Liver-directed gene targeting as a potential therapy for Fabry Disease

Himanshi Saxena

A thesis submitted for the fulfilment of the requirements of the Open University (UK) for the degree of

Doctor of Philosophy

at

International Centre for Genetic Engineering and Biotechnology (ICGEB), Trieste, Italy

Dr Andrés Fernando Muro
Director of Studies

Dr Gloria Gonzalez-Aseguinolaza
External examiner

Submitted August 2023

Declaration of original work

I, Himanshi Saxena, declare that I am the sole author of this thesis, and the work presented in this Ph.D. thesis, entitled "Liver-directed gene targeting as a potential therapy for Fabry Disease," is the result of my original research. To the best of my knowledge, all sources, people, publications, and contributions have been diligently acknowledged.

Himanshi Saxena

ICGEB, Trieste (Italy)

Acknowledgement

With heartfelt gratitude, I proudly present this thesis as a testament to my unwavering dedication and hard work, while acknowledging that this extraordinary expedition wouldn't have been possible without the support, guidance, and encouragement of countless remarkable individuals.

This doctoral journey is a difficult one to embark on, especially when it comes during a pandemic. However, it certainly makes things easier if your PI is an understanding and supportive person. Therefore, I would start by thanking my supervisor Dr. Andrés Muro, for this opportunity, constant guidance, and his trust in my abilities. I extend a special thanks to the collaborators in Udine, for their constant availability and contribution to this thesis and a sincere appreciation to the Telethon Foundation for funding the project.

I am grateful for the amazing support system I had to help me get through everyday life. Sonal, thank you for sharing the love of food and travel and most importantly being my home away from home! I would like to thank the Mouse molecular biology group members, Sandra, Giulia, Bhaswati, and Luca for their support. Michela, thank you for being there since the very beginning, for fresh perspectives, sushi dinners, and especially for introducing me to the realm of cats. I would like to extend my warm words to Antonio, through all the homemade pizzas, teasing, and playful banter, I enjoyed every moment of annoying you like a sibling. Thank you, Ilenia, for being such a caring friend. Laura Di, thank you for sharing our mutual courage of things that are ‘do-able’, the laughter and most importantly embracing me like a sister. I am grateful for the opportunity to explore my abilities as a mentor. So, thank you Martina for being a wonderful student and good friend.

Although I am grateful for the family I made in Italy, I would not be here if not for my family in India, I am grateful to my amazing and supportive parents and Harshit bhaiya for believing in me. Thank you, Anu and Praffy for keeping me grounded and at the same time being my personal cheerleaders. I would like to express my deepest gratitude to Abhishek, without whom this journey would not have been possible. Thank you for your extraordinary patience and unconditional support. I appreciate your ability to make me smile even on the greyest of days and inspire me to be a better human being.

“Act as if what you do makes a difference. It does” -William James

“Let success be your noise” -Frank Ocean

I would like to acknowledge the authors of these quotes, which have been an unwavering beacon of motivation throughout my Ph.D. journey and have profoundly influenced my life's purpose and passion

for science. During moments of doubt and uncertainty, these thoughts served as a powerful reminder to work hard, and that even seemingly small actions and unstirring contributions can have profound consequences. This has also influenced the way I approached challenges with optimism and positive intent in my personal relationships and professional pursuits. During this journey, every experiment conducted, every data point analyzed, and every laugh and tear has empowered me on a path that aligns with my values, relations, and vision for contributing to the greater good.

Abstract

Fabry disease (FD) is an X-linked inherited, lysosomal storage disorder caused by mutations in the Alpha Galactosidase-A (GLA) gene. This gene encodes for the GLA enzyme which is responsible for the catabolism of glycosphingolipids like globotriaosylceramide (Gb3). Accumulation of Gb3 in lysosomes results in systemic clinical manifestations and reduced lifespan. Enzyme replacement therapy (ERT) and chaperone therapy are the available treatments for FD however, noncurative and with limitations.

We developed a potential therapeutic approach based on the permanent genetic modification of hepatocytes to express the GLA enzyme by targeting the albumin locus *in vivo*. To model late-onset and early-onset FD, we treated juvenile (P30) and neonatal (P5) Fabry mice with an AAV8 donor vector containing mAlb homology arms and a codon-optimized version of the human GLA cDNA. This treatment was coupled with the AAV-mediated delivery of the CRISPR/SaCas9 platform to increase targeting efficiency. Treatment of juvenile Fabry mice (donor, 3.0E13 vg/kg; SaCas9, 6.0E12 vg/kg) resulted in elevated GLA enzyme activity which was stable till the termination of the experiment at 5 months of age, accompanied by a 70-80% reduction in Lyso-Gb3 accumulation in liver, kidneys and heart, compared to untreated mutant mice. To increase the safety of the procedure, concerns related to the use of programmable nucleases were avoided by applying a nuclease-free approach. Juvenile animals were treated only with the donor vector (3.0E13 vg/kg), coupled with the treatment with fludarabine, which enhances the gene targeting rate. This nuclease-free strategy resulted in increased plasma GLA activity compared to donor-only treated mice, accompanied by 80-95% of lyso-Gb3 clearance.

When we treated neonatal P5 Fabry mice with donor and SaCas9 AAVs, the treatment was significantly more efficient than in juvenile animals due to the increased targeting rate observed in proliferating hepatocytes present in a growing liver. In fact, we were able to completely clear lyso-Gb3 in plasma and in the different organs with the highest dose of 3.0E14 vg/kg of donor vector, while a dose of 3.0E13 vg/kg resulted in a reduction of 95-98% in plasma and target organs.

A dose escalation study with AAV-mediated episomal gene therapy was also done as a proof-of-principle in juvenile Faby KO mice using a strong liver-specific promoter and the human codon-optimized GLA transgene. Animals treated at 3.0E12 vg/kg and higher doses were able to reduce substrate accumulation by 98-100% in plasma and target tissues. Treatment with the lowest dose of the AAV vector (3.0E11vg/kg) resulted in the clearance of 85-95% lyso-Gb3 in the bloodstream and tissues proving the efficacy of the treatment for late-onset FD. ERT-treated animals were considered for comparative evaluation of the treatment.

This data is inclined towards a promising one-shot therapy using an AAV-based integrative gene-editing approach for early-onset and AAV-based episomal gene therapy for late-onset FD to revert the phenotype irrespective of the Fabry disease-causing mutation. To test the translational applicability of this integrative strategy, AAV-LK03 vectors containing human ALB homology arms have been tested in human liver cell lines and will be validated in primary cultures of human hepatocytes, and in humanized mice to generate consistent preclinical support.

List of contents

List of Tables

List of Figures

Introduction

1.1 Inherited rare diseases

Rare diseases cover a wide range of 7,000-8,000 genetically inherited disorders. The definition of rare diseases changes among different countries. For example, in the European Union and Australia, it is defined as a disease whose prevalence corresponds to 1 affected person in 2,000, while it is 1 in 10,000 according to China, 1 in 50,000 in Japan, and 200,000 affected persons according to the United States of America (Nguengang Wakap et al. 2020) (Khosla and Valdez 2018). The lack of a single epidemiology data across a continent makes these rare diseases a non-priority issue in the medical community. Regardless of their nomenclature and definitions, rare diseases are significantly common affecting 350 to 446 million people globally (30 million out of 500 million in the European continent) (Bax 2017) (Nguengang Wakap et al. 2020). The term "rare diseases" is often interchangeably used with "orphan diseases" or diseases that have been under-estimated and under-appreciated by the medical and research community like Huntington's disease and even a few common issues like pediatric Severe combined immunodeficiency (SCID) and pediatric diabetes, and lysosomal storage disorders (LSD) like Fabry disease. Eighty percent (80%) of these disorders have a genetic cause that is usually a recessive mutation in the genome, which is often heritable (Tambuyzer 2010).

The advancements in DNA sequencing techniques and big data analysis have paved the way for discovering and diagnosing rare disorders. Orphanet is an open platform in which all the sequencing data are stored, providing modifiable gene-sequencing panels, genetic tests, and directories from diagnostic laboratories for rare diseases (Pavan et al. 2017). Other than this, Whole-Exome Sequencing (WES) has also helped in the identification of genetic mutations (Nguyen and Charlebois 2015). Although the exome comprises 2% of the entire genome, it is estimated that 85% of the heritable Mendelian disease-causing mutations are in this region. There is enough evidence to support that genetic aberrations in the rest of the 98% genomic component, the non-coding sequences, are the causative of many genetic diseases as well. Other than sequencing, genetic counseling, family tree studies, and prenatal analysis are methods to assist diagnose the possibility of the presence of rare disease-causing mutations (Cornel et al. 2021). Due to a lack of enduring solutions for rare diseases, patients often rely on dietary therapies in case of metabolic disorders or Enzyme Replacement Therapy (ERT) for a limited number of conditions to improve their quality of life. Ultimately, patients must undergo organ transplants to revert the phenotype. Research being done on rare diseases like lysosomal storage disorders (Hunter syndrome, Fabry disease, Pompe disease, etc.) with gene therapy to target the core genetic cause has brought in hope for a more reliable treatment.

1.2 Lysosomal Storage Disorder

1.2.1 The lysosome

In order to better understand Lysosomal Storage Disorders (LSDs) it is vital to skim through the significance of the lysosome. Nearly 60 years ago in 1963 the Nobel Laureate, Christian de Duve introduced *"The Lysosome"* in the Scientific American journal as *"This small particle acts as the digestive tract of the living cell. Its enzymes dissolve the substances ingested by the cell under certain circumstances can dissolve the cell itself"* (de Duve 1963). This discovery has become an aid in the identification of over 50 LSDs and hence novel curatives.

Lysosomes are cell vacuoles that use acid hydrolases to digest the extracellular material taken up by the cell's macrophages by phagocytosis and clean up the cell's intracellular compartment by autophagy. The endocytic role of lysosomes not only contributes to their function but also their formation. The extracellular material is endocytosed by a clathrin-coated endocytic vesicle followed by budding from the plasma membrane and eventually fusing with the endosomes. These endosomes progressively mature to late endosomes characterizing the lowering of the internal pH of the vacuole. These events trigger the formation of the lysosome by stimulating the recognition of acid hydrolases synthesized in the rough endoplasmic reticulum, in the trans-Golgi network by mannose-6-phosphate (M6P) residues

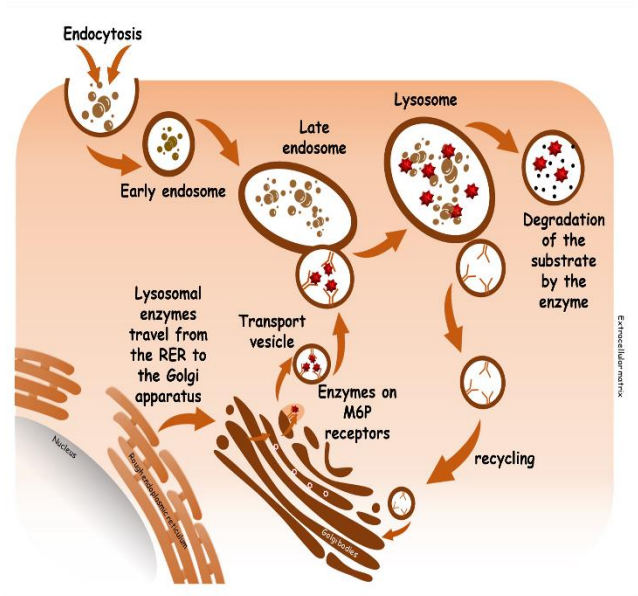

Figure 1. Formation of lysosomes. Lysosomes are membrane-bound organelles formed by the fusion of endocytic vesicles-enclosing extracellular substrate and transport vesicles with acid hydrolases bound to M6P receptors. With optimal pH the acid hydrolases dissociate from the receptors and engage in catabolizing the substrate acting as degrading bodies.

and their receptors. These hydrolases are then packed in the clathrin-coated vesicles and fuse with the late endosomes. The low pH of the endosomes allows the dissociation of the hydrolases from the M6P receptors. Once the late endosomes containing the target molecules acquire the necessary hydrolase mature and form the lysosome as depicted in Figure 1 (Luzio et al. 2000) (von Knebel Doeberitz and Wentzensen 2008).

There are about 60 enzymes constituting the family of lysosomal hydrolases. Glycosidases (Alpha-Galactosidase A, Cytosolic Beta-Glucosidase, Hyaluronidase1/4, etc.) use carbohydrates, glycoprotein, and glycolipids as their substrates; nucleases like DNase I/II and Phospholipase D3/D4 act on RNA and DNA molecules; phosphatases play their role in the removal of phosphate groups from its substrate (polysaccharides and mucopolysaccharides, and sulfates) by hydrolysing phosphoric acid monoesters. Proteases like the Cathepsin family and Napsin digest proteins, peptides, and collagen, and Lipases (LIPA and LIPL4) break down cholesteryl esters and triglycerides. The proper functioning of the lysosome and its enzymes is vital for cell homeostasis. The table assembled below classifies lysosomal enzymes based on the target substrate along with their genes since mutations in the gene encoding these lysosomal enzymes are known to cause lysosomal storage disorders (Table 1).

1.2.2 Understanding LSDs

Lysosomal storage disorders or LSD are a group of around 50 inherited metabolic diseases dealing with deficiencies and malfunctioning acid hydrolases of the lysosomes. Most LSDs occur due to mutations in the genes encoding these enzymes, translating to misfolded or inefficient protein production, ER retention, and aberrations in lysosomal intracellular trafficking and signaling mechanisms. Pathologically, this condition leads to the accumulation of non-degraded substrates in the lysosomes inside the cell, eventually manifesting clinical symptoms. Lysosomal storage disorders are classified based on the type of accumulating substrate. For example, defects in enzymes responsible for Glycosaminoglycans (GAG) catabolism are categorized as mucopolysaccharidoses, defects in enzymes for sphingolipid catabolism are sphingolipidoses, for glycolipids and glycoproteins; glycoproteinoses (Parkinson-Lawrence et al. 2010). LSDs also cover diseases with defects in the machinery leading to the maintenance of lysosomes like post-translations processing of lysosomal enzymes, defects in channels and transporters of these enzymes or substrates, or even defects in the machinery of lysosome synthesis itself.

Category	Lysosomal storage disorder	Genes encoding lysosomal enzymes
Sphingolipidoses	Fabry disease	*GLA*
	Farber lipogranulomatosis	*ASAH1*
	Gaucher disease	*GBA*
	GM1 gangliosidosis	*GLB1*
	GM2 gangliosidosis (Tay-Sachs disease)	*HEXA*
	GM2 gangliosidosis (Sandhoff disease)	*HEXB*
	GM2 activator deficiency	*GM2A*
	Krabbe disease	*GALC*
	Niemann-pick disease	*SMPD1*
Mucopolysaccharidosis	Hurler Syndrome (MPSI)	*IDUA*
	Hunter Syndrome (MPSII)	*IDS*
	MPS III-A/B/C/D	*SGSH/ NAGLU/ HGSNAT/ GNS*
	MPS IV-A/B	*GALNS/GLB1*
	MPS VI	*ARSB*
	MPS VII	*GUSB*
	MPS IX	*HYAL1*
Glycoproteinoses	α-Mannosidosis	*MAN2B1*
	β-Mannosidosis	*MANBA*
	Fucosidosis	*FUCA1*
	Aspartylglucosaminuria	*AGA*
	Schindler disease	*NAGA*
	Sialidosis type I/II	*NEU1*
	Galactosialidosis	*CTSA*
Membrane protein disease	Cystinosis	*CTNS*
	Danon disease	*LAMP2*
	Sialic acid storage disease	*SLC17A5*
	Niemann-pick disease type C1/C2	*NPC1/ NPC2*
	Mucolipidosis IV	*MCOLN1*
Post-translational modification defects	Multiple sulfatase deficiency	*SUMF1*
	Mucolipidosis II α/β	*GNPTAB*
	Mucolipidosis III γ	*GNPTG*
Glycogen storage disease	Pompe disease	*GAA*
Lipid Storage disease	Acid lipase deficiency	*LIPA*

Table 1. Classification of Lysosomal Storage diseases. Lysosomal storage disorders can be broadly classified based on the substrate that accumulates in the lysosomes of the affected cells. The table represents a few categories and major diseases associated with the storage molecule and the respective acid hydrolase or lysosomal enzyme responsible for the catabolism of the substrate.

1.2.3 Reviewing treatments and trials for LSDs

There are several treatments available for patients suffering from lysosomal storage disorders like hematopoietic stem cell transplantation (HSCT), enzyme replacement therapy (ERT) (Mindy 2018), substrate reduction therapy (SRT) (Coutinho, Santos, and Alves 2016), and pharmacological chaperone therapy (PCT) (Parenti, Andria, and Valenzano 2015) to name a few. ERT has proven to be effective for many of these disorders (listed in Table 2). The first recombinant enzyme approved was Alglucerase

Lysosomal Storage Disorder	Enzyme Replacement Therapy	FDA Approval
Fabry disease	Agalsidase α (Fabrazyme™)	2003
	Agalsidase β (Replagal™)	2003
	PRX-102 (pegunigalsidase alfa)	2023
Gaucher's disease	Velaglucerase (VPRIV™)	2010
	Taliglucerase (Elelyso™)	2012
	Imiglucerase (Cerezyme®)	1991
Pompe disease	Aglucosidase (Myozyme™)	2006
	Aglucosidase (Lumizyme™)	2010
	Avalglucosidase alfa	2021
MPS I	Laronidase (Aldurazyme™)	2003
MPS II	Idursulfase (Elaprase™)	2006
MPS IV A	Elosulfase Alfa (Vimzim™)	2014
MPS VI	Galsulfase (Naglazyme™)	2005
Lysosomal acid lipase deficiency	Sebelipase α (Kanuma™)	2015
CLN2	cerliponase alpha (Brineura®)	2017
MPS VII	Vestronidase alfa (Mepsevii™)	2017
Gaucher disease	Imiglucerase (Cerezyme®)	1991

*FDA=Food and Drug Administration

Table 2. FDA-approved ERT for LSDs. There are several FDA-approved Enzyme Replacement Therapy (ERT) available for the treatment of lysosomal storage disorders. Most recently Pegunigalsidase alfa has been accepted for FDA approval in 2023 for Fabry disease.

for Gaucher's disease type 1, which dates back to 1991 (Whittington and Goa 1995). Following this, other enzyme replacement products for Gaucher disease were approved like Imiglucerase (Zimran et al. 1995), and Taliglucerase alpha. Fabrazyme and Replagal were approved in recent years for Fabry disease (Pisani et al. 2012). According to the Canadian Agency for Drugs and Technologies in Health (CADTH) Common drug review, the cost of treatment using Fabrazyme and Replagal per patient per year is 312,186 USD and 299,821 USD respectively with a life-long course of treatment, this unrealistic cost comes along with a considerable loss in the quality of life. Currently, the standard treatment to manage the phenotype of diseases like Gaucher disease, Pompe disease, neuronal ceroid lipofuscinosis type 2 (CLN2), Fabry disease, and mucopolysaccharidoses is dependent on their respective enzyme replacement therapy products (Silva et al. 2022).

Pharmacological Chaperone therapy (PCT) works on the principle that molecules called chaperones help to stabilize protein folding and unstable conformations. Velaglucerase alfa was first approved for Gaucher patients for whom ERT was not an option (Cox et al. 2008). Migalastat is the only approved drug using PCT for Fabry disease (Germain et al. 2016), however, there are clinical trials ongoing for similar drugs for other LSDs. Ambroxol an over-the-counter drug just completed phase-2 clinical trials for type 1 Gaucher disease (Zimran, Altarescu, and Elstein 2013). Despite important research, chaperone therapy targets only a small proportion of patients due to its mutation-specific mode of action.

A promising tool for the treatment of LSDs is gene therapy. Jacob Favret in his review of lysosomal storage diseases explains the different approaches to treatment represented in Figure 2 (Favret et al. 2020). Recently many gene therapy studies based on *in vivo* AAV-mediated delivery of a functional copy of the defective gene have advanced to the clinics. Reports suggest encouraging progress using adeno-associated viral vectors serotype 8 (AAV8) because of its efficient transduction abilities along with an appreciable safety profile and long-lasting expression in non-replicative cells *in vivo*. There is incessant research being done in the field of engineered AAV capsids to increase transduction efficiency and safety. AAV-DJ and AAVLK03 are some engineered AAV capsids that are capable of enhanced specie-specific infectivity that have reached clinics and are being tested in phase-1 and phase-2 trials, making AAV a good candidate for use in pre-clinical and clinical research (Wang et al. 2015). For some LSDs, the delivered gene expresses the correct enzyme which is secreted from its depot organ like the liver and taken up by other organs using M6P receptors. This "cross-correction" is being applied to gene therapy treatments of various LSDs like Fabry disease.

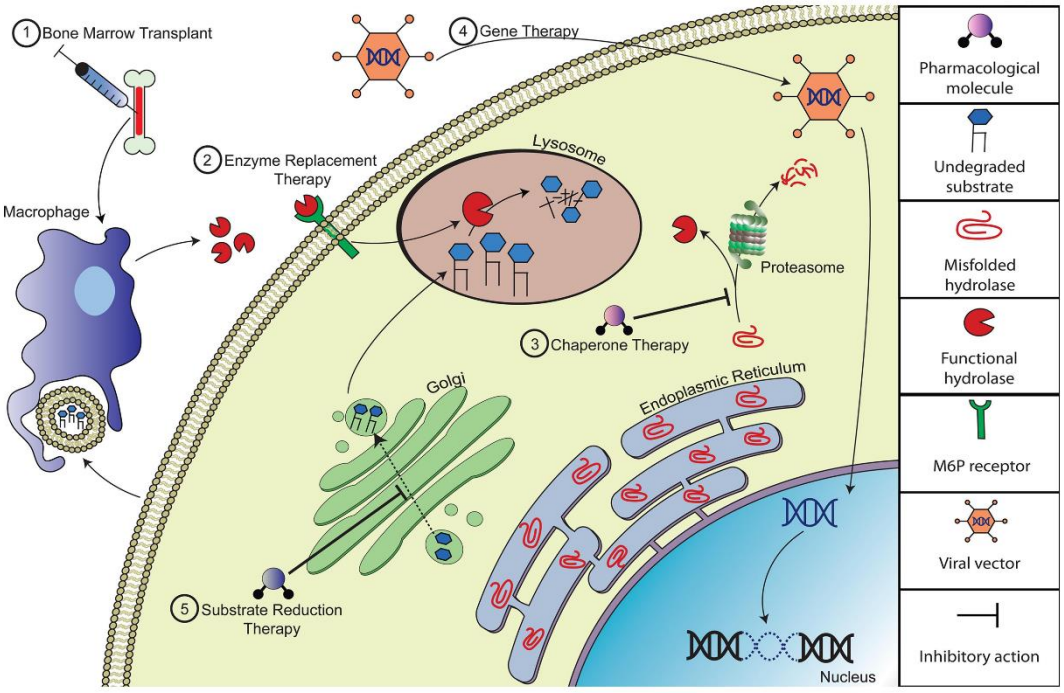

Figure 2. Potential therapeutic approaches to treat substrate accumulation in LSDs. This image from Favret *et al.* reviewed the different therapeutic approaches being researched and tested to target substrate accumulation in LSDs. 1) Bone marrow transplantation (BMT) (2) Enzyme replacement therapy (ERT) compensates for the loss of endogenous hydrolase activity by providing recombinant enzyme (3) Pharmacologic chaperone therapy (PCT) can improve the catalytic activity of the misfolded lysosomal enzyme by promoting folding and acquisition of functional conformation of the nascent mutant peptide (4) Gene therapy (GT) (5) Substrate reduction therapy (SRT) involves the delivery of small molecule inhibitors that reduce biosynthesis of the specific accumulating substrate. (Favret J M. *et al.*, 2020)

Adult Fabry patients have been involved in a clinical trial with AAV6 (NCT04046224) and with other engineered capsids (NCT04040049, NCT04519749) to test safety and tolerability. Other than this, a phase-1/2 clinical trial delivering AAV8 to late-onset Pompe disease patients is ongoing (NCT04093349, NCT04174105). Also, in a multi-center phase-1/2 clinical trial (NCT03173521) AAV8-based vector has been administered to MPS IV patients.

Ex vivo gene therapy using lentiviral vectors works by correcting the patient's cells by manipulating the genetic structure to produce a functional protein followed by re-implantation into the patient. In 2018, a phase-1/2 clinical trial was initiated for Mucopolysaccharidosis Type I, using lentiviral mediated gene therapy which has recently shown promising preliminary clinical data. Similarly, in the case of Gaucher disease, a successful preclinical mouse data was followed by a phase 1/2 clinical trial by Avrobio where lentiviral modified HSCs are being administered to patients.

A list of recent ongoing clinical trials with gene-based therapies is presented in Table 3 (Kido, Sugawara, and Nakamura 2023). Patients treated with ERT and PCT have noticed more manageable phenotypes of the disease condition. However, the course and high cost of the therapies reduce the quality of life substantially. Therefore, targeting lysosomal storage disorders at the root cause is essential and the research with gene-based therapies comes with a hope of a potential therapeutic for LSDs.

1.3 Fabry disease

1.3.1 Overview and research history

Fabry disease (OMIM 301500) is a rare lysosomal disorder often reminded as Anderson-Fabry disease after the researchers who brought light to it. Other nomenclatures include Alpha-galactosidase A deficiency or GLA deficiency, Angiokeratoma corporis diffusum, Diffuse Angiokeratoma, Ceramide trihexosidosis (Brady et al. 1967), and Hereditary dystopic lipidosis. It is an X-linked inborn error of metabolism which occurs due to the deficiency of the Alpha galactosidase enzyme intended to catabolize globotriaosylceramide or Gb3 and its isoforms, instead progressively accumulates in the lysosomes of the cells (Figure 3). There are more than 1000 mutations registered in the GLA gene translating into a defective enzyme with reduced (non-classical variant) and minimal or null (classical variant) Alpha-D- Galactosidase A enzyme activity.

Disease	Clinical Trial	Intervention	Sponsor	Status
Fabry	NCT05039866	ST-920; AAV2/6 (GLA)	Sangamo Therapeutics	LTFU
	NCT04455230	FLT190; AAVS3 (GLA)	Freeline Therapeutics	LTFU
	NCT04519749	4D-310; AAV (GLA)	4D Molecular Therapeutics	Phase 1/2
	NCT04999059	AVR-RD-01; LV (GLA), *ex vivo*	AvroBio	LTFU
	NCT02800070	LV (GLA), *ex vivo*	Ozmosis Research Inc.	Phase 1
Pompe	NCT05567627	GC301; AAV9 (GAA)	GeneCradle Therapeutics	NA
	NCT04093349	SPK-3006; AAV (GAA)	Spark Therapeutics	Phase 1/2
	NCT04174105	AT845; AAV8 (GAA)	Audentes Therapeutics	Phase 1/2
	NCT03533673	ACTUS-101; AAV2/8 (GAA)	Asklepios Biopharmaceutical	Phase 1/2
	NCT02240407	AAV9 (GAA)	University of Florida	Phase 1
Gaucher	NCT05815004	AVR-RD-02; *LV (GBA) ex vivo*	AvroBio	Phase 2/3
	NCT05324943	FLT201; AAVS3 (GBA)	Freeline Therapeutics	Phase 1/2
Krabbe	NCT04771416	PBKR03; AAVHu68 (GALC)	Passage Bio, Inc.	Phase 1/2
	NCT04693598	FBX-101; AAVrh10 (GALC)	Forge Biologics, Inc.	Phase 1/2
MPS I	NCT04628871	SB-318; AAV2/6 (ZFN)	Sangamo Therapeutics	LTFU
	NCT03580083	RGX-111;AAV9 (IDUA)	Regenxbio Inc.	Phase 1/2
	NCT03488394	LV (IDUA), *ex vivo*	IRCCS San Raffaele	Phase 1/2
MPS II	NCT05238324	HMI-203; AAV (IDS)	Homology Medicines, Inc.	Phase 1
	NCT04571970	RGX-121; AAV9 (IDS)	Regenxbio Inc.	Phase 1/2
	NCT04628871	SB-913; AAV2/6 (ZFN)	Sangamo Therapeutics	LTFU
MPS IIIA	NCT04088734	ABO-102; AAV9 (SGSH)	Abeona Therapeutics, Inc	Phase 1/2
	NCT04201405	LV (SGSH), *ex vivo*	University of Manchester	Phase 1/2
	NCT03612869	LYS-SAF302; AAVrh10 (SGSH)	Lysogene	Phase 2/3
	NCT01474343	SAF-301; AAVrh10 (SGSH + SUMF1)	Lysogene	Phase 1/2
MPS IIIB	NCT04655911	ABO-101; AAV9 (NAGLU+CMV)	Abeona Therapeutics, Inc.	LTFU
	NCT03300453	AMT-110; AAV2/5 (NAGLU)	UniQure Biopharma B.V.	Phase 1/2
MPS VI	NCT03173521	AAV2/8 (ARSB)	Fondazione Telethon	Phase 1/2
GM1 gangliosidosis	NCT04273269	LYS-GM101; AAVrh10 (GLB1)	Lysogene	Phase 1/2
	NCT04713475	PBGM01; AAVrh68 (GLB1)	Passage Bio, Inc.	Phase 1/2
	NCT03952637	AXO-AAV-GM1; AAV9 (GLB1)	NHGRI	Phase 1/2
Tay-Sachs/Sandhoff	NCT04669535	AXO-AAV-GM2; AAVrh8-HEXA +HEXB	University of Massachusetts	Phase 1
	NCT04798235	TSHA-101; AAV9 (HEXA + HEXB)	Taysha Gene Therapies, Inc.	Phase 1/2
Cystinosis	NCT05146830	AVR-RD-04/CTNS-RD-04; LV (CTNS)	AvroBio	LTFU
Metachromatic leukodystrophy	NCT04283227	OTL-200; LV (ARSA)	Orchard Therapeutics	Phase 3
	NCT02559830	LV (ARSA + ABCD1), *ex vivo*	Shenzhen Second People's Hospital	Phase 1/2
	NCT01801709	AAV10 (ARSA), Intracranial	European Leukodystrophy Association	Phase 1/2
CLN2	NCT04273243	AT-GTX-501; AAV9 (CLN6)	Amicus Therapeutics	LTFU
	NCT01414985	AAV10 (CLN2)	Cornell University	Phase 1/2
CLN3	NCT03770572	AT-GTX-502; AAV9 (CLN3)	Amicus Therapeutics	Phase 1/2
CLN5	NCT05228145	NGN-101; AAV9 (CLN5)	Neurogene Inc.	Phase 1/2
CLN7	NCT04737460	AAV9 (CLN7)	Benjamin Greenberg	Phase 1
Danon disease	NCT03882437	RP-A501; AAV9 (LAMP2B)	Rocket Pharmaceuticals Inc.	Phase 1

Table 3. Gene therapy-based clinical trials for Lysosomal Storage diseases. Gene therapy and genome editing are proving to be potential treatment approaches to lysosomal storage disorders. The table lists clinical trials with gene-based therapies, most of which are in Phase-1 and -2. However, many treatments are undergoing long-term follow-up studies and have the potential for FDA approval. The list was updated in April 2023 from *clinicaltrials.gov*

Currently, enzyme replacement therapy therapeutics Replagal and Fabrazyme, and more recently chaperone therapy product Galafold, have been made available in the market to treat Fabry disease. There is a dire need for awareness of Fabry disease among the general population. In a study on global research on Fabry disease, it was noticed that from 1973 to 2018 a total number of 1,975 articles were published with the USA leading in the research followed by Germany, Italy, the UK, France, and Japan. The global market for the treatment of Fabry disease blooms with an estimated 3.12 billion USD growth by 2025 according to Value Market Research (Klingelhöfer et al. 2020).

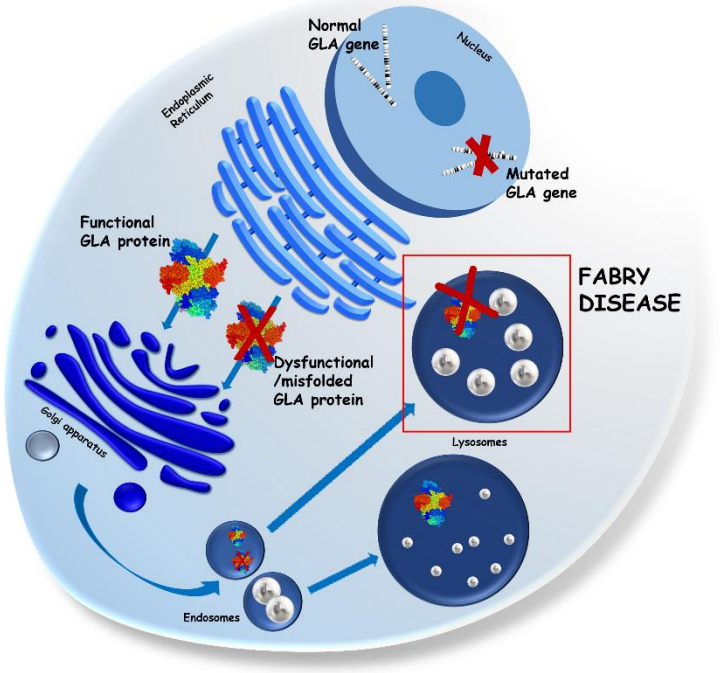

Figure 2. Fabry disease. Fabry disease is caused due to a mutation in the GLA gene encoding Alpha-galactosidase A enzyme responsible for the degradation of larger Gb3 and its isotopes into smaller molecules in the lysosome. Due to the mutation in the gene, a misfolded or inefficient GLA is produced and is unable to hydrolyse Gb3 substrates resulting in substrate accumulation in the lysosome and a systemic response known as Fabry disease.

Anderson-Fabry disease came into light for the first time in 1898 when two dermatologists independently reported cases indicating the novel disease. Johannes Fabry in Germany diagnosed a 13-year-old patient suffering from nodular purpura and albuminuria as a case of Angiokeratoma Corporis Diffusum. While in the same year in England, William Anderson reported a systemic disorder in his 39 years old patient suffering from Angiokeratomas, proteinuria, varicose veins, lymphedema along with deformities in the fingers (Anderson 1898). Several similar cases followed the initial description of the disease. It was identified to possess hereditary traits when Pompen in 1947 reported the death of two brothers with the same disease (Pompen, Ruiter, and Wyers 1947). A breakthrough in the context of the disease came with the discovery of Gb3 in 1963 by Sweeley and Klionsky. It was found that the accumulation of this lipid in the lysosomes was the main cause of Fabry disease. Eventually, the

defective α-Galactosidase A gene was identified to be the primary contributing agent of Anderson-Fabry disease.

1.3.2 Molecular basis and pathophysiology

Fabry disease is caused by the deficiency of Alpha D-Galactosidase A (E.C. 3.2.1.22) an enzyme translated from the GLA gene (Gene ID: 2717) present on the long arm of the X chromosome at q22.1 (Xq22.1). It is a 12kb gene with a 1290 base pair long coding sequence with 8 exons and 429 amino acids. Structural studies of the gene describe it as a homodimer glycoprotein, where each monomer in the dimer contains two domains: a C-terminal antiparallel β domain and a (β/α) barrel with the active site. The GLA protein is secretory as well as cellular in nature and abundantly available in most organs in a healthy individual. The functional significance of the protein relies on its catalytic capabilities in that hydrolysis of the terminal alpha-galactosyl moieties from glycolipids and glycoproteins (Garman and Garboczi 2004). Predominantly, it is responsible for the catalytic cleavage of the terminal galactose from Gb3 (Globotriaosylceramide) (Garman and Garboczi 2004). Gb3 or ceramide trihexoside is formed by the linkage of galactose and lactosylceramide making it a lipid moiety that is also a cluster of differentiation (CD77). Accumulation of glycosphingolipids, such as globotriaosylceramide (Gb3) isoforms, globotriaosylsphingosine (lyso-Gb3) and isoforms, and galabiosylceramide (Ga2) isoforms, are measured in human plasma and urine and are standard substrate markers of Fabry disease (Garman and Garboczi 2004) (Figure 4.).

According to fabry-database.org, more than 1000 mutations have been reported in the gene including 1518 missense and 297 nonsense accounting for a large percentage of the mutations. However, it is crucial to note that not all of them lead to a defective GLA protein, but more than 800 mutations have already been held responsible for the condition. These mutations in the GLA gene translate to misfolded or inefficient GLA protein depending on the mutation, which is unable to degrade Gb3 molecules inside the lysosomes. As a result, there is progressive accumulation of the substrate in the cells leading to clinical manifestations.

Suffering patients experience a systemic response that varies with each individual. A few mentioned: acroparesthesias, heat intolerance, tinnitus (nervous system), vomiting, diarrhea, and nausea along with loss of weight target the gastrointestinal tract. Angiokeratomas and hypohidrosis are some of the most common abnormalities affecting the skin, the eyes suffer from corneal and lenticular opacities and vasculopathy. The two most affected organs include the kidneys which start to malfunction and lead to proteinuria, hyperfiltration, and show increased urine Gb3 levels, and the heart which displays signs of arrhythmias, ECG abnormalities, and valvular insufficiency to mention a few (Germain 2010).

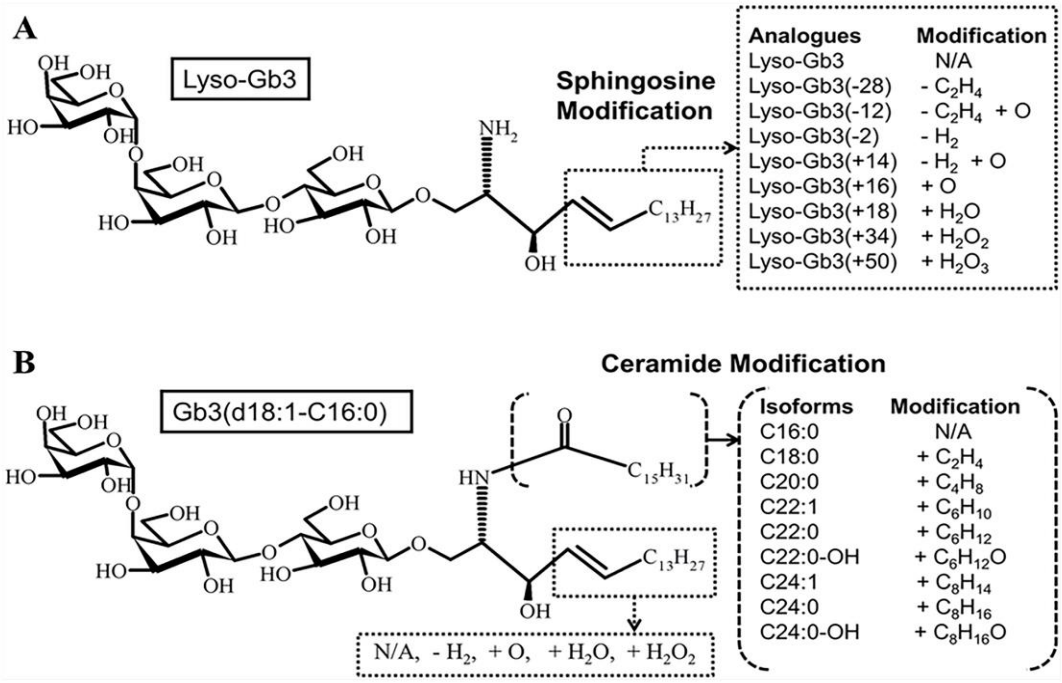

Figure 4. Substrate markers of Fabry disease. Accumulation of substrates like Globotriaosylceramide (Gb3) and globotriaosylsphingosine (lyso-Gb3) and their isoforms found in tissues, blood and urine are quantified using Mass-spectrometric techniques as markers of Fabry disease.

Based on these severe phenotypes, FD is classified according to the affected organ, with the renal and the cardiac variants covering the majority of the cases. However, Fabry disease is more often classified on the basis of its onset; the classical variant or early-onset FD, and the atypical or late-onset FD. The GLA enzyme activity in late-onset patients ranges from 3 to 30%, with symptoms evident in the third decade of life whereas, in the case of classical form, patients have mutations causing minimal or no residual GLA enzyme activity (1-3%) affecting the quality of life from an early age and reducing life expectancy. Children with classical FD suffer intolerance to heat, skin abnormalities, gastrointestinal problems, and burning pain in the limbs known as Fabry crises which often extend to renal and cardiac symptoms toward adulthood (Michaud et al. 2020).

1.3.3 Epidemiology and diagnosis

FD is an X-linked inherited disorder associated with the defective GLA gene present on the X chromosome and therefore, majorly affects the male population. It is also widely accepted that heterozygous females carrying the defective gene have been reported with mild to severe symptoms

due to random X inactivation. Based on the skewing of X inactivation, some cells express normal range of GLA whereas, some other cells will have minimum or null GLA expression, leading to mosaic GLA expression at cellular levels (Hughes 2008).

FD involves multiple organs and varied clinical manifestations with variables like age and sex, it often remains underdiagnosed in a common population. The true prevalence of the disease should be studied regionally due to its pan-ethnic nature which creates an alarming inconsistency in the number of cases globally. In Taiwan, a newborn screening predicts an unexpected 1 in 1,500 FD affected males (Lin et al. 2009). During a newborn and family screening in Italy, the numbers reach up to 1 in 3,100 males with an 11:1 ratio of late-onset to classical phenotype, proving the higher undiagnosed incidence of late-onset FD. Another study in the Netherlands involving pre-natal and post-natal diagnosis accounts for 1 in 500,000 FD patients. Similar numbers were diagnosed in the UK (1 in 300,000 as well). This discrepancy has led to misjudged prevalence figures in the community (Spada et al. 2006).

In case the patient is suspected to be suffering from Fabry disease, genetic and enzymatic evaluations are done. Clinical tests for the activity of the α-Galactosidase enzyme in plasma are done for both classical and non-classical FD. Genetic testing confirms the type of mutation in the enzyme locus and its repercussions. This type of genetic testing is recommended for females since enzymatic assay is most likely to indicate residual activity. Furthermore, genetic counseling or familial studies have helped diagnose Fabry's disease. In families with this X-linked disorder, prenatal evaluation is done through the analysis of amniotic fluids and gene sequencing for suspected mutations (Michaud et al. 2020).

1.3.4 Research, treatments, and trials

Due to the complex symptoms of the disease which vary from each individual, the diagnosis is often delayed and mostly neglected. It is crucial and perchance rare for a general practitioner to identify a patient's symptoms as those of Fabry disease. Therefore, a major undiagnosed population is often treated with organ-specific treatments in the case of late-onset FD. Currently, patients diagnosed with Fabry disease are treated with ERT. Studies are attempting novel treatments are therapeutics for Fabry disease.

ERT stands first in line to show some success in the treatment of Fabry disease. Recombinant alpha-galactosidase enzyme is intravenously infused once every two weeks, in an attempt to provide for the deficiency. There are two recombinant products available for the purpose since 2001: Fabrazyme or Agalsidase beta and Replagal or Agalsidase alpha. Studies have shown improvement in the clinical manifestations during the early stage of the disease involving the heart and kidney, and a reduction in pain has also been observed. Despite the success, the long-term effect is yet to be determined. Keeping in mind the half-life of the enzyme, multiple infusions, liver-directed ineffective biodistribution, and immune response against the recombinant product do not ascertain a permanent and stable cure (Rombach et al. 2013). Several missense mutations have been studied which tend to produce a normal

GLA protein but result in reduced enzymatic activity due to protein instability. Chaperones are substances that bind to the mutated protein and assist it in proper folding, restoring stability, maturation, and trafficking to the lysosomes. Migalastat is 1-deoxygalactonojirimycin, a galactose analog or chaperone from Amicus Therapeutics is an oral drug taken every other day to treat FD. The long-term efficacy of the drug is being studied. A major drawback to this therapy is its eligibility for particular mutations which cannot be applied to all GLA mutations (McCafferty and Scott 2019).

Recent research with substrate reduction therapy (SRT) aims for the reduction of the substrate Gb3 as the name suggests. To reduce the accumulation of Gb3 in the lysosomes glucosylceramide synthetase inhibitors are used to slow down the rate of Gb3 production. N-butyldeoxynojirimycin, an imino sugar analog is under observation for this therapy. Though SRT aims to control the Fabry condition by inhibiting Gb3 accumulation and not restoring function GLA, it might spring better results if used alongside ERT (Guérard et al. 2018). Another potential approach is promoter activation therapy which aims at the amplification of the residual enzyme in Fabry patients. Small molecule promoter activators can be targeted to bind the GLA promoter in the cells to boost transcription and produce an increased amount of mutated GLA protein to degrade Gb3 and promote trafficking. This technique cannot be used in patients suffering from the classical form of Fabry disease (Figure 5) (Motabar et al. 2010).

The basic goal of gene therapy development for FD aims at the over-expression of GLA protein in the target organ, efficient secretion, reabsorption by the cells of the different organs via mannose-6-phosphate receptors and eventually degrade the accumulating substrate in the lysosomes. There are phase-1 and -2 clinical trials ongoing for Fabry disease (Domm et al. 2021). There is a promising progress trend for some therapies including long-term follow-up studies for two AAV-based therapies by Sangamo therapeutics (ST-920) and Freeline therapeutics (FLT190) and an *ex vivo* study using lentiviruses by AvroBio (AVR-RD-01). The increasing research in the field is indicative of a gene therapy-based treatment for Fabry disease.

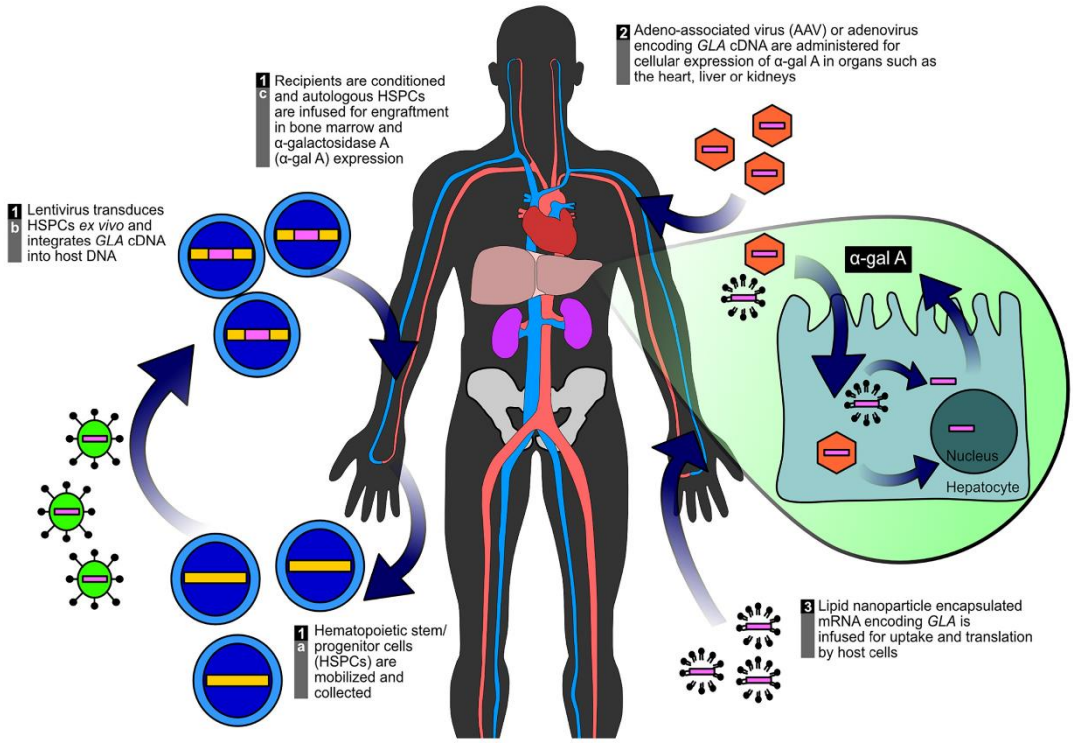

Figure 5. Potential gene-based therapies applied to clinical and preclinical trials for Fabry disease. Domm J M. *et al*. reviewed in his publication the different gene therapy techniques being used for Fabry disease including *in vivo* and *ex vivo* strategies using Adeno-associated virus and Lentiviruses respectively. Non-viral vectors are also being discussed and tested in the clinics. All these gene therapies share a common goal to deliver a therapeutic payload of GLA enzyme to treat Fabry disease.

1.3.5 Fabry mouse models

The deposition of Gb3 and Lyso-Gb3 leads to a gradual systemic response including renal failure, premature myocardial infractions, and keratomas in patients. To study the disease and explore alternative treatments animal models are valuable. For FD, a mouse model widely used was developed by T. Ohshima and their group by gene targeting completely abolishing alpha-galactosidase A activity. Though the phenotype is not severe, and the mouse does not show clinical symptoms, accumulation in lysosomes has been observed at around 5 months of age. This model is being widely used to obtain preclinical data in clinical trials as well (Ohshima, Gary J Murray, et al. 1997). Another mouse model generated by crossing GLA knockout mice with a Gb3 synthase expressing transgenic mice (G3Stg/GLAko) displays phenotypic symptoms like progressive kidney impairment, albuminuria, and much higher Gb3 accumulation in organs and serum. This is a promising model for use in preclinical research, however, is not commercially available (Taguchi et al. 2013).

1.4 Genetic manipulation as a therapeutic tool

1.4.1 Gene therapy

Gene therapy is a promising component of therapeutic medicine for a variety of acquired and inherited diseases like hemophilia, eye disorders, neurodegenerative disorders, and cancers with product approvals in the USA and Europe. Presently there are more than 2500 approved clinical trials that are ongoing around the world which majorly target cancers followed by monogenic diseases and cardiovascular diseases.

Gene therapy is the transfer of genetic material to repair, regulate, add, or delete a genetic sequence to prevent, halt or reverse a pathological process. In the case of monogenic diseases, the genetic material transferred usually refers to a "healthy" variant of the mutated gene. The principle of augmentation of gene therapy in the long-term expression of transferred genes at therapeutic levels is sufficient to revert the hyper/hypo physiological level to normal levels.

AAV-based episomal gene therapy is an emerging field of research and development where a therapeutic gene of interest is delivered to the target cells using AAV as cargo. This infection is exploited by the AAV to transduce the therapeutic gene into the cell's nucleus where it remains as an episome which are small circular DNA molecules that exist independently of the host genome. Post-infection, the transgene is expressed by the cell's machinery transiently. Vector loss due to cell duplication is a major concern leading to loss of efficacy of the treatment, however, liver-directed AAV-based episomal gene therapy has shown success in adults where hepatocyte duplication rate is rather low.

Gene therapy is widely classified based on the mode of administration; *ex vivo* or *in vivo,* and the mode of delivery; viral vectors (Table 4.), or non-viral vectors. When the therapy is executed by extracting defective cells from the patient's body, genetically manipulating them to normal or healthy cells, and then re-infusing them into the patient, an *ex-vivo* procedure is performed. On the other hand, *in vivo,* therapy involves treating the patient by directly administering the corrected gene via local or systemic administration of a vector carrying the therapeutic DNA into the patient's body.

	Adenovirus	Adeno-associated virus	Retrovirus	Lentivirus
Size	~90-100nm	~25nm	~80-100nm	~80-100nm
Genome	dsDNA	ssDNA	ssRNA	ssRNA
Packaging capacity	~8kb- 36kb	~4.7kb	10kb	8kb
Transduction	Dividing and non-dividing cells	Dividing and non-dividing cells	Dividing cells	Dividing and non-dividing cells
Transduction efficiency	High	Moderate	Moderate	Moderate
Integration	Non-integrating	Non-integrating	Integrating	Integrating
Expression	Transient	Transient or stable	Stable	Stable
Immunogenicity	High	Low	Moderate-High	Moderate-High
Gene therapy strategy	*in vivo*	*in vivo*	*ex vivo*	*ex vivo*
Biosafety	BSL-2	BSL-1	BSL-2	BSL-2

Table 4. Viral vectors used in gene-based therapies. Gene transfer for gene-based therapies can be facilitated using viral vectors like Adenovirus, Adeno-associated virus, Lentivirus and Retrovirus. Adeno-associated viruses (AAV) are most commonly used in *in vivo* clinical trials due to their safety profile and packaging capacity, whereas Lentiviruses have shown promising abilities in *ex vivo* gene delivery systems. *BSL=Biosafety level, ds= double-stranded, ss=single-stranded

1.4.1.1 Viral vectors

Retroviral vectors

Retroviruses belong to the *retroviridae* family and were one of the first viral vectors to be used in gene therapy clinical trials. They are lipid-enveloped particles with a single-stranded RNA as their genetic material. The RNA of these vectors is 9Kb to 11Kb in size with long terminal repeats (LTR) at each end flanking the *gag*, *pol*, *env* essential genes required for packaging. The envelope is responsible to interact with the receptors on the target cells thus controlling the host tropism. The target range of these vectors was explored by pseudotyping where the vector binding proteins are engineered to substitute with other unrelated viral strains. Once received by the target cells the RNA genome is reverse transcribed into double-stranded linear DNA which integrates into the host genome. The drawback of using retroviruses as vectors is their random integration which gives rise to the possibility of insertion near oncogenes with the risk of tumorigenesis. Also, these are highly immunogenic and can transduce only dividing cells (Elsner and Bohne 2017).

Lentiviral vectors

Lentiviruses are a genus of the retroviridae family as well derived from HIV. In addition to the retroviridae genes *gag, pol, env* there are two regulatory genes known as tat and rev essential for viral replication and four accessory genes *vif, vpr, vpu, and nef* which are mandatory for *in vivo* pathogenesis and replication. Lentiviruses can infect dividing and non-diving cells and therefore they are highly used in terminally differentiated and stem cells as well. There have been multiple modifications made to the genome of the vector to increase safety however, recently the Self-inactivating (SIN) third-generation lentivirus has proven to be very efficient and safer in clinical trials (Dull et al. 1998) (Miyoshi et al. 1998).

Adenoviral vectors

Adenoviruses have a double-stranded DNA as their genetic material with a capsid that is icosahedral and non-enveloped and a packaging capacity of approximately 35Kb between two inverted terminal repeats (ITRs). However, a second vector known as the helper vector is required to carry the genes required for viral replication. Adenoviruses are highly immunogenic which makes them incompatible with their use in monogenic diseases and *in vivo* therapy, but are good candidates for the production of vaccines (Boussettine et al. 2023).

Adeno-Associated Virus (AAV)

Adeno-associated virus (AAV) was discovered as a contaminant of adenovirus in 1965. This is an emerging luminary in the vector world of gene therapy. AAV is one of the smallest known single-stranded DNA viruses (~4.7kb) with a 22 nm icosahedral capsid, belonging to the parvovirus family. At the termini, AAV has two 145 bp inverted terminal repeats (ITR) flanking the two viral genes rep (replication) and cap (capsid), encoding the structural and non-structural proteins obligatory for virus formation and multiplication. The rep region, through two promoters and alternative splicing, encodes four regulatory proteins; Rep78, Rep68, Rep52, and Rep40, involved in genome replication. The cap gene, has three capsid proteins, VP1 (virion protein 1), VP2, and VP3, with a molecular weight of 87kDa, 72kDa, and 62kDa, respectively in the available in ratio 1:1:10 (Gonçalves 2005b).

These viruses are usually non-pathogenic although a co-infection with a helper virus; usually adenovirus or herpes simplex virus can result in a productive infection. AAV lifecycle also consists of two phases: lytic and lysogenic phases. During infection, if helper genes (from adenovirus or any lentivirus) are available then the lytic pathway is followed. These helper genes from adenovirus (i.e., E1A, E1B, E2A, E4) assist productive infections characterized by genome replication, viral gene expression, and virion production, whereas the herpes virus provides the DNA polymerase and helicases. In the absence of any helper genes, AAV adopts the lysogenic pathway where genome replication and gene expression reduce. The genome establishes latency by integrating chromosome 19

on a 4kb region known as the AAVS1 locus. AAV has 12 serotypes, some of human origin whereas others of non-human origin with diverse tissue tropism. Despite the high seroprevalence of AAV, serotype 2 is the most common in human beings with about 50-80% seropositivity globally (Balakrishnan and Jayandharan 2014). Studies have reported 58.5% and 56% seropositivity in a cohort of 546 Hemophilia A patients and 101 males with Duchenne Muscular Dystrophy (Klamroth et al. 2022) (Verma et al. 2022). Intracellular trafficking of AAV vector is a major rate-limiting step in most cell types and any improvement in the area would directly increase its efficiency as a gene therapy viral vector. The general transduction follows the binding of the virus to a receptor, its endocytosis, intracellular trafficking through the endosomal compartments, escaping from the compartment, trafficking to the nucleus, uncoating, viral genome conversion to double-stranded DNA, and finally expression (Gonçalves, 2005).

1.4.1.2 Non-viral vectors

Non-viral vectors demonstrate much lower immunogenic reactions and toxic effects, the production mechanism is easier and hence they are cheaper to produce as compared to viral vectors and their drawbacks. The progress made in long-term gene expression and biosafety of non-viral vectors has led to increased use in clinical trials in the past decade. However, they are unable to fulfill the ideal vector properties. These vectors are generally used to deliver small DNA (oligodeoxynucleotides), plasmid DNAs, and RNA molecules including siRNAs, miRNAs, ribozymes, and mRNAs. Intracellular delivery is possible by disrupting the membrane barrier of the cell using physical means like electroporation, sonoporation, ultrasound-assisted microbubbles, gene gun, etc. Liposomes have demonstrated enhanced biocompatibility, low immunogenicity, and capability to carry large molecules making them efficient vector candidates. Cationic polymers are another alternative being studied as potential non-viral vectors. Vectors like lipoplexes and polyplexes have demonstrated appreciable results *in vitro* but fail to replicate the same potential in *in vivo* settings (Sarvari et al. 2022).

There is a large number of studies ongoing to explore other non-viral vectors like nanoshells, cell-penetrating peptides, conjugated polymers, sleeping beauty transposon, and SPION (superparamagnetic nanoparticle). Lipid nano particles (LNPs) are a promising vehicle to deliver therapeutics and most recently have been successful to deliver mRNAs for example in the case of the COVID-19 vaccine from Moderna against the coronavirus was approved in 2020. Moreover, antisense oligonucleotides have also seen popularity specially in case of Duchenne muscular dystrophy (DMD) with Exondys51, Vyondys53, and Amondys45 approved in 2016, 2019, and 2021 respectively from Sarepta therapeutics. Tegsedi from Ionis pharmaceuticals and Onpattro from Alnylam were approved in 2018 for Amyloidosis. For the treatment of Transthyretin amyloidosis (ATTR amyloidosis), NTLA-2001 (NCT04601051) is being researched to deliver CRISPR/Cas9 system via LNPs (Gillmore et al. 2021).

1.4.2 Genome editing

With the progressing gene therapy research, genome editing was a breakthrough in the field opening up new endeavors by precise targeting into the genome using engineered and programmable enzymes to manipulate DNA.

1.4.2.1 Understanding double-stranded breaks

The “programmable enzymes” or endonucleases are designed to target a specific genomic region and execute double-strand breaks (DBS), progressively triggering the cell’s repair mechanisms. Based on the stage in the cell cycle, either of the endogenous repair mechanisms can be stimulated: Non-homologous End Joining (NHEJ) or Homology-Directed Repair (HDR) (Figure 6).

Non-homologous end joining or NHEJ machinery can recognize and join diverse DNA, and chromosomes resulting in chromosomal translocations. NHEJ is an efficient but error-prone mechanism since repeated repairs can cause small insertion and deletion mutations at the site of the double-stranded break, denominated INDELs (INsertions-DELetions). These INDELS can lead to a frameshift in the open reading frame of the DNA coding region and eventually loss of function of the gene. For example, Huntington's disease and achondroplasia are gain of function mutations in HTT and FGFR3 genes, respectively, which are actively treated using NHEJ-based therapies. NHEJ-based DNA repair is more frequent since it occurs both in diving and post-mitotic cells throughout the cell's life cycle, predominant during the G1, S, and G2 phases of the cycle (Weterings and Chen 2008).

In contrast, HDR-based repair occurs primarily in the S/G2 phases of the cell cycle. It utilizes a “correct” template with homology to the sequence near the DSB. Homologous recombination (HR) is a cellular mechanism responsible for maintaining genome integrity and stability, and repairs of DSBs, incomplete telomers, and damaged DNA replication forks. In the case of meiosis, the diversity of precursor cells results due to the exchange of information between maternal and paternal alleles, followed by precise segregation of the two homologous chromosomes mediated by HR (Gilles and Averof 2014).

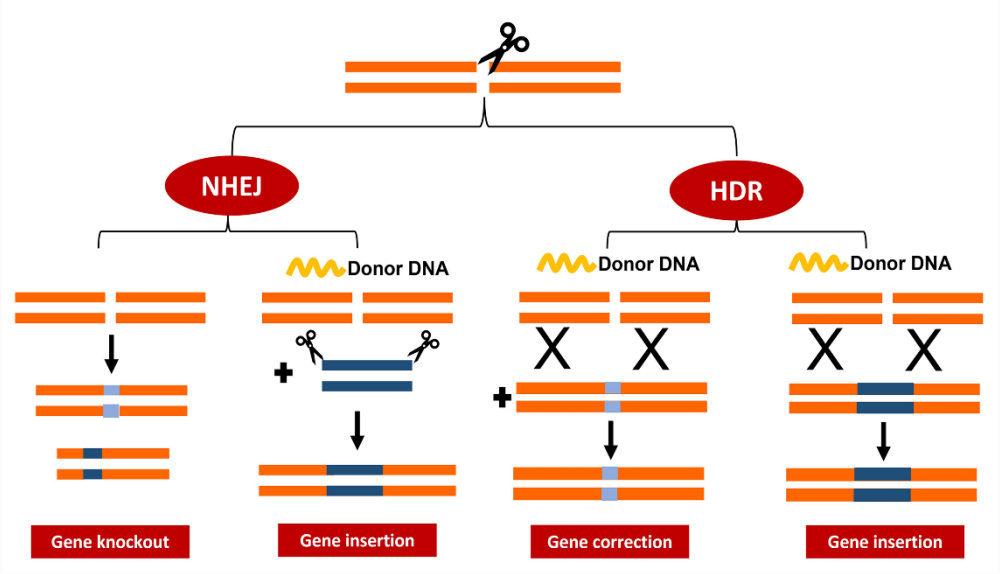

Figure 6. Repairing double-strand break. The cell's repair mechanism approaches the double-strand break with two different mechanisms: non-homologous end joining (NHEJ) or Homologous directed repair (HDR). NHEJ is capable of joining two diverse ends of DNA generating small insertions and deletions (INDELS) whereas, HDR repairs DSBs by homologous recombination (HR) efficiently creating gene insertions in the presence of a donor DNA

1.4.2.2 CRISPR/Cas and other advanced nucleases

Major advancements have taken shape over the years in the field of site-specific genome targeting, especially with the discovery of nucleases and their manipulation for precise and efficient editing. There are four major categories of nucleases; Mega nucleases (MegNs), Transcription Activator-Like Effector Nucleases (TALENs), Zinc-finger Nucleases (ZFNs), and Clustered Regularly Interspaced Short Palindromic Repeats (CRISPR)/ CRISPR-associated system 9 (Cas9) (Figure 7).

Meganucleases (MegNs) are naturally occurring endodeoxyribonucleases translated from the self-splicing elements of the genome. They work by exploiting their molecular function to act as invasive DNA using its endonuclease activity surrounding the introns and invade the coding sequence using its splicing activity. MegNs are regarded as highly specific since they cleave the dsDNA at a specific recognition site of 14-40 bp and can be used for the development of therapies for inherited diseases from nonsense or frameshift mutations. However, the preparation of custom MegNs is complex and inefficient, and the probability to find an enzyme that can target the desired locus is small which makes them challenging to work with (Wang and Doudna 2023).

Zinc-finger nucleases or ZFNs are engineered by joining several zinc-finger domains, the DNA binding domain, and Fok1, the endonuclease domain to create the DSB where each finger domain recognizes 3

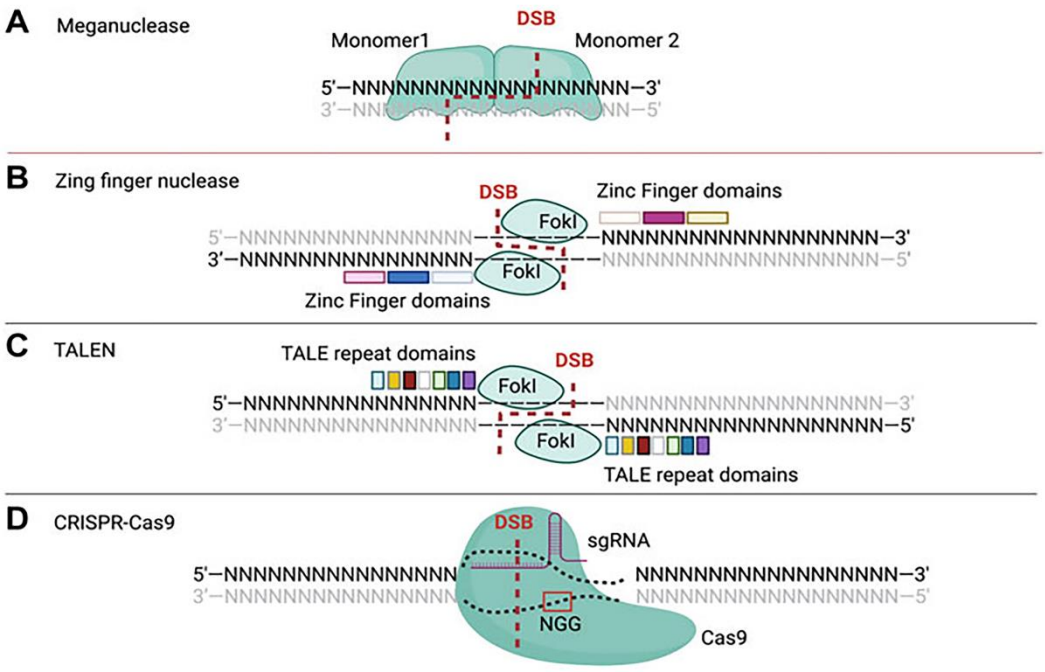

Figure 7. Genome editing nucleases. The figure from Yaoyao Lu *et al*. depicts the major nucleases used to treat genetic disorders using editing techniques. A) Meganucleases (MegN) B) Zinc Finger nucleases C) Transcription Activator-Like Effector Nucleases (TALENS) and D) Clustered Regularly Interspaced Short Palindromic Repeats (CRISPR)/ CRISPR-associated system 9 (Cas9).

bases. Though the pre-existing combinatorial assembly of zinc fingers aids in its designing, the specificity of ZFNs depends on the sequences adjacent to the target sequence in the genome known as "context-dependent specificity" which causes fragmentation and non-specific cleavage (Lu et al. 2022).

Working on improving the limitations faced with ZFNs, TALENs, or Transcription activator-like effector nucleases were developed. Similar in rearrangement, TALENs are made by fusing the FokI restriction endonuclease domain with a DNA binding domain consisting of conserved repeats derived from transcription activator-like effectors or TALE. A TALE is made of a transport signal, a DNA-binding domain with one nucleotide recognition site, and a carboxy-terminal for nuclear localization and transcription activation (Lu et al. 2022).

CRISPR/Cas9 system is the most recent or third-generation gene editing tool first identified in 1987 in the adaptive immune system of *E.Coli* as a defense mechanism that is RNA-based and is involved in the recognition and degradation of parasites. Originally, CRISPR is the foreign genetic material present in the host chromosome in a sequence of repetitive loci separated by stretches of variable sequences called spacers, flanked by Cas9 genes hence, the name Clustered Regularly Interspaced Short Palindromic Repeats. Short sequences from the invading virus/plasmids are incorporated and expressed

in the form of CRISPR-derived RNAs (crRNAs), following which the CRISPR-associates protein or Cas joins the crRNA to form an active endonuclease complex or CRISPR/Cas system. The system's specificity is based on the complementarity between the crRNA and the target viral DNA. This efficient defense system was computationally confirmed to be functional in 40% of sequenced bacteria and 90% of archaea. CRISPR/Cas systems are classified into 2 classes: Class 1 and Class 2, further into 6 types (types I to VI) and several subtypes. CRISPR-Cas9 system of Class 2, type II category is one of the best characterized and utilized in recent research (Makarova et al. 2011).

A ground-breaking study published in 2012 demonstrated that nucleotide-based recognition could generate customizable nuclease for gene editing by the use of the CRISPR system of *Streptococcus pyogenes* involving a Cas9 protein and a combination of crRNA and a Trans-acting antisense RNA (tracRNA) to form a chimeric single guide RNA (sgRNA/gRNA). The 5' end of the sgRNA contains a customizable 20 nucleotide sequence complementary to the target DNA which defines the specificity of the system, whereas the 3' end of the gRNA is the invariable tracRNA which efficiently directs the Cas9 protein to the site-specific DNA target sequence. To increase precision, the interaction of Cas9 and the target DNA is aided by the protospacer adjacent motif (PAM) located downstream of the 20-nucleotide gRNA sequence (Wang and Doudna 2023). Figure 8 represents targeted genome editing using the CRISPR Cas9 system.

Since the development of CRISPR/Cas technology, research was biased towards spCas9 or *Streptococcus pyogenes* Cas9 which is 1368 amino acid and a PAM consisting of NGG nucleotides 3' to the target site. However, Cas9 nucleases from other bacterial species were identified like *Streptococcus thermophilus, Neisseria meningitides,* and *Staphylococcus aureus*. Recently, saCas9 or *Staphylococcus aureus* which recognizes an NNGRRT PAM site, due to its small size (1053 amino acids) which makes it easier to be packaged into an Adeno-associated virus (AAV) and reduces off-targets due to its more complex PAM is proving to be a promising candidate for clinical research (Ran et al. 2015).

1.4.3 Advancements and clinical trials

Currently, the AAV-based gene therapy market blooms with recent approvals. Spark Therapeutic's Luxturna was approved for rare inherited retinal dystrophy in 2017 and Novartis's Zolgensma for Spinal Muscular Dystrophy was approved in 2019. The first gene therapy product Glybera for hereditary lipoprotein lipase deficiency was approved in 2012 however, due it was soon withdrawn due to commercial reasons. In 2022, new therapies with AAV5 were approved for Haemophilia, Roctavian (Blair 2022) for adults with severe hemophilia A by BioMarin and Hemgenix (Sachin Navale et al. 2022) for Haemophilia B from UniQure.

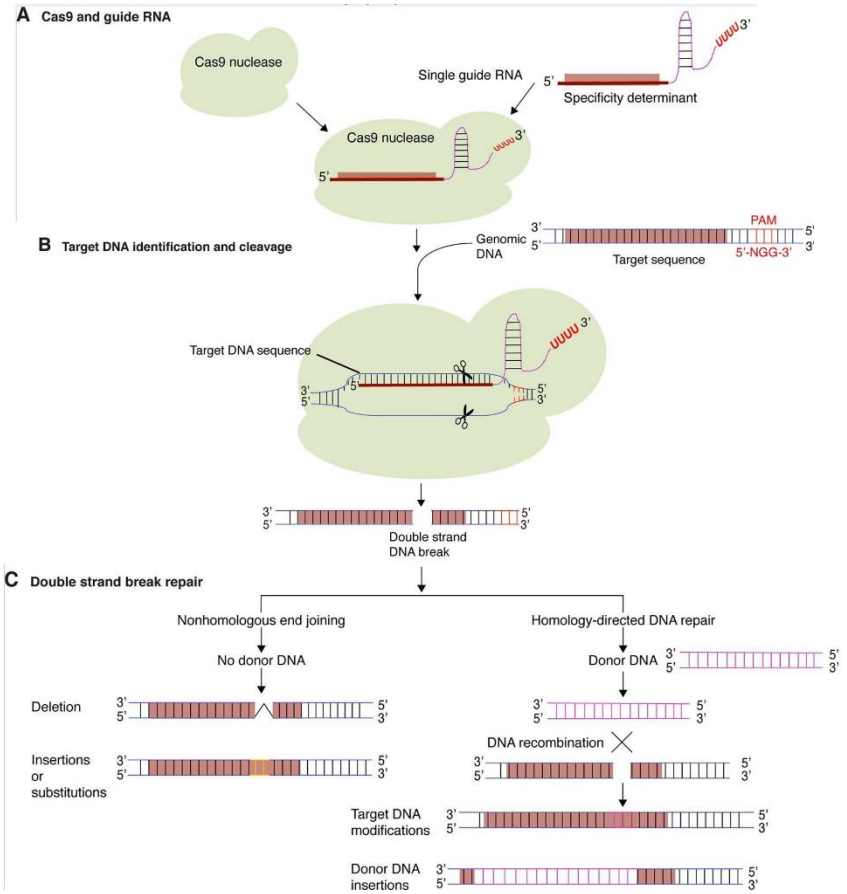

Figure 8. Targeting using CRISPR-Cas9. A) CRISPR-Cas9 system consists of a Cas9 protein and guide RNA which determine target DNA specificity by sequence complementarity. (B) Guide RNA and Cas9 form a complex that cleaves target DNA creating a double-strand DNA break. (C) Cellular DNA repair mechanisms, non-homologous end joining (NHEJ) and homology-directed repair (HDR), repair the double-strand DNA break. In the process, short insertions, deletions, nucleotide substitutions, or gene insertion may occur. (Kaoutar El-Mounadi et.al.,2020)

The discovery of a novel gene editing system has dramatically opened up new opportunities for research and clinical therapy in various fields. Many phase-1 and -2 clinical trials are going on globally using genome editing interventions with CRISPR/Cas technology (Khirallah et al. 2023). Some of them are listed in Table 5. Cancer immunotherapy research has been on a boost since the development of engineered chimeric antigen receptor T cells (CAR-T cells) using the CRISPR-Cas system which has the potential to treat leukemia and lymphomas. CRISPR has also proven to be helpful in the development of human iPSCs (induced pluripotent stem cells) based models for human diseases.

There have been notable improvements to the CRISPR/Cas system as well. Researchers have developed a dead-Cas9 or dCas9 which lacks the DNA cleavage activity but still has the DNA binding activity by introducing two-point mutations (H840A and D10A) into the nuclease domains. CRISPR-dCas9

system's sequence-specific recruitment is being exploited by fusing transcription activators and inhibitors to the dCas9 to activate (CRISPRa) or inhibit (CRISPRi) transcription of target genes, or even fusing fluorescent proteins for genome imaging (Xu and Li 2020).

Base editor systems have been developed to enhance the efficiency of site-directed mutagenesis by coupling cytosine deaminase (cytidine base editor, CBE) or adenosine deaminase (adenine base editor, ABE) with dCas9. This complex is able to introduce point mutations in the target sites of the sgRNA without the need for a double-strand break avoiding the generation of random insertions and deletions. This system is being widely used in cell lines, bacteria, human embryos, and plants for site-directed mutagenesis (Doudna 2020).

Anzalone *et al.* very recently developed prime editing technology consisting of a catalytically impaired Cas9 protein fused with a prime editing guide RNA (pegRNA) encoding the desired edits and the ability to specify target sites and reverse transcriptase (RT). Following the cleavage by Cas9 at the target site,

Disease	Clinical trial	Intervention	Mechanism	Status
Severe sickle cell disease	NCT05329649	CTX001	CRISPR/Cas9-mediated BCL11A disruption in autologous CD34+ HSPCs	Phase 3
Sickle cell disease	NCT04819841	GPH101	CRISPR/Cas9-mediated HBB correction in autologous CD34+ HSPCs	Phase 1/2
Hereditary angioedema	NCT05120830	NTLA-2002	CRISPR/Cas9-mediated KLKB1 knockout delivered by LNPs; intravenous injection; *in vivo*	Phase 1/2
COVID-19 respiratory infection	NCT04990557	PD1 and ACE2-knockout T-cells	CRISPR/Cas9-mediated knockout of PD1 and ACE2 in T cells to induce long-term immunity against COVID-19; ex vivo	Phase 1/2
Severe sickle cell disease	NCT04774536	CRISPR_SCD001	CRISPR/Cas9-mediated HBB correction in CD34+ HSPCs; *ex vivo*	Phase 1/2
Acute myeloid leukemia	NCT05066165	NTLA-5001	CRISPR/Cas9-edited autologous TCR-T cells targeting WT1	Phase 1/2
β-Thalassemia	NCT04925206	ET-01	CRISPR/Cas9-mediated BCL11A disruption in CD34+ HSPCs	Phase 1
B cell acute lymphoblastic leukemia	NCT04557436	PBLTT52CAR19	CRISPR/Cas9-edited CD52 and TRAC CAR-T cells targeting CD19	Phase 1
Metastatic gastrointestinal epithelial cancer	NCT04426669	Biological: TILs Drugs: cyclophosphamide, fludarabine, aldesleukin	CRISPR/Cas9-mediated CISH disruption in TILs	Phase 1/2
Relapsed or refractory B cell non-Hodgkin lymphoma	NCT04637763	Genetic: CB-010 Drug:cyclophosphamide Drug:fludarabine	CRISPR/Cas9 gene-edited allogeneic CAR-T cells targeting CD19	Phase 1
Refractory herpetic viral keratitis	NCT04560790	BD111	CRISPR/Cas9 mRNA-mediated HSV-1 genome disruption; corneal injection; *in vivo*	na
Hereditary transthyretin amyloidosis	NCT04601051	NTLA-2001	CRISPR/Cas9-mediated TTR knockout delivered by LNPs; intravenous injection; in vivo	Phase 1
Leber congenital amaurosis 10-IVS26	NCT03872479	EDIT-101	CRISPR/Cas9-mediated removal of CEP290 mutation delivered by AAV; subretinal injection; *in vivo*	Phase 1/2
Relapsed or refractory B cell malignancies	NCT04035434	CTX110	CRISPR/Cas9 gene-edited allogeneic CAR-T cells targeting CD19; *ex vivo*	Phase 1
Relapsed or refractory CD19+ leukemia or lymphoma	NCT04037566	Genetic: XYF19 CAR-T cells Drug: cyclophosphamide Drug: fludarabine	CRISPR/Cas9-edited autologous CD19 CAR-T cells with HPK1 disruption	Phase 1
Relapsed or refractory leukemia and lymphoma	NCT03398967	Universal dual specificity CD19 and CD20 or CD22 CAR-T cells	Universal CRISPR/Cas9 gene-edited allogeneic CAR-T cells targeting CD19 and CD20 or CD22; *ex vivo*	Phase 1/2
Mesothelin-positive multiple solid tumors	NCT03545815	Anti-mesothelin CAR-T cells	CRISPR/Cas9-edited PD1- and TCR-knockout mesothelin-directed CAR-T cells	Phase 1

*Last updated in April 2023 from *Clinicaltrials.gov*

Table 5. Clinical trials using CRISPR/Cas genome editing interventions to treat inherited genetic disorders. The list is a database of recent clinical trials for genetic disorders being approached with CRISPR/Cas technology. *Clinicaltrial.gov*

the RT uses pegRNA as a template to write new genetic information using reverse transcription. Prime editing can mediate deletions, insertions, and all base substitutions without the need for a double-strand break or donor DNA template. This breakthrough has expanded the scope of genome editing accurately and efficiently, however, more research is yet required (Anzalone et al. 2019).

CRISPR/Cas technology is now widely being used for the development of cell and animal models of human diseases; it is also rapidly being exploited for molecular diagnostic technology and is proving to be inexpensive and accessible. Feng Zhang *et al.* developed SHERLOCK (Specific High Sensitivity Enzymatic Reporter UnLOCKing) (Kellner et al. 2019): a Cas13a-based *in vitro* nucleic acid detection platform. Cas13 can cleave nearby non-target RNAs after having been activated by cleaving the target-specific sequence, an activity known as 'collateral cleavage'. Researchers are using this technology to detect viruses and pathogenic bacteria and identify tumor DNA mutations. Similarly, Doudna *et al.* developed DETECTR (DNA endonuclease targeted CRISPR *trans* reporter) based on Cas12 enzyme also possessing collateral cleavage activity which is being used to detect cervical cancer-associated HPV in cell lines and clinical patient samples (Petri and Pattanayak 2018).

These advancements and new technologies have paved the way for clinical research for genetically inherited disorders.

1.5 Liver-directed gene targeting

1.5.1 AAV transduction in hepatocytes

The liver is the largest and most vital organ maintaining the metabolism of the human body. The cells of the liver or hepatocyte are parenchymal in nature and makeup about 67% of the residing liver cells (Figure 9) (Azparren-Angulo et al. 2021). Important factors involved in hepatocyte-directed gene transfer are the successful passage through the hepatocyte fenestrae and the long-term expression of the transgene DNA. Considering that the diameter of a healthy human liver fenestrae is 107 nm, AAV vectors can easily facilitate this journey.

Referring to the successful gene therapy treatment in hemophilia patients, it can be implied that hepatocytes can be easily transduced with AAV ensuring the safe and long-term expression of the transgene. Recent studies demonstrate that even though AAV2 was earlier considered the optimum choice for liver transduction, serotype 8 (AAV8) has shown better results in rescuing the phenotype in genetic disease (Zhao et al. 2023). Some novel serotypes like LK03 and NP59 and also AAV3B have reached superior transduction efficiency in mouse and human hepatocytes. Using a liver-restricted promoter has also been studied to decrease the immune response generated due to the reduced

expression of the transgene in antigen-presenting cells. Therefore, AAV-mediated liver-directed gene transfer has the potential to remedy hepatic disorders, mainly inborn errors of metabolism. However, a major loophole is the loss of AAV viral particles due to hepatocyte duplication when treating pediatric patients which is vital in early-onset disorders (Zabaleta et al. 2023).

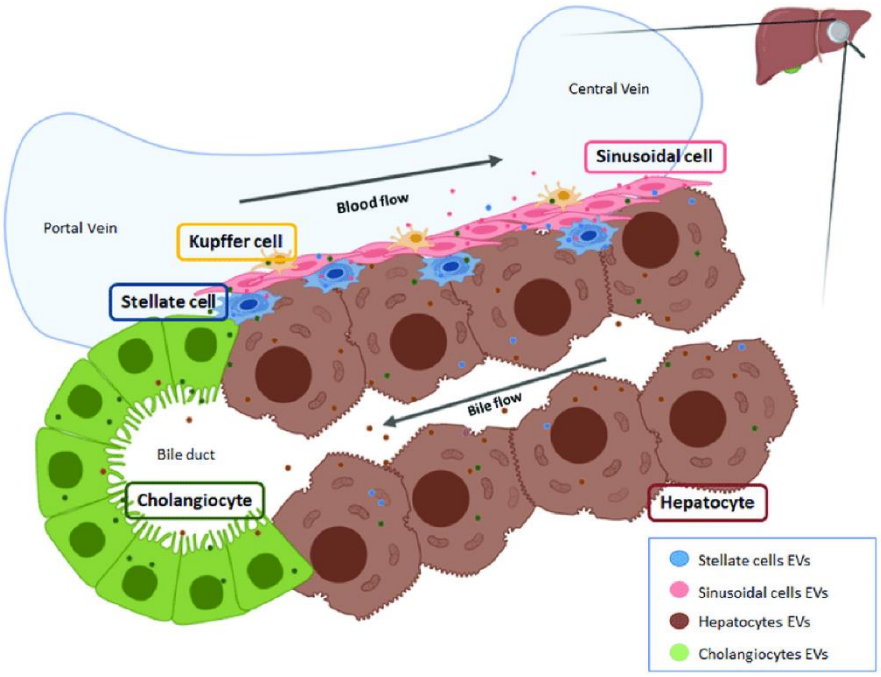

Figure 9. The organisation of human liver cells. The figure by Maria A. A. *et al.* defines the liver architecture and its cells. The liver is composed of sinusoidal cells, Kupffer cells, Stellate cells and Hepatocytes occupying ~70% of the overall liver cell population.

Liver-directed AAV gene therapy has evolved to be safe and efficient, however, the major obstacle remains the vector DNA loss associated with hepatocyte proliferation in cases of liver damage and pediatric settings. AAV episomes are lost with the growing liver due to the duplication of the hepatocytes and eventually the efficacy of the treatment is significantly reduced ultimately raising the need for re-administration, an option that is not feasible due to the production of anti-AAV antibodies raised after the first AAV administration (Cunningham et al. 2008). Several ongoing studies are determined to resolve the issues related to the re-administration of AAV vectors. An alternate approach to this problem is to modify the genome permanently, using AAV vectors to integrate the therapeutic cDNA into the target locus. The integrated cells with the therapeutic cDNA divide and express the therapeutic protein, maintaining the efficacy of the treatment, and eliminating the need for re-administration.

1.5.2 GeneRide™ Technology

In a study published in 2015 by the team of Prof. Mark. Kay, at Stanford, recombinant AAV (rAAV) was used to deliver a promoterless construct containing the human coagulation factor 9 cDNA, with a preceding P2A peptide, flanked by mouse albumin homology arms to hemophilia B mice, in the absence of nucleases. This construct targets the albumin gene in the liver, as a "safe harbor locus", using the two homology arms at each end. This strategy facilitates the use of the endogenous albumin promoter for the production of both albumin itself and coagulation factor 9. Even though the transgene and the albumin are fused at the RNA and DNA levels, the P2A peptide enables ribosomal skipping and results in the production of separate proteins for albumin and Factor 9. The strategy also denominated Gene Ride, is expected to integrate into at least 0.5% of hepatocytes with efficient ribosomal skipping (Figure 10) (A Barzel et al. 2015). In a study published in 2017, the albumin locus of a Crigler-Najjar syndrome type I (CNSI) mouse model was targeted with a promoterless therapeutic cDNA which led to complete rescue of the neonatal lethality and a long-term stable reduction in plasma bilirubin levels (Porro et al. 2017). In order to increase the recombination of the donor vector, the Gene Ride technology was coupled with CRISPR/Cas9 system which increased the targeting efficiency by 26-folds with EGFP reporter cDNA. When applied to Crigler-Najjar mice targeting the UGT1A1 cDNA in the albumin locus with the aid of CRISPR technology corrected the phenotype completely with a 90-fold increase in recombination rate (De Caneva, Porro, Bortolussi, Sola, Lisjak, Barzel, Giacca, Mark A Kay, et al. 2019).

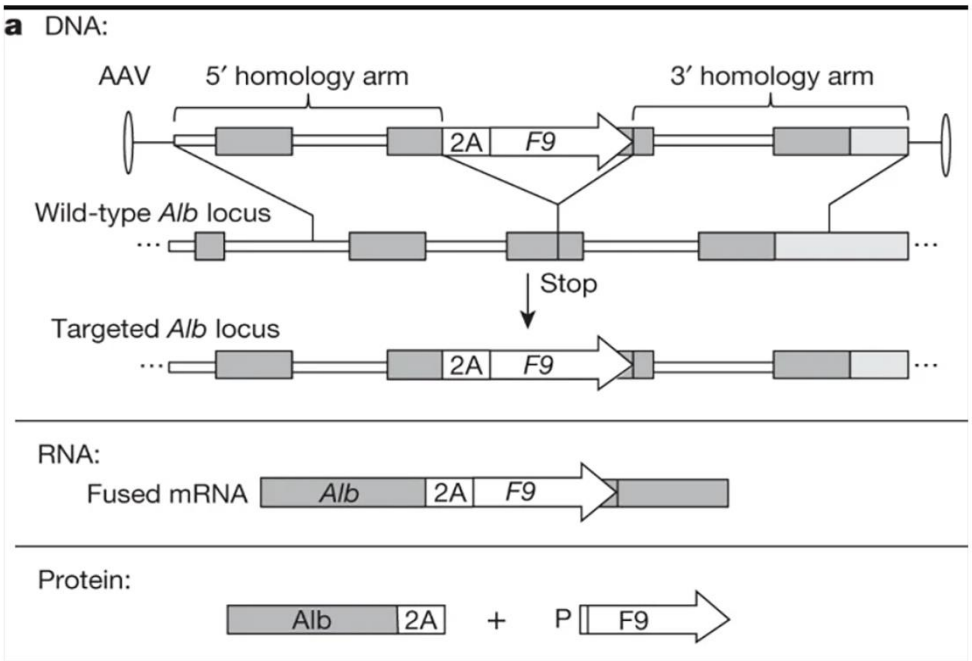

Figure 10. Schematic of Gene Ride™ technology. The schematic is the original diagram from "Promoterless gene targeting without nucleases ameliorates haemophilia B in mice" by Barzel *et al.* where Gene ride was used to target haemophilia B.

1.5.3 Nuclease-free approach to gene targeting

Nucleases have shown their potential in gene targeting by increasing HR (homologous recombination) rate. However, they came in with a number of safety issues like off-target activity, transactivation of oncogenes, pre-existing immunity against the nucleases, and toxicity. An approach using a donor vector containing albumin homology arms without nucleases is the next challenge. Various studies have shown the effect of chemical compounds and small molecules on the rate of homologous recombination to achieve better therapeutic efficiency. For example, the small-molecule RS-1 was found to enhance the homologous recombination activity of hRAD51, a protein that carries out the central steps of homologous recombination (Jayathilaka et al. 2008). In another recent study, a series of FDA-approved compounds were tested [i.e., mTOR inhibitor (Torin-1), proteasome inhibitor (MG132), HDAC inhibitors (Trichostatin A, FK228), topoisomerase inhibitor (Teniposide), and ribonucleotide reductase (RNR) inhibitors] concluding that a drug called fludarabine, which is an RNR enzyme inhibitor, was able to increase rAAV homologous recombination rate *in vivo* (Tsuji et al. 2022). The safety study revealed no toxic side effects and also precise integration into the albumin locus using the GeneRide™ construct. It is theorized that fludarabine works in non-dividing cells by antagonizing basal levels of the DNA repair mechanism also benefitting from its transient presence in the cells. The long-term effects of this drug are yet to be studied. Nevertheless, it can prove to be a promising tool for higher rates of recombination.

This project aims at the development of a therapeutic approach based on the genetic modification of hepatocytes to permanently express a human GLA enzyme. It employs the GeneRide™ technique to deliver the *hGLA* cDNA into the albumin locus, exploiting the use of its endogenous strong and liver-specific promoter. This strategy will be applied in Fabry knockout mice to rescue the diseased phenotype. The rate of HDR will be enhanced using the SaCas9 nuclease, however, to avoid the risks of its potential side effects, a nuclease-free approach using an HDR-enhancer drug will be tested in parallel. This compound, fludarabine, has been proven to significantly increase the recombination rate. As the principal end-point assessment, GLA enzyme activity will be measured and the reduction in Gb3 accumulation will be monitored in the kidney, heart, and liver to test the efficiency of the two strategies to revert the phenotype to wild-type levels (Figure 11).

As an evaluation of this therapy with the currently available treatments for FD, ERT-treated Fabry mice will be used as control. In order to support the clinical translation of this potential therapy, the strategy will be tested in a human-like environment *in vitro* and *in vivo*. Donor constructs with human albumin homology arms with the *hGLA* and *EGFP* cDNAs will be tested in human cell lines like HuH7 and primary cultures of human hepatocytes. Furthermore, the *in vivo* proof-of-principle will be obtained by treating chimeric mice with the liver repopulated with human hepatocytes with the EGFP transgene. In this work, we aim to develop an alternative, cost-effective, treatment, that can be potentially applied to

Fabry patients. With this strategy, a single treatment would be enough to restore the diseased phenotype, but importantly, it can be applied to different disease-causing mutations and can be also implemented to cure other LSD. Therefore, we will evaluate the therapeutic potential of this treatment, considering its safety profile.

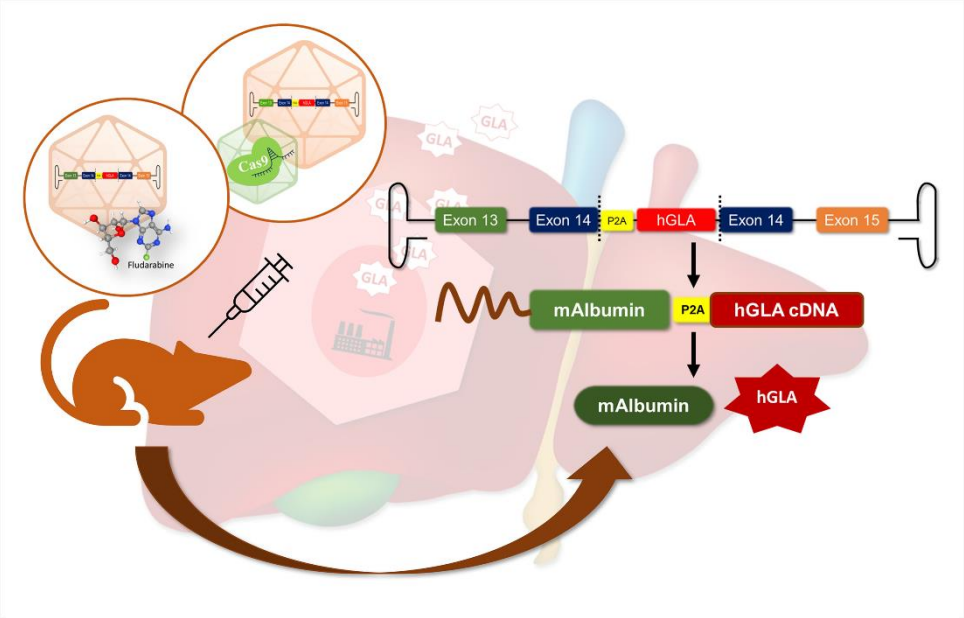

Figure 11. Liver-directed gene targeting as a potential therapy for Fabry disease. The schematic demonstrates the strategy to treat Fabry disease by exploiting the Gene ride technology incorporating the *hGLA* cDNA. CRISPR/Cas9 was coupled with the Donor AAV to increase the rate of recombination, however, the use of Fludarabine drug with the AAV vector holds promising evidence of a safer and more efficient one-shot therapy for FD.

Aims

The main aim of this study is to develop potential therapeutic treatments targeting late-onset and early-onset Fabry disease irrespective of the disease-causing mutation, using liver-specific AAV-based episomal gene therapy and integrative genome editing tools.

To achieve this goal, it is essential to gather preliminary data in C57BL/6 WT mice by:

- Studying the association of liver-directed episomal and integrative AAV-based therapies with age to select an optimum postnatal age for AAV delivery
- Constructing an advanced codon-optimized version of the human GLA gene to achieve optimum expression and enzyme activity

For the assessment of AAV-based therapy for late-onset FD in juvenile Fabry KO mice, it will be necessary to:

- Perform a dose-response experiment to test the episomal AAV vector strategy
- Evaluate the integrative genome editing vector coupled with CRISPR/Cas9 system
- Evaluate the nuclease-free integrative genome editing approach with fludarabine, a drug that increases gene targeting rate

Whereas, in order to assess the AAV integrative genome editing strategy for the early-onset FD in neonatal mice, it will be necessary to:

- Study the dose-response of integrative genome editing vector coupled with CRISPR/Cas9 in neonate Fabry KO mice
- Optimization of the fludarabine dose in C57BL/6 WT neonatal mice

The clinical potential of the integrative strategy will be tested in human primary hepatocytes and humanized mice by generating an AAV vector containing human albumin homology arms. The rationale behind these aims is to permanently constrain the hepatocytes to produce *hGLA* and convert the liver into a biofactory of *hGLA* production avoiding the need for vector re-administration and reducing the elevated costs of existing standard treatments for FD including enzyme replacement therapy.

Materials and methods

3.1 Construction and preparation of plasmids and AAV vectors

3.1.1 Codon-optimization of human GLA gene

The human mRNA transcript 201 sequence (*hGLA* WT) was extracted from the NCBI database. Codon optimization was done using different online tools using different optimization algorithms (IDT Codon Optimization Tool, JCAT Java Codon Adaptation Tool, COOL Codon Optimization Online by the National University of Singapore). GC content was registered using ENDMEMO GC content calculator, CpG Islands were identified by EMBOSS CPG PLOT by EMBL-EBI, and Cryptic Splice Sites were identified using Splice Site Prediction by Neural Network at Fruitfly.org. Further, the four codon-optimized sequences obtained were manually edited to reduce splice site score, and base modification to avoid additional Open reading Frames and CpG Islands. To enable cloning, a Kozak sequence was added at the 5' end (5 GCCGCCACC 3'). A SalI Site was added at the 5' end and a NheI+ EcoRI site was added at the 3' end of the GLA sequences. All four codon-optimized sequences along with wild-type sequences (hGLA_WT, hGLA_CO01, hGLA_CO02, hGLA_CO03, and hGLA_CO04) were synthesized by Genscript and cloned in the pUC57-Kana plasmid at the SalI and NheI sites.

3.1.2 Plasmid construction

Episomal hGLA plasmids (pSMD2_hGLA WT/CO)

All the codon-optimized cDNA were cloned into the pSMD2 vector containing the alpha-1-antitrypsin (hAAT), liver-specific, promoter, and the apolipoprotein E (ApoE) enhancer. The hGLA_WT and codon-optimized constructs were inserted using SalI and NheI restriction sites into the pSMD2 episomal AAV ITRs containing vectors.

Integrative mALB arms hGLA/ EGFP plasmids (pAB hGLA_WT/CO or pAB288-ALB-EGFP)

The hGLA_WT and hGLA_CO02 cDNAs were inserted into a donor vector using SalI and NheI restriction sites (pAB288). The pAB288 vector contained a P2A peptide flanked by mouse albumin homology arms and AAV ITRs at both ends. The vector had a modified PAM site to facilitate genome editing using nucleases. The modified version of the pAB288 vector was generated by mutating the PAM recognition site as described previously.

Integrative hALB arms hGLA plasmids (pAB hALB Hap1/Hap2_EGFP)

Two albumin homology arms containing constructs were created with the SNPs at the positions mentioned in Table 6 corresponding to haplotype 1 and haplotype 2. The right homology arm (1401

base pair) starts at the stop codon in exon 14 and ends with the locus whereas the left arm corresponds to 1302 bases upstream of the latter. A 2A peptide and EGFP transgene sequences were added upstream to the stop codon in the exon 14, flanked by the two homology arms.

Guide RNA and saCas9 plasmids (pX602-sgRNA-Cas9/ pX602-hsgRNA)

The sgRNA used to target the mouse albumin gene was previously constructed based on (De Caneva et al., 2019). In the case of the human albumin targeting CRISPR/Cas9 system, human single guide RNA (sgRNA) was designed based on the saCas9 PAM (NNGRRT) sequence identified in the genomic region flanking the albumin stop codon located in exon 14 of the human albumin gene. The PAM region was modified to TTAAAC. The guide RNA oligonucleotide was cloned into pX602 plasmid encoding saCas9 under the transcriptional control of thyroid-binding globulin (TBG).

Original PAM: TTAAAC

Modified PAM: TTAAAC

Guide RNA: 5' AGCATCTCAGGTAACTATATT 3'

3.1.3 Plasmid preparation

After the plasmids were cloned, XL10 Gold ultracompetent bacterial cells were used for transformation. 50µl cells were added to the ligation reaction and incubated in ice for 30 minutes. The cells were heat-shocked at 42°C for 45 seconds and placed on ice immediately for 2 minutes. Bacteria were recovered by adding 200µl LB medium followed by incubation for 1 hour at 37°C on a shaker. Cells were later plated on appropriate antibiotic-containing agarose plates and incubated overnight at 37°C. Isolated colonies were picked to perform colony PCR by amplifying cloned regions in the plasmid, followed by verification of amplicon size on an agarose gel. After identifying the positive clones the corresponding colony was used to inoculate the primary culture in LB broth containing antibiotic. This culture was used for a miniprep or for inoculation of a secondary culture with 400ml antibiotic containing LB broth which was incubated overnight at 37°C in a shaking incubator. This bacterial culture was used for plasmid isolation at three different scales depending on the requirement (5ml for miniprep, 50ml for midiprep and, 400ml for megaprep). The plasmids were isolated from this bacterial culture on different scales using Wizard® Plus SV Minipreps DNA Purification Systems (Promega Cat#A1330) for small-scale (5ml), NucleoBond Xtra Midi kit for transfection-grade plasmid DNA (Macherey-Nagel Cat#740410.50) for medium-scale up to 50ml and NucleoBond Xtra Maxi kit for transfection-grade plasmid DNA (Macherey-Nagel Cat# 740414.1) for large-scale up to 400ml culture. The plasmid isolation was carried out according to the manufacturer's instructions. The DNA was quantified using NanoDrop™. The plasmids were verified by restriction digestion using restriction endonucleases (from New England Biolabs) and validated by Sanger sequencing (Eurofins Genomics). All the plasmid DNA was stored at -20°C.

3.1.4 rAAV vector production

All AAV stocks were prepared by AAV Vector Unit at ICGEB, Trieste. Serotype AAV8 was used for all the preparations of episomal vectors and integrative vectors containing mouse albumin homology arms. AAV LK03 serotype was used for the preparation of an integrative vector containing human albumin homology arms and the corresponding saCas9-guide RNA-containing vector.

3.2 Cell culture

3.2.1 Cell maintenance

HuH7 cells were maintained in Dulbecco's Modified Eagle Medium (DMEM) with 10% of Fetal Bovine Serum (FBS) and antibiotics at 37°C in 10cm^2 cell culture-safe dishes. Cells were passaged at 80% confluency by removing the existing medium. PBS was added to the cells to wash any leftover remains of the medium. After the PBS was discarded 3ml 1x trypsin was added to the cells and incubated for 5 minutes. The trypsin was deactivated by adding a fresh medium to collect the cells in a 15ml tube. The tube was centrifuged at 5000rpm for 5 minutes at room temperature. The supernatant was discarded, and the pellet was resuspended in a cell culture medium and plated in 10cm^2 cell culture-safe dishes (1:10) until confluent.

3.2.2 Plasmid transfection

Transient transfection was performed using Lipofectamine 2000 reagent (Lipofectamine™ 2000 Transfection Reagent; Cat# 11668019; Invitrogen). HuH7 cells were plated on a 12-well plate to reach 70-80 % confluency at the time of transfection. According to the manufacturer's instruction, two solutions were prepared, sol#A containing Lipo2000 reagent diluted in OptiMEM, and sol#B constituted of the DNA diluted in OptiMEM. For transfection mix A and B were mixed and incubated for 5 minutes at room temperature. The growth medium in the cells was replaced by the transfection mix. DMEM growth medium was added 4-6 hours post-transfection. cells were incubated at 37°C for 48 hours.

3.2.3 AAV Transduction

The efficiency of human albumin arms containing vectors AAVLK03_pAB_hALB_Hap1/Hap2_EGFP was tested by *in vitro* transduction. HuH7 cells were seeded in a 96-well plate on day 0 such as to accommodate triplicates for the following conditions: Donor Hap1/Hap2, Donor Hap1/Hap2+Fludarabine, and Donor Hap1/Hap2+Cas9. Cells were treated with Fludarabine on day 1 by replacing the growth medium with fresh DMEM containing 100µM

fludarabine. Drug-treated cells were incubated for 16-18 hours. On day 2, Transduction with AAV vectors was performed by diluting AAV vectors at 500,000 MOI in OptiMEM. The existing media in the cells with and without the drug was replaced with AAV containing OptiMEM. In the case of Donor vector+Cas9 treatment, AAVLK03_px602_hsgRNA and AAV donor vector were diluted (1:5) in OptiMEM together at 100,000MOI and 500,000MOI respectively, and added to the cells. Fresh DMEM+10% FBS with antibiotics was added to the cells 4 hours post-transduction. The cells were incubated for 72 hours at 37°C. Once 100% confluency was achieved, the cells were trypsinized, collected, pooled together, and plated into 24 well plate to provide a larger surface area to expand. Once confluency was obtained after 72 hours in the 24-well plate, the cells were collected and plated in a 12-well plate. The cells were allowed to expand until they reached 100% confluency in a $10cm^2$ dish. The transduced cells and mock untreated cells were harvested for analysis.

3.3 Animals

3.3.1 Murine maintenance

All the animals were housed and handled according to the institutional guidelines and the Italian Ministry of Health in the ICGEB bio-experimental facility in Trieste. C57BL/6 WT and Fabry KO mice were maintained in a temperature-controlled environment with 12/12 hours of light/dark cycles and received a standard chow diet and water *ad libitum.* Fabry KO mice or B6;129-Gla^{tm1Kul}/J (Strain #003535) were bought from Jackson laboratory and were housed in ICGEB bio-experimental facility. Hemizygous males and homozygous females were used for mating to generate hemizygous males for experimentation.

3.3.2 Genotyping

Fabry KO mice were genotyped according to the protocol provided by Jackson's laboratory. Ears were marked for mice identification and the tip of the tails were cut and harvested. Genomic DNA was extracted using KAPA2G Fast Genotyping Mix (Roche cat#KK5121). Approximately 0.5cm biopsies were incubated in 50µl of extraction mix containing 5µl of Kapa Express Extract buffer, 0.5µl of Kapa Express Extract enzyme, and 44.5µl of water. After a lysis incubation for 20 minutes at 70°C, a 5 minutes incubation at 95°C was performed to inactivate the enzyme. The extract was diluted 10-fold with 10 mM Tris-HCl (pH 8.0–8.5). Genotyping was done by amplifying the genomic region of human GLA exon 3 using a touchdown PCR reaction using 5x DNA polymerase reaction buffer, 0.25-unit GoTaq Flexi DNA polymerase, 25mM MgCl2, 5mM dNTPs, 100ng/µl primers (Table 7), water and, genomic DNA. The PCR protocol was designed with the initial denaturation at 94°C for 3 minutes, and 10 cycles of 94°C for 30 seconds, 65°C for 30 seconds with a touchdown of -0.5°C and 68°C for 30

seconds. Followed by 23 cycles of 94°C for 30 seconds, 62°C for 30 seconds, 72°C for 30 seconds. A final elongation at 72°C for 7 minutes was done before reaction cool down at 4°C. The bands corresponding to wild-type (295bp), hemizygotes/mutant (202bp), and heterozygotes (295bp+202bp) were identified by running the PCR product on a 2% agarose gel.

Primers used for Fabry KO genotyping	
Primer name	**Sequence 5'→ 3'**
oIMR5947_common	AGG TCC ACA GCA AAG GAT TG
oIMR5948_WT REV	GCA AGT TGC CCT CTG ACT TC
oIMR7415_MUT REV	GCC AGA GGC CAC TTG TGT AG

Table 6. Primers for Fabry KO genotyping

3.3.3 Animal treatments

AAV treatments

AAV viral vector treatment was done intravenously via the retro-orbital route of injections dosed as AAV viral genomes per weight of the animal (vg/kg) in all cases by anesthetizing animals with isoflurane. The study in C57BL/6 WT animals was done by treating males at postnatal days P1, P5. P10, P15, P20, P30. All the animals were sacrificed at P60. C57BL/6 WT neonatal male mice were also treated at P5 to test the human albumin arms containing integrative vectors. These animals were sacrificed two weeks post-treatment at P15. Untreated wild-type animals were used as controls. The liver was harvested at sacrifice for molecular analysis and the right lobe of the liver was collected in 4% PFA (Paraformaldehyde) solution for immunofluorescence analysis. The study in Fabry KO (B6;129-Gla^{tm1Kul}/J) juvenile and neonatal animals was done by treating hemizygous males at P30 and P5 respectively. Untreated age-matched B6;129sf2/J and B6;129-Gla^{tm1Kul}/J were used as wild-type and mutant controls. All the experiments in Fabry mice were terminated at 5 months of age (P150) by sacrificing the animal and harvesting the liver, kidneys, and heart. The tissues were snap-frozen and later crushed using mortar-pistol into homogenous powder and stored at -80°C until further use. Blood was collected at intermediate time points from the submandibular (facial) vein in 0.5M EDTA by anesthetizing animals (isoflurane). Plasma was isolated from the collected blood by centrifugation at 3000 rpm for 15 minutes at room temperature. Plasma was stored at -80°C until further use.

Fludarabine treatment

Fludarabine treatment was done in Fabry KO by treating P30 male mice intraperitoneally at 125mg/kg drug (total 375mg/kg) three times a day with an interval of 3-4 hours for three consecutive days. This treatment was coupled with a single AAV retro-orbital injection on day one preferably between the first and second dose. The animals were incubated and sacrificed as mentioned above.

3.4 Nucleic acid and protein extraction

3.4.1 Genomic DNA extraction

Wizard® SV Genomic DNA purification System (Promega Cat# A2361) was used to extract genomic DNA from murine liver powder homogenates according to the manufacturer's instructions. 25mg tissue was incubated with lysis buffer (200µl of Nucleic Solution, 50µl of EDTA, 5µl of RNAse and 20µl of Proteinase K) over night at 55°C. Samples were mixed by vortexing post-incubation and centrifuged for 20 minutes at 13,000 rcf. The supernatant was collected, mixed with 250µl of Wizard® SV lysis buffer in a new 1.5ml tube, and incubated at room temperature for 5 minutes. The lysate was transferred to Wizard® SV mini-column and centrifuged at 13,000 rcf for 2 minutes. The flow through in the collection tube was discarded and the column was washed with column wash solution at 13,000 rcf for 1 minute, this step was repeated three times before a dry spin for 2 minutes. The DNA was eluted with Nuclease-free water by incubating for 2 minutes at room temperature followed by collection in a fresh 1.5 ml tube by centrifugation at 13,000 rcf for 1 minute. The DNA extracted was quantified using NanoDrop™.

3.4.2 RNA extraction and reverse transcription

RNA was isolated using a NucleoZOL solution from Macherey-Nagel. For murine livers, 500µl NucleoZOL was used for 50mg tissue homogenate, whereas in the case of cells, 1ml NucleoZOL per $10cm^2$ cell culture dish was used after removing the growth medium followed by the collection of cells in a 1.5ml tube. 400µl water per 1ml NucleoZOL was added and vigorously shaken for 15 seconds at room temperature and then incubated for another 15 minutes followed by centrifugation at 12,000 rcf for 15 minutes. The supernatant containing the solubilized RNA was collected leaving a small volume of DNA/protein/polysaccharides containing liquid above the pellet in a 1.5ml tube. Isopropanol (500µl/500µl supernatant) was added to the supernatant and incubated at room temperature for 10 minutes and then centrifugation at 12,000 rcf for 10 minutes. The supernatant was discarded, and a white RNA pellet was observed. The pellet was washed using 500µl of 75% ethanol by centrifuging at 8000 rcf for 3 minutes. The pellet was partially dried after the removal of the ethanol and later dissolved in nuclease-free water. The RNA extracted was quantified using NanoDrop™.

About 1µg of total RNA was reverse-transcribed using M-MLV reverse transcriptase (Invitrogen, Carlsbad, CA, United States) following the manufacturer's instructions. The RT-reactions were conducted in a volume of 12µl containing 1µg of total RNA, 1µl of 10mM dNTPs mix (10mM of each dNTP), 5µl of oligo dT (0.1µg/µl) and, water to a volume of 12µl.
Mixes were heated at 65°C for 5 minutes and then chilled on ice. Thereafter, 4µl of 5x First-Strand buffer and 2µl of 0.1M DTT were added to the mix and incubated for 2 minutes at 37°C, followed by

the addition of 1µl of M-MLV RT (200 units). The RT reaction was incubated for 1 hour at 37 °C. The enzyme was heat-inactivated for 15 minutes at 70 °C. cDNA was stored at -20°C.

3.4.3 Protein extraction

Whole livers were harvested, reduced to powder using a mortar pistol with liquid nitrogen, and stored at -80°C. Around 20-25mg of liver powder was homogenized using a mechanical homogenizer (IKA ULTRA-TURRAX T25), in 100µl protein lysis buffer. The homogenate was centrifuged at 13,000 rcf for 15 minutes at 4°C. Supernatants were transferred into a fresh tube and stored at -80°C. Bradford (Bio-Rad) method was used to determine total protein concentration. Coomassie Brilliant Blue G-250 (200µl) was added to 1µl protein lysate in a transparent 96-well plate. Bovine Serum Albumin (BSA) at different concentrations were used as standard samples. Using a multi-plate reader (Perkin Elmer Envision Plate Reader, Waltham, MA), the absorption of the samples and standards was measured at 595nm. The protein concentration was determined by plotting the absorbance obtained against the BSA standards reference curve. Different lysis buffers were used depending on the analytical purposes. Lysis buffer for the purpose of western blot analysis was composed of 50mM Hepes (pH 7.4), 150mM Sodium chloride (NaCl), 1mM EDTA, 0.5% NP40, Protease inhibitor, and water, whereas the buffer used to extract proteins to perform GLA enzymatic assay consists of 28mM citric acid, 44mM Disodium phosphate, 1% TritonX-100, Protease inhibitor and water.

3.5 Viral genome copy number analysis

Viral genome particles were quantified using a real-time quantitative PCR (RT-qPCR) method. The pSMD2 episomal vectors were analyzed using primers amplifying the region between the hAAT promoter region of the vector (Table 8).

pSMD2 specific primers	
pGG2_906 FW	GCC ACT AAG GAT TCT GCA GT
pGG2_105 REV	CTG CAC TTA CCG AAA GGA GT

Table 7. Primers for viral genome copy number analysis

A reference curve was prepared using pSMD2_hGLA_WT plasmid serially diluted from 10^{10} to 10^{0} copies. The AAV viral vector treated genomic DNA samples and the standards were added to the master mix which was composed of iQ SYBER Green Supermix (Biorad), forward and reverse primers, water, and genomic DNA and run in a C1000 Thermal Cycler CFX96 Real-Time System (Bio-Rad) with a reaction protocol starting at 98°C for 30 seconds and 40 cycles of 5 seconds at 95°C and 25 seconds at

62°C. Melting curves were generated at 95°C for 10 seconds and increased from 65°C to 95°C at 0.5°C/second. The viral genome particles per cell (vgp/cell) were determined by based on the standard curve obtained.

3.6 mRNA expression analysis

Quantitative real-time RT-PCR (qRT-PCR) was performed to determine the gene expression of immune markers in the liver of mice treated with episomal gene therapy and also to determine the fused ALB+EGFP mRNA expression. Diluted cDNA reverse transcribed from RNA extracted from HuH7 cells or liver homogenates was used as a template for the qPCR. In the case of the study with immune markers, gene-specific primers were used, whereas to quantify gene expression of the fused mRNA a primer on the EGFP transgene was coupled with a primer specific to exon 12 of the endogenous albumin (mALB for murine liver/ hALB for HuH7 cells) to amplify the fusion. GAPDH-specific primers were used to amplify the housekeeping gene for normalization The primers are listed in Table 9.

Gene	**Primer**	**Sequence 5'→3'**
mIL6	mIL6-FW	CAACGATGATGCACTTGCAG
	mIL6-REV	TCTGAAGGACTCTGGCTTTG
mCD86	mCD86-FW	TGTGTTCTGGAAACGGAGTC
	mCD86-REV	CTGATTCGGCTTCTTGTGAC
mNFkB1	mNFkB1-FW	AGCAGGACATGGGATTTCAG
	mNFkB1-REV	AGGTGGATGATGGCTAAGTG
mGRP78	mGRP78-FW	GTTCTTCAATGGCAAGGAGC
	mGRP78-REV	TGAGACTTCTTGGTGGGTAC
mCHOP	mCHOP FW	ACCACACCTGAAAGCAGAAC
	mCHOP REV	TCTTCCTCTTCGTTTCCTGG
mGAPDH	mGAPDH-FW	GCATGGACTGTGGTCATGAG
	mGAPDH-REV	CCATCACCATCTTCCAGGAG
hGAPDH	hGAPDH-FW	CTGGGCTACACTGAGCAC
	hGAPDH-REV	AAGTGGTGCGTTGAGGGCAAT
hALB Exon 12	hALB exon12 FW	CTGAGAAGGAGAGACAAATC
mALB Exon 12	mALB exon12 FW	CACACTTCCAGAGAAGGAGAAGC
EGFP	pAB-EGFP 1635 REV	ACCACCCCGGTGAACAGC

Table 8. Primers for mRNA expression analysis

The assay was performed on a 96-well real-time PCR plate using the iQ SYBER Green Supermix (Bio-Rad), forward and reverse primers, water, and diluted cDNA on a C1000 Thermal Cycler CFX96 Real-Time System (Bio-Rad). The qRT-PCR protocol used consists of an amplification reaction and the generation of a melting curve. Amplification reactions were conducted as follows: 1 cycle of 30 seconds at 98°C; 40 cycles of 5 seconds at 95°C, and 25 seconds at 62°C. Melting curves were generated as follows: 10 seconds at 95°C and increasing the temperature from 65°C to 95°C at 0.5°C increment per second. Data were analyzed using the ΔΔCt method.

3.7 Western blot

Proteins extracted from liver homogenates of treated and untreated mice (15µg) or plasma diluted 1:50 were used to perform an SDS-PAGE. The samples were denatured in 1x protein loading buffer (250mM Tris-HCl pH 6.8, 10% SDS, 0.5% Bromophenol blue, 50% Glycerol, 500mM DTT) for 5 minutes at 95°C and loaded onto the electrophoretic chamber along with a protein marker (Sharpmass VII Plus Euroclone) at 120V. After the appropriate separation of the bands and completion of the run, the proteins were transferred to a Polyvinylidene fluoride (PVDF) membrane using a Lightning Blot™ System (Perkin Elmer) using a PVDF membrane activated with water and buffer 2 (25mM Tris, 10% Methanol, water) and the gel sandwiched between 3mm Whatman paper, soaked in transfer buffers 1 (200mM Tris, 10% Methanol, water) and buffer 3 (25mM Tris, 10% Methanol, 40mM Glycine, water). Proteins on the membrane post-transfer were stained with Red Ponceau solution for 5 minutes and then imaged. The membrane was blocked in blocking buffer (5% milk in 0.1% PBS-Tween 20) for 2-4 hours followed by incubation in primary antibody diluted in the blocking buffer overnight at 4°C on a shaking surface. The membrane was later washed with wash buffer (0.1% Tween 20 in PBS) before incubating it with the secondary antibody diluted in the wash buffer for ~2 hours at room temperature on a shaking surface. Finally, the membrane was washed again with wash buffer to remove excess traces of antibodies and developed with Enhanced Chemiluminescence (ECL – ThermoFisher Scientific) to be imaged using a ChemiDoc imaging system (Biorad). The list of primary and secondary antibodies is listed in Table 10.

The band intensities on the images were measured using Image Lab software 6.0.1 (Biorad) for a quantitative evaluation of the western blot analysis.

	Antibody	Source	Supplier	Cat. No.	Dilution
Primary Antibodies	Human alpha-Galactosidase A / *hGLA*	Rabbit (Monoclonal)	Sino Biological	12078-R001	1:3000
	EGFP	Mouse	Santa Cruz Biotechnology	sc-81045	1:3000
	HSP70/HSP73 (1B5)	Rat (Monoclonal)	Enzo Life Science	ADI-SPA-815-D	1:3000
Secondary Antibodies	Anti-Mouse IgG/HRP	Goat (Polyclonal)	Dako	P0447	1:3000
	Anti-Rat IgG/HRP	Goat (Polyclonal)	Bethyl Laboratories	A110-305P	1:3000
	Anti-Rabbit IgG/HRP	Goat (Polyclonal)	Dako	P0448	1:3000

Table 9. Antibodies for western blot analysis

3.8 Histology

The right lobe of the liver and/or one kidney were harvested during the sacrifice of the treated and untreated mice in 4% PFA (4% paraformaldehyde in 1x PBS). The tissues were fixed in the solution at 4°C for 24 hours. The buffer was changed to 20% sucrose solution (20% sucrose, 0.02% sodium azide, and, PBS) post-incubation. The tissues were frozen at optimal cutting temperature compound and sliced into 4µm slices on histological slides. The slides with tissue sections were stored at -20°C until further use.

Similarly, in the case of HuH7 cells, the medium was removed from the well plate, and cells were washed with PBS. 4% PFA was added to the cells and incubated for 20 minutes at room temperature followed by PBS wash.

3.8.1 Counterstaining

Counterstaining was done to stain the nucleus of the cells and observe EGFP-positive cells. The sections were thawed at room temperature for 20 minutes, whereas the cells in PFA did not require thawing. The cells and tissues were washed with PBS for 5 minutes. The washing was repeated three times before

proceeding. Nuclei-staining Hoechst diluted in PBS was added to the sections and incubated for 10 minutes. To remove excess Hoechst, the slides were washed three times with PBS for 5 minutes each and then rinsed with water. The sections were then mounted with Mowiol and covered with a coverslip and left to dry. Once the slides were counter-staining and mounted, fluorescent images were taken with Leica fluorescent microscope. The images were analyzed using ImageJ software 1.53e and QuPath-0.3.2. for EGFP-positive cells.

3.8.2 Immunofluorescence

Immunofluorescence was done with Fabry KO animals to differentiate between the hemizygous and the wild-type male mice. The slides with liver and kidney sections were thawed at room temperature for 20 minutes followed by a PBS wash. Antigen retrieval was done with 10mM Sodium citrate buffer pH 6.0 by baking the slides in the microwave for 40 minutes (refresh the solution to avoid temperature increasing above 65°C). The slides were washed with PBS and blocked with blocking buffer (5% BSA in 0.4% PBS-Triton X 100) for 2 hours at room temperature. Later, excess blocking buffer was removed, and the sections were incubated with the primary antibody in 2.5% BSA in 0.4% PBS-triton X 100 for 2 hours at room temperature. The slides were washed with three cycles of washing buffer (0.1% PBS-Triton X 100) for 5 minutes each, followed by incubation with a secondary antibody diluted in wash buffer for 2 hours at room temperature. Finally, the slides were washed with wash buffer to remove traces of antibodies and incubated with Hoechst diluted in PBS to stain the nucleus for 10 minutes. The stain was washed with PBS and rinsed with water before mounting with a Mowiol using a coverslip. The mounted slides were left to rest until dry and later fluorescent images were taken with Leica fluorescent microscope. The antibodies used are listed in Table 11.

Antibody	Source	Supplier	Cat. No.	Dilution
Anti-GB3	Mouse (Monoclonal)	Amsbio	AMS.A2506	1:250
Alexa Fluor™ 488 Phalloidin	-	Invitrogen	A12379	1:500
Anti-mouse IgG/Alexa Fluor™ 568	Goat (Polyclonal)	Invitrogen	A11004	1:500

Table 10. Antibodies used for immunofluorescence

3.9 GLA enzyme assay

GLA enzyme activity test was done with HuH7 cell extract and supernatant medium, and murine plasma and tissue including liver, kidney, and heart as a phenotypic marker of Fabry disease. Protein extracted from the cells and tissues using citrate lysis buffer mentioned in the protein extraction section was used as samples, along with crude supernatant and plasma diluted according to the requirement with PBS. Initially, 4MU (4-Methylumbelliferone, Cat# M1381 Sigma Aldrich) was used to prepare stocks of different concentrations (2pmoles, 4pmoles, 10pmoles, 20pmoles, 40pmoles, 80pmoles, and 100pmoles) to be used as standards to generate a reference curve. In a black opaque 96-well plate, a 2µl enzyme-containing sample (protein from cell/tissue, supernatant medium, or blood plasma) was added. To this, 20µl of 4MUG (4-Methyl-umbelliferyl-alpha-D-galactopyranoside, Cat#M7633 Sigma Aldrich) (2.46mM 4MUG in 0.1M Citrate/ 0.2M phosphate buffer pH 4.5) substrate was added and mixed gently by pipetting. The plate was incubated at 37°C for the reaction to take place. After 1 hour of incubation, 200µl of stop solution (200mM glycine-NaOH Buffer pH 10.4) was added to stop the reaction. Previously prepared standards were also added to the plate diluted in 200µl of stop solution. The released fluorescence from the samples and the standards was measured at excitation 365nm and emission 450nm wavelengths with a multi-plate reader (Perkin Elmer Envision Plate Reader, Waltham, MA),

For the analysis, the RFU obtained was normalized with the appropriate blank samples, and 4MU units (B) released by the samples were calculated using the standard curve. To calculate enzyme activity,

$$\text{Enzyme activity (nmoles/ml/hr or nmoles/mg/hr)} = \frac{(B/1000) \times D}{V \times P}$$

Where, B= 4MU (pmoles)

V= Volume of samples used (ml)

P= Concentration of proteins (µg/µl)

D= Dilution

3.10 Mass-spectrometry for Lyso-Gb3 analysis

Lyso-Gb3 level was evaluated as a phenotypic marker of Fabry disease in murine plasma and tissues (liver, kidney, and heart) of treated and untreated animals. In the case of tissues, 20mg of powdered tissue homogenate was weighed and homogenized using a mechanical homogenizer (IKA ULTRA-TURRAX T25) with 350µl of water. Liver (20mg) from an untreated hemizygous 5-month-old mouse was homogenized in 350µl of water and was used as a reproducibility control whereas, 30mg liver from an untreated wild-type 5-month-old mice was used as a matrix control in all assays for the assessment of murine tissues. Tissue and plasma lyso-Gb3 concentrations were determined by liquid chromatography-mass spectrometry (LCMS) at Centro Servizi di Laboratorio (CSL) in Hospital Santa Maria della Misericordia in Udine. Homogenized samples or plasma were mixed with precipitation solution (10ml internal standard solution (1ng/mL-10ng/mL), 10ml acetone, 2.22ml water) containing internal standard (1ng/mL Lyso GlcCer d5 - Lyso-SM d9; 10ng/mL Lyso Gb3 d7 in Methanol). The mix was vortexed and incubated on an orbital shaker for 30 minutes and then centrifuged at 16,000 rcf for 10 minutes. The clear supernatant observed was collected in a clean tube and dried under a stream of nitrogen. Once the liquid was evaporated the dried content was reconstituted with 100µl mobile phase (55% FMA: water + 0.1% HCOOH, 45% FMB: CH_3CN +0.1 %HCOOH) was mixed using a vortex for 30 seconds. The reconstituted mix was centrifuged at 16,000 rcf for 5 minutes and 100µl supernatant was used for analysis by injecting 2µl in Citrine Sciex 6500QT with Poroshell 120 EC-C8 2.7µm and 3.0x50mm columns. The analysis was done against a calibration curve prepared by spiking the pure standards in water: methanol 50:50 solution (range 0.1ng/ml-200ng/ml for LysoGb3, Lyso GlcCer, and range 1ng/ml -2000ng/ml for Lyso SM/509).

The absolute values of lysoGb3 accumulation in plasma (ng/ml) and tissues (ng/mg) were converted to percentages for ease of understanding. In the case of plasma, the mean of lyso-Gb3 accumulation in untreated hemizygous males (n=5) at P150 was considered as 100%. Whereas, in the case of tissues, the mean of lyso-Gb3 accumulation in the specific organ (liver/kidney/heart) of untreated hemizygous males (n=5) was considered as 100% accumulation. All the treated and untreated wild-type substrate levels were re-calculated as percentages based on this criterion.

3.11 Digital droplet PCR

The on-target recombination rate was measured using ddPCR of liver genomic DNA as described previously (Tsuji et al., 2022). Genomic DNA (100-200ng) was digested with SpeI for 1 hour. The digested genomic DNA (25ng) was added to a 25µl PCR reaction containing ddPCR Supermix for Probes (No dUTP) (Bio-Rad), 900nM target-specific primers, and 250nM amplicon-specific probes (Table 12). The droplets were generated using 22µl of the PCR reactions and 70µl of oil according to the manufacturer's instructions. Reaction cycles were as follows: 95°C for 10 minutes, 50 cycles of 95°C for 30 s, 60°C for 30 s, and 72°C for 6 minutes, and one cycle of 95°C for 10 minutes and held at 4°C until droplet reading.

	On-target (endogenous Alb)	**Non-target (P2A)**
Primers 5'→3'	GGGCAAGGCAACGTCATGG	CTGCTGTGCACCAGTTGATGTT
	CCAGGGTTCTCTTCCACGTC	TGCTTTCTGGGTGTAGCGAACT
Probes 5'→3'	GCCCAAGGCTACAGCGGAGC (FAM)	TCTGGTGCTGAGGACACGTAGCCCAGT (HEX)

Table 11. Primers and probes used for ddPCR analysis

3.12 ALT assay

Plasma from animals treated with episomal AAV vectors and untreated controls was used to determine alanine aminotransferase (ALT) activity, 15 days, and 30 days post-infection. The enzyme activity was measured using an ALT Assay kit from Abnova (Cat#KA4189). ALT standards were prepared, and samples were used to carry out the enzymatic reaction producing glutamate as a blue-colored product, whose absorbance was measured using a multi-plate reader (Perkin Elmer Envision Plate Reader, Waltham, MA), absorbance ration A_{570nm}/A_{610nm} as per manufacturer's instructions. The equation obtained from the standard curve plotted using the absorbance (ABS) values were used to calculate the ALT levels (µM/ml) in the samples.

3.13 TIDE analysis

The efficiency of the CRISPR/Cas9 system with the single guide RNA designed to target the human albumin gene was tested in vivo in HuH7 liver-derived human cells, using TIDE (Tracking of Indels by Decomposition) analysis. HuH7 cells were transfected with the pX602_hsgRNA plasmid. The transfected and mock untreated cells were collected 24 hours post-transfection. Genomic DNA isolated from these cells was used as a template to amplify the albumin region of the CRISPR target site using a PCR reaction composed of 5x DNA polymerase reaction buffer, 0.25-unit GoTaq Flexi DNA polymerase, 25mM MgCl2, 5mM dNTPs, water, and primers specific to the albumin region around the PAM site as mentioned in table 13. Genomic DNA was added to the master mix. The PCR run followed a temperature cycle of initial denaturation at 95°C for 3 minutes, followed by 95°C for 30 seconds, 47°C for 30 seconds, and 72°C for 30 seconds for 30 cycles, followed by final elongation of 7 minutes at 72°C and a cool down at 4°C. The PCR product was run on an agarose gel and the band corresponding to the amplicon was purified from the gel. Sanger sequencing of the amplicon DNA was done with Eurofins Genomics and the raw sequence obtained was used as input to determine cleavage efficiency using the TIDE web tool (https://tide.nki.nl/).

Primers	**Sequence 5'→3'**
pAB_hALB_Hap2 FW	AGCTTCCATCCAGAGATTAT
hALB Int14_1102 REV	TTGAATTTTGACCCTTTGGAA

Table 12. Primers used for TIDE analysis

3.14 SNP hALB genotyping

TaqMan predesigned SNP genotyping assay from Thermofisher Scientific was used to genotype the SNP ID rs962004, using fluorophores for human ALB Haplotype 1 (FAM/ TTGTTGAGCTT) and Haplotype 2 (VIC/ TTGTTGAGCTC). Genomic DNA (20ng) isolated from untreated HuH7, and four different human blood samples were used to increase confidence in the genotyping assay. Water was used as the negative control. A reaction mix containing 2x iQ supermix (Biorad), 20x SNP assay mix, and water. DNA was added to the mix and run on a C1000 Thermal Cycler CFX96 Real-Time System (Bio-Rad). The generated dot plot was generated according to the Fluorophore-specificity in the sample.

3.15 Statistical analysis

Statistical analyses were performed for all the assays using GraphPad Prism 8.2.1. Data in the graphs were plotted as mean with the corresponding standard deviation (SD). Statistical analysis of data containing different time points was done using a mixed-effect model (REML). The comparison of groups was done using one-way or two-way ANOVA was used. A p-value below 0.05 was considered significant (* $p<0.05$, ** $p<0.01$, *** $p<0.001$).

Results

4.1 Generation and evaluation of codon-optimized human GLA constructs

Codon optimization is a technique that aims at improving expression profiles and translational capabilities of genes and cDNAs by manipulating the nucleic acid sequence without altering the amino acid sequence. In nature, most amino acids are encoded by more than one codon, and each organism has a favorable codon for a particular amino acid known as codon biasing. The approach is based on the replacement of less used codons by the optimal ones, maintaining the original primary sequence. To obtain an advanced version of human GLA (*hGLA*), transcript 201 of the wild-type human GLA sequence was codon-optimized, modifying its codon composition based on biasing templates. Online codon-optimization tools like IDT Codon Optimization tool (https://eu.idtdna.com/CodonOpt), JCAT or Java Codon Adaptation Tool (http://www.jcat.de/) and COOL or Codon Optimization On-Line by the National University of Singapore, were used to generate different *hGLA* variants. These *hGLA* constructs were then manually analyzed and further optimized for parameters like GC content, CpG islands, cryptic splice sites, and the absence of alternative open reading frames in the coding and non-coding strands. Following automated and manual optimizations, four codon-optimized constructs were generated: hGLA_CO01, hGLA_CO02, hGLA_CO03, and hGLA_CO04 with 76.52%, 78.11%, 80.23%, and 80.76% sequence identity with hGLA_WT, respectively.

A Kozak consensus sequence and NheI and SalI unique cloning sites flanking either end to facilitate cloning were added to all sequences. The *hGLA* cDNAs were cloned into the plasmid pSMD2, which contains the AAV ITRs flanking a liver-specific promoter from human Alpha-1 antitrypsin (α-1hAAT), the human apolipoprotein E enhancer (ApoE) (Ronzitti et al., 2016), the HBB2 intronic sequence for enhanced expression, and the bovine growth hormone polyadenylation sequences, namely, pSMD2_hGLA WT, pSMD2_hGLA CO01, pSMD2_hGLA CO02, pSMD2_hGLA CO03 and pSMD2_hGLA CO04 as represented in Figure 12.

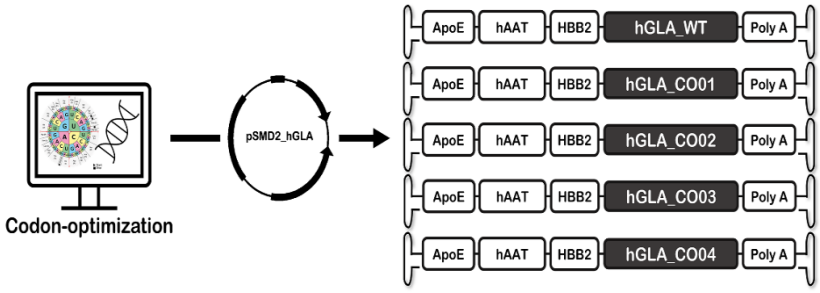

Figure 12. Synthesis and construction of codon-optimized *hGLA* constructs. The human GLA 201 transcript was used as a template to generate four codon-optimized variants of the gene using online tools and manual alterations to the codon composition, resulting in hGLA_CO01, hGLA_CO02, hGLA_CO03, and hGLA_CO04 with 76.52%, 78.11%, 80.23% and 80.76% sequence identity with hGLA_WT respectively. These codon-optimized cDNAs along with WT *hGLA* cDNA were cloned into pSMD2-hAAT-ApoE episomal plasmid containing liver-specific promoter.

4.1.1 *in vitro* characterization of codon-optimized *hGLA* constructs

Codon-optimized episomal *hGLA* plasmids and wild-type constructs were tested *in vitro* to determine the expression and compare the activity of the produced codon-optimized proteins against the wild-type *hGLA* protein. The *hGLA* plasmids were transfected into HuH7 cells as described in the Materials and Methods Section. Untreated cells were considered mock control for the assay and an EGFP containing plasmid was co-transfected as transfection control (Figure 13).

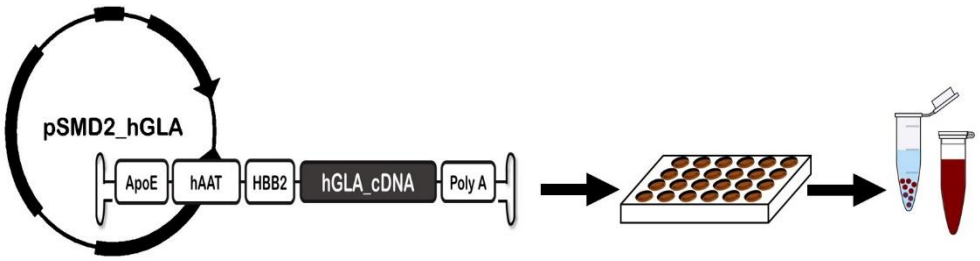

Figure 13. Experimental set-up for the assessment of codon-optimized sequences *in vitro*. Experimental design for the assessment of the four codon-optimized sequences *in vitro* in HuH7 cells. The cloned pSMD2_hGLA_CO sequences were transfected in HuH7 cells using lipofectamine 2000. An eGFP-containing plasmid was co-transfected as transfection control and untreated cells were considered mock control. Cells were harvested to extract proteins and growth medium was collected 48 hours post-transfection.

Since HuH7 is a human liver cell line with endogenous GLA expression, we expect to observe above-basal levels of GLA protein production and GLA enzyme activity in the cell extract by transfecting these cells. Due to its secretory nature, we also expected a fraction of the produced protein to be observed in the cell culture medium. Proteins (5 µg) extracted from the harvested cells and 5 µl of cell medium were used to measure GLA enzyme activity. According to the data in Figure 14, It was evident that the codon-optimized *hGLA* sequences were more efficient than the wild-type sequence, showing higher levels of GLA enzyme activity. The data are represented as relative to the wild-type values obtained in the enzyme activity assay. The constructs hGLA_CO01, hGLA_CO02, hGLA_CO03, and hGLA_CO04 showed a 2.1x, 2.0x, 1.5x, and 1.2x increase in the GLA activity in cells respectively, while the secreted GLA activity was 4.2x, 4.5x, 2.3x and 1.6x higher than hGLA_WT for the codon-optimized constructs in that order (Figures 14A and 14B).

Before, the selection of the optimum construct it was necessary to evaluate the protein production abilities. Therefore, SDS-PAGE was performed for proteins extracted from both the cell extract and the cell culture medium. Western blot analysis was done to compare protein levels of codon-optimized *hGLA* and wildtype sequences in both cases, using co-transfected-EGFP as a control for transfection efficiency. An anti-GLA antibody (1:3000; 49KDa; Sino Biological Cat# 12078-R001) was used to obtain *hGLA*-specific bands. With the Western blot image analysis, it was evident that codon-optimized

sequences were able to express higher protein levels than wild-type ones. hGLA_CO01, hGLA_CO02 and hGLA_CO03 had similar expression profiles in cells being 2x, 1.9x and 1.7x higher compared to hGLA_WT. The proteins detected in the cell supernatant were 6.5x for hGLA_CO01, 5.3x for hGLA_CO02, and 2.7x for hGLA_CO03. The hGLA_CO04 treated cells however did not match hGLA_WT levels in protein production in cells even though 1.8x higher proteins were detected in the cell culture medium. (Figure 14C-14F).

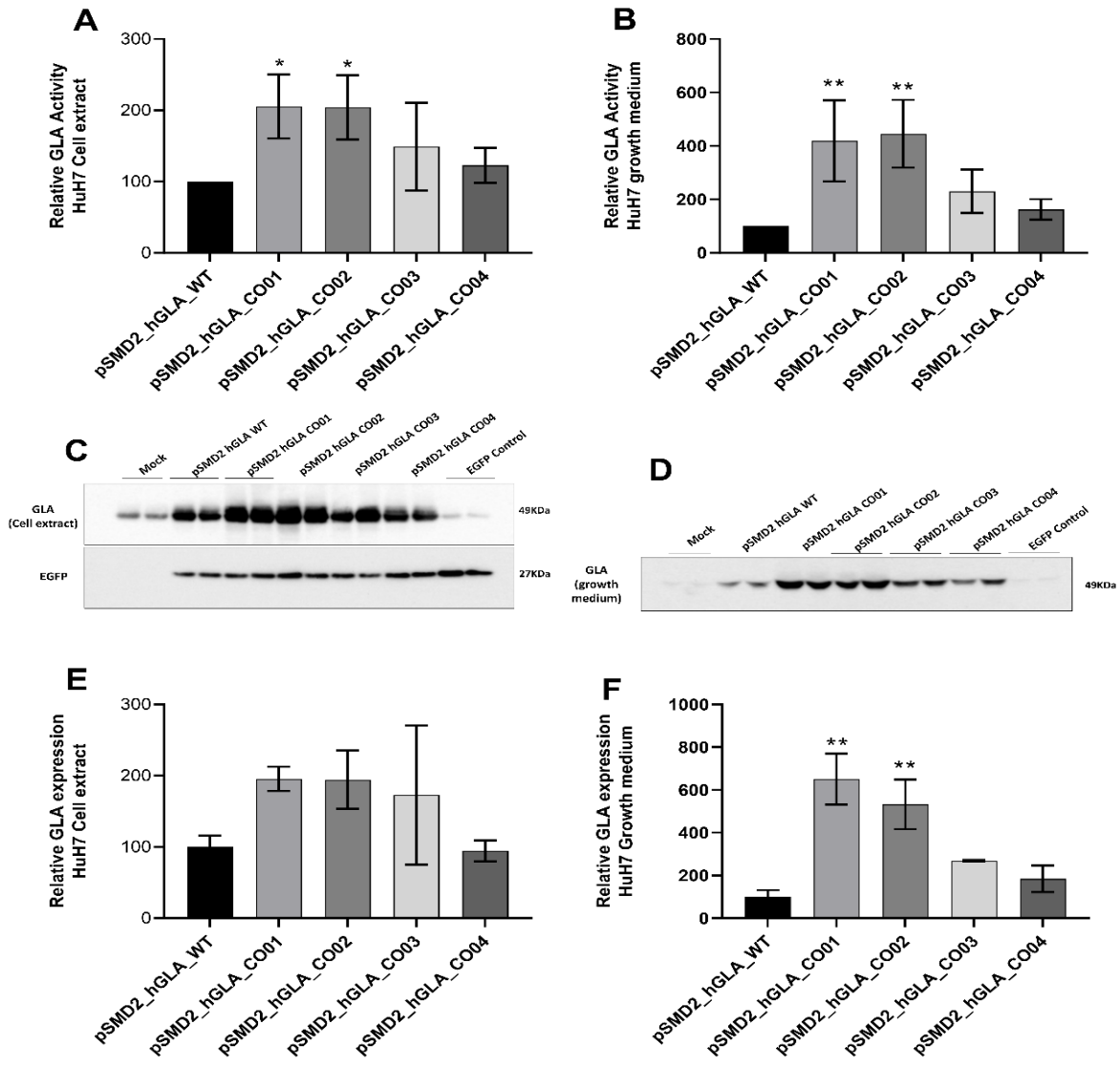

Figure 14. Assessment of codon-optimized sequences *in vitro*. An enzymatic reaction was performed to evaluate the relative GLA activity of the codon-optimized versions and the wild-type *hGLA* sequence A) This data represents the mean of three independent assays (n=2), each with 5µg proteins extracted from the cell extract. B) similar assay was done using 5µl growth media (n=2). C-D) Western blot assay was done for cell extract and growth medium using *hGLA* specific antibody and normalized with transfection control. E-F) This data quantitatively represents the Western blot analysis (n=2). Mean±SD. One-way ANOVA (p*<0.05, **<0.001, ***<0.0001)

These data coincide with the information obtained from the enzyme assay and therefore it can be claimed with confidence that codon-optimized *hGLA* sequences CO01, CO02, and CO03 were more efficient than the wild-type hGLA sequence. Moving forward, it was necessary to evaluate these constructs *in vivo* for their GLA enzyme activity and protein production abilities.

4.1.2 *in vivo* characterization of codon-optimized *hGLA* constructs

Following the promising *in vitro* data, where the codon-optimized sequences demonstrated better efficiency than wild-type both in terms of protein expression and enzyme activity, it was necessary to validate the same *in vivo* since the ultimate aim for the assessment of the codon-optimized constructs is the selection of an advanced version when compared to WT to use is in Fabry KO mouse model. For this, AAV8-pSMD2-hGLA virus stocks of the most efficient codon-optimized *hGLA* variants were prepared, (i.e. CO01, CO02, and CO03 as well as for hGLA_WT). Liver-specific expression of the *hGLA* cDNA variants is driven by the human α1-aat promoter and ApoE enhancer sequences. One-month-old (post-natal day 30, P30) C57BL/6 WT mice (n=5) were treated with a dose of the episomal vectors (3.0E+12 vg/kg) via retro-orbital injections, expecting to obtain a higher *hGLA* expression than the endogenous *mGLA*, in order to be able to evaluate the *hGLA* cDNA. Age-matched untreated animals were considered as control. These mice were sacrificed three weeks post-injection (P51), the liver was harvested, and blood was collected for plasma analysis (Figure 15).

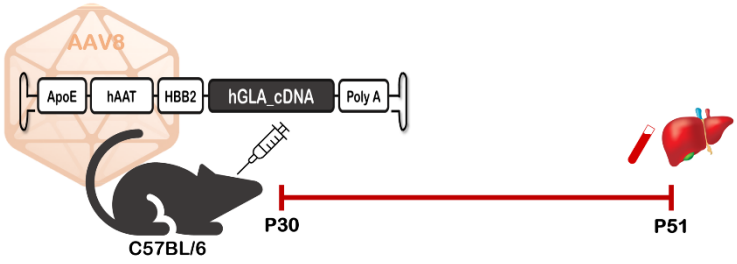

Figure 15. Experimental set-up for the assessment of codon-optimized sequences *in vivo*. Experimental design for the assessment of the codon-optimized sequences *in vivo* in C57BL/6 WT mice. AAV8 viral stocks were prepared for hGLA_CO plasmids. AAV8_pSMD2_hGLA WT, AAV8_pSMD2_hGLA_CO01, AAV8_pSMD2_hGLA_CO02 and AAV8_pSMD2_hGLA_CO03 vectors used to infect WT animals (n=5) at 3.0E+12vg/kg intravenously (retro-orbital) at P30. Age-matched untreated mice were used as a control to indicate endogenous mGLA. The experiment was terminated after 3 weeks, harvesting the liver and collecting blood for plasma analysis.

To determine GLA activity, the fluorescent enzyme assay was performed with 3 ng liver proteins (nmole/mg/hr) and plasma diluted 1:10,000 in PBS (nmoles/ml/hr). The GLA enzyme activity in the liver in mice treated with AAV8 pSMD2_hGLA CO02 and AAV8 pSMD2_hGLA CO03 was 2.1x and

1.7x higher than in hGLA_WT treated animals. Likewise, when the secreted GLA in the bloodstream was measured the values were in line with those observed in the liver homogenates, hGLA_CO02 and hGLA_CO03 had 3.4x and 2.3x higher activity than hGLA_WT. The animals with hGLA_CO01 treatment could not match the activity of the WT construct either in the liver cells or in the plasma (Figure 16).

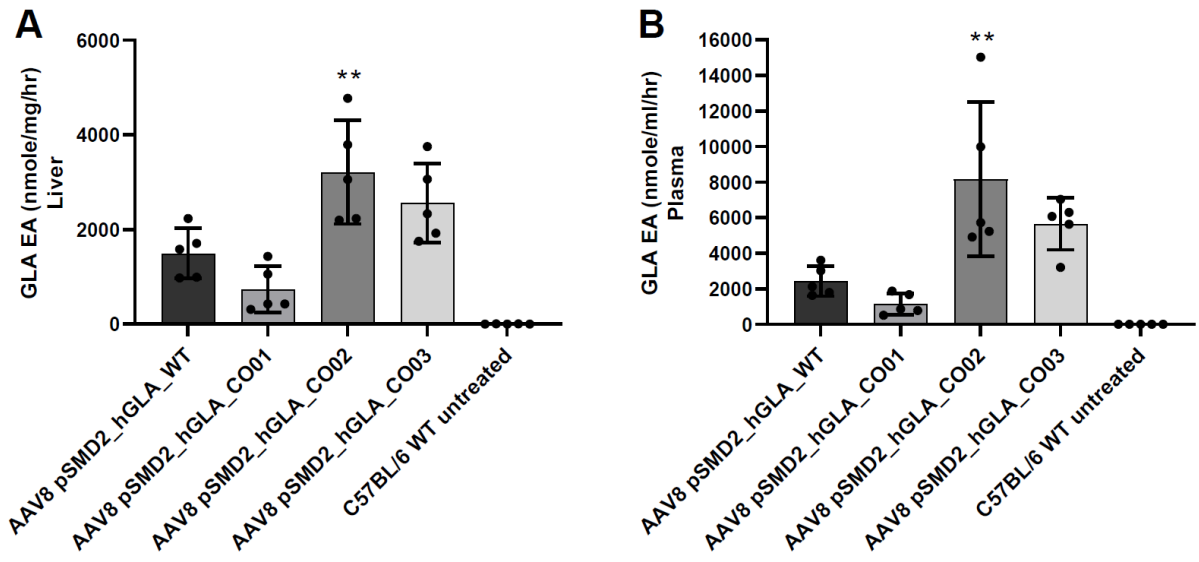

Figure 16. GLA enzyme activity analysis in C57BL/6 WT mice. C57BL/6 WT Mice (n=5) treated with AAV8 codon optimized vectors and wild type were sacrificed after 3 weeks of treatment. GLA enzyme activity was tested using a fluorescent enzyme assay with A) proteins extracted from liver homogenates (3ng) (nmoles/mg/hr) and B) plasma isolated from crude blood collected at the termination of the experiment (nmoles/ml/hr). The graphs represent the mean of GLA enzyme activity. Age-matched untreated mice were used as control and showed endogenous activity ranging from 2-6 nmoles/mg/hr in the liver and 0.5-3 nmoles/ml/hr in blood plasma. Mean±SD. One-way ANOVA (p*<0.05, **<0.001, ***<0.0001)

AAV8 viral genome particles in genomic DNA extracted from liver homogenates were also measured using quantitative RT-PCR analysis as represented in (VGP/cell) Figure 17. Importantly, the VGC of mice treated with AAV8_pSMD2_hGLA CO02 was 5.6-fold lower than those present in mice treated with the hGLA WT construct, suggesting that the increase in GLA activity observed was sub-estimated and the CO02-variant may be more efficient than what it was determined in the enzyme assays.

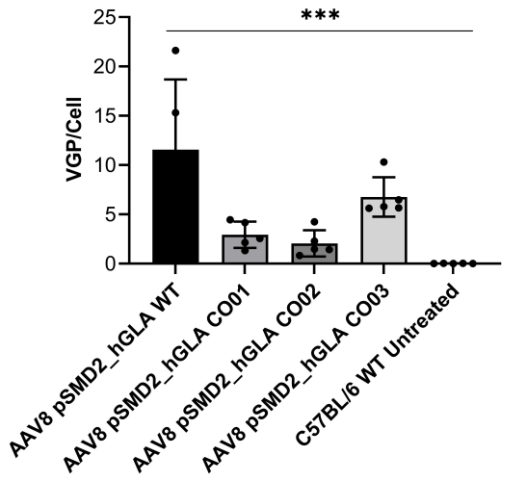

Figure 17. VGP in C57BL/6 mice treated with AAV8 pSMD2_hGLA CO. Genomic DNA was extracted from liver homogenates of mice treated with AAV8 pSMD2_hGLA codon optimised vectors and WT and viral genome particles were measured using quantitative PCR. Untreated C57BL/6 WT mice were used as control (n=5). Mean±SD One-way ANOVA (p*<0.05, **<0.001, ***<0.0001)

For a more confident result, *hGLA* protein expression was analyzed by Western blot. Plasma (1:50) and liver proteins (15 µg) from treated animals as well as untreated control groups were run on an SDS-PAGE gel and blotted onto a nitrocellulose membrane. A GLA-specific antibody was used to identify human GLA proteins. Housekeeping genes, HSP70 (liver proteins), and mIgG (plasma) were used for normalization. According to the quantification of the band intensities, AAV8_pSMD2_hGLA CO02 and AAV8_pSMD2_hGLA CO03 reflect an increase in the relative expression by 1.3-fold in liver and 1.4-fold in plasma as compared to the wild-type sequence. AAV8_pSMD2_CO01 levels were still lower than that of wild-type *hGLA* expression (Figure 18).

Considering the data obtained from the enzyme assay and the western blot it was concluded that hGLA_CO02 and hGLA_CO03 had better potentials than the wildtype in C57BL/6 mice and HuH7 cells. However, instead of going forward with both sequences, hGLA_CO02 was given preference based on its notable increase in enzyme activity levels.

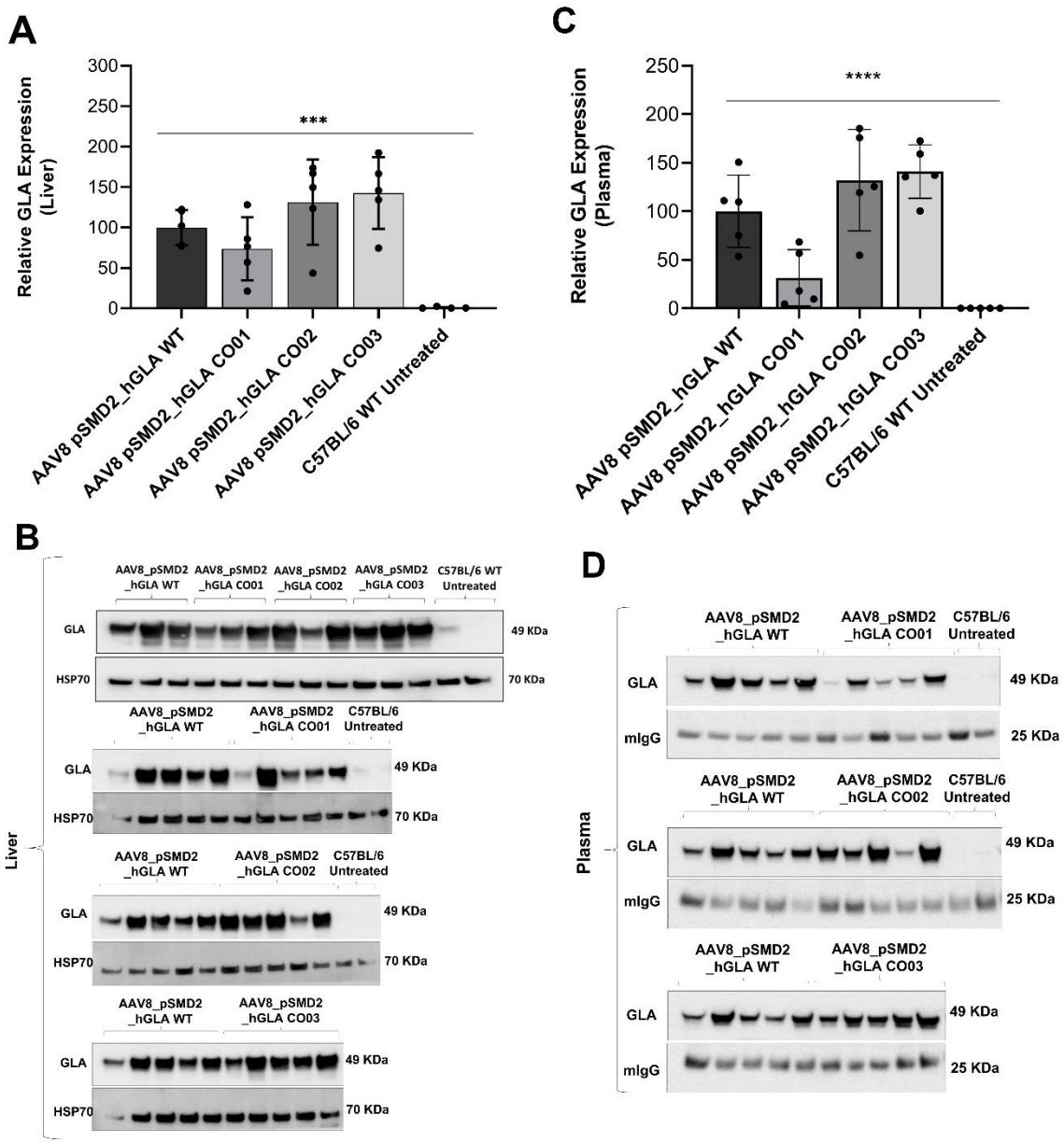

Figure 18. Western blot analysis in C57BL/6 mice treated with AAV8 pSMD2_hGLA CO. A and B) Proteins were extracted from the liver homogenates of C57BL/6 WT mice treated with AAV8 pSMD2 hGLA codon optimized variants and hGLA_WT. Western blot analysis was done with 15µg proteins using Anti-GLA antibody (1:3000), represented with comparative blots of hGLA_CO and hGLA_WT proteins and a representative image. Anti-HSP70 antibody (1:3000) was used for normalisation. Quantification represents the relative GLA expression in the liver. C and D) Blood collected from treated and untreated mice were used to extract plasma. A 1:50 dilution of plasma (PBS) was used to do the western blot analysis. The blots represent comparative expression profiles of GLA normalised using mouse IgG-specific antibody and its quantitative analysis. Age-matched untreated C57BL/6 WT mice were used as control (n=5). Mean±SD, One-way ANOVA (p*<0.05, **<0.001, ***<0.0001)

4.2 Determination of optimal conditions for gene-based therapies

Despite their resemblances in phylogenetic traits and physiological similarities, determining the appropriate 'age matching' in humans and mice is still a work in progress, and many studies have been conducted to decipher the correlation between humans and mice in terms of lifespan and age. This knowledge is a vital aid to designing experiments targeting monogenic diseases with different onsets, for example in the case of Fabry disease where the early onset is usually diagnosed in the first decade of human life and the late onset, on the other hand, is recognized near to the third decade of life. When performing gene-based therapies, it is also important to optimize experimental conditions to obtain optimum efficiency. In the case of liver-directed AAV gene therapy, due to the duplication of the hepatocytes in a growing liver, AAV episomes are lost, eventually compromising the efficacy of the treatment. So far AAV based episomal gene therapies have shown success in adults with fully-developed and mature liver cells in contrast to children with growing livers and in cases of liver damage. Alternatively, genome editing therapy with AAV vectors targeting the liver to permanently modify the genome exploits hepatocyte proliferation to target the efficiency issues of the treatment. The cells integrated with the treatment, divide, and pass on the therapeutic gene to the daughter cells, maintaining the efficacy of the therapy.

An experiment (Figure 19) was designed to determine the optimum age for liver-directed gene therapy using an AAV8 donor vector with hAAT liver-specific promoter referred to hereafter as episomal treatment, and genome editing with a promoter-less AAV8 donor vector with mouse albumin homology arms and EGFP transgene referred hereafter as integrative treatment coupled with an AAV vector containing gRNA and saCas9 to increase HR.

C57BL/6 WT male animals (n=5) were intravenously treated (retro-orbital) at different postnatal ages of P1, P5, P10, P15, P20, and P30 at a dose of 3.0E+12vg/kg with AAV8-pGG2-AAT-EGFP for Episomal treatment and a higher dose for integrative treatment i.e., 3.0E+14vg/kg for AAV8-pAB288-ALB-EGFP (Donor vector) and AAV8 pX602-sgRNA-Cas9 (1:1; Donor: Cas9). All the animals treated at different time points were sacrificed at 2 months of age. The liver was harvested for histological and expression analysis (Figure 19).

Proteins were extracted from liver homogenates for expression assessment. Western blots analysis of liver proteins identified minimum EGFP expression in mice treated with episomal treatment at early time points and the gradual increase in band intensity in animals treated at P15, P20, and a 51x increase with animals treated at P30 when compared to the initial time point. Animals treated with integrating donor vector and Cas9 at P1, P5, and P10 reached up to 72-88% efficiency however, treatment after 15 and 20 days of birth sees a 2.4x and 3.7x decrease in the intensity of EGFP expression bands compared to treatment at P1.

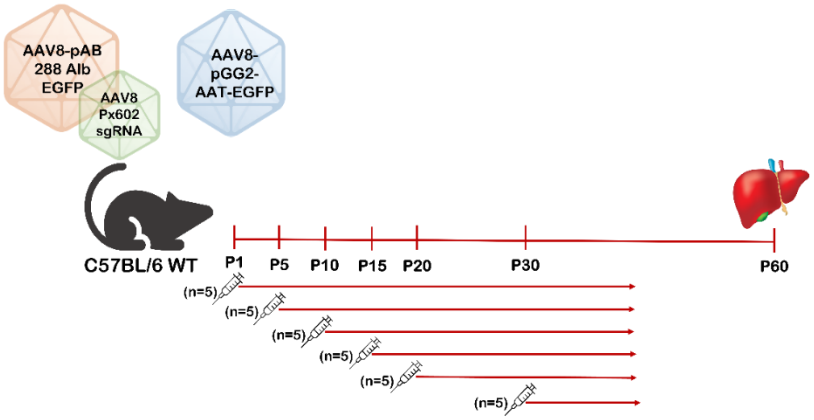

Figure 19. Experimental set-up to determine the optimal age of AAV-based gene therapies in C57BL/6 mice. An experiment was designed to assess the efficacy of AAV-based gene therapies at different postnatal ages. C57BL/6 WT male mice (n=5) were treated with either AAV8-pGG2-AAT-eGFP episomal donor vector (3.0E+12vg/kg) with a liver-specific promoter or AAV8-pAB288-ALB-eGFP integrating donor vector (3.0E+14vg/kg) coupled with AAV8 pX602-sgRNA-Cas9 (3.0E+14vg/kg) at P1, P5, P10, P15, P20 and P30 via retro-orbital route of injection. Age-matched untreated mice were considered as control. The experiment was terminated at 2 months of age regardless the time of treatment. The liver was harvested and processed for expression and histological evaluation.

The blots are representative images of the treated groups (Figure 20 A and B). Similar results were obtained with immunofluorescence analysis of liver sections after 2 months of treatment where figure 20C shows representative images of the treated groups. Neonatal mice treated with episomal therapy count very few EGFP (green) positive cells. However, there was a 10-fold between animals treated at P20 (2% EGFP-positive cells) and P30 with 20% EGFP-positive cells compared to treatment at P1. In the case of animals treated with integrative treatment 1-day after birth counts to 60-90% EGFP positive cells, which gradually decrease with age of treatment, P5 (42%), P10 (30%), P15 (17%), and P20 (11%), and a non-significant hike with 60% EGFP positive cells can be observed with mice treated at P30 (Figure 20 C and D). This data can be confirmed since protein expression analysis and immunofluorescence quantification follow the same trends for both therapies. These results fall in line with the expectation and confirm the theory explained before. During the first few days after birth, the liver grows at the maximum rate accompanied by hepatocyte duplication which leads to AAV episome loss and dilution. Therefore, there is almost no expression observed after 2 months when animals were treated 1 day, 5 days, and 10 days after birth. The expression gradually starts to increase in the later time points and an increase in expression is observed with animals treated at 1 month of age when the liver growth rate is rather stable. On the contrary, genome editing with Cas9 was able to integrate EGFP transgene in the hepatocyte which rapidly expanded to the daughter cells in the early time points of treatment when the liver growth is at its peak, reaching maximum efficiency.

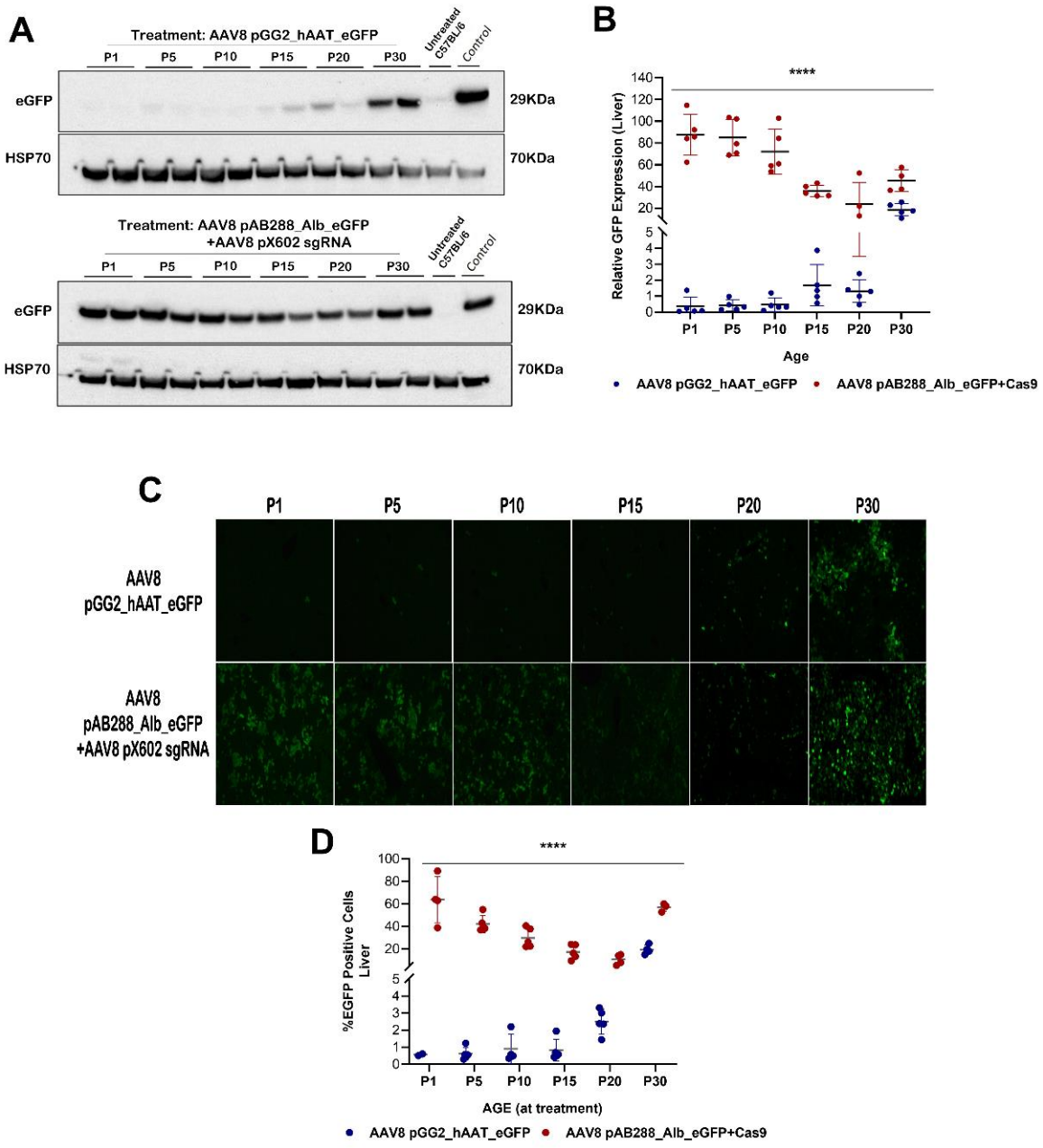

Figure 20. Determining the optimal age of AAV-based gene therapies in C57BL/6 mice. C57BL/6 WT male mice (n=5) were treated with either AAV8-pGG2-AAT-eGFP episomal donor vector with a liver-specific promoter or AAV8-pAB288-ALB-eGFP integrating donor vector coupled with AAV8 pX602-sgRNA-Cas9 at P1, P5, P10, P15, P20 and P30 via the retro-orbital route of injection. A) Western blot images show a gradual increase in band intensity with episomal treatment with increasing age of treatment, whereas there is a slight decrease in intensity with integrative treatment. B) Quantitative analysis of the western blots represented as relative GFP expression in the liver homogenates, confirms the trend followed by both treatments is statistically significant. C) Immunofluorescence was done on liver sections of treated mice showing eGFP-positive cells in green. D) Quantification of immunofluorescence images is shown as the mean percentage of GFP-positive cells. Age-matched untreated C57BL/6 WT mice were used as control (n=5). Mean±SD, Mixed-effect analysis (p*<0.05, **<0.001, ***<0.0001).

4.3 Characterisation of Fabry knock-out mouse model

Fabry knock-out mice B6;129-Gla tm1Kul/J were brought to the ICGEB animal facility from Jackson Laboratory, Main, USA (Cat no. 003535). Also known as α-Gal A KO (*α-Gal A*$^{-}$), these mice were developed by Dr. Ashok B Kulkarni and have a 1kb region including the exon 3 and intron 3 region which was replaced by a neomycin resistance cassette (Oshima T et. al, 1997).

The colony was expanded by mating heterozygous females with wild-type males. Mating cages were also set up between mutant females and hemizygous males to generate hemizygous males for experimentation. For the characterization of the colony, male Fabry KO animals (n=2) aged 2-, 3-, 4-, 5-, and 6 months were sacrificed, the liver, kidney, and heart were harvested, and blood was collected to extract plasma. GLA enzyme activity assay was done for all samples. The values of GLA enzyme activity of 5 months wild-type animals measured an average of 5.1 nmoles/mg/hr, 4.6 nmoles/mg/hr, 0.45 nmoles/mg/hr, and 2.05 nmoles/ml/hr for liver, kidney, heart, and plasma, respectively. The hemizygous (mutant) animals in the liver, kidney, heart, and plasma reached a mean of 0.22 nmoles/mg/hr, 0.23 nmoles/mg/hr, 0.08 nmoles/mg/hr, and 0.5 nmoles/ml/hr respectively at the age of 5 months implying the lack of GLA enzyme activity (Figure 21A-21D).

Further, as a test of the phenotypic characterization of Fabry disease, the accumulation of lyso-Gb3 was determined by UHPLC MS/MS at a facility located in "Azienda Sanitaria Universitaria Integrata" in Udine, Italy. To determine the basal Lyso-Gb3 levels of plasma in untreated Fabry KO mice, 5-month-old male hemizygous (mutant) and wild-type blood plasma were sent for Lyso-Gb3 analysis. Figure 21E indicates the significant lyso-Gb3 accumulation in mutants (142.30 ng/ml), whereas wild-type male mice presented a very low value (0.49 ng/ml). This result offers confidence in the Fabry KO mouse colony and the representation of a clear Fabry disease phenotype in 5 months old hemizygous mice. This strain does not reveal evident phenotypic traits like the accumulation of Gb3 and lyso-Gb3 before the age of 5 months. Therefore, in the studies that follow, mice treated at different time points have all been sacrificed at least at 5 months of age to effectively judge the efficiency of the treatment by measuring the accumulation of substrate.

Immunofluorescence was also done to confirm the accumulation of Gb3 in tissue sections of the liver and kidney of 5 months old hemizygous and wild-type male mice. An anti-Gb3-specific antibody [Anti-Gb3 Monoclonal Antibody; A2506; TCI] was used to see the Gb3 accumulation in red, indicated by white arrows in mutant liver and kidney sections. The Gb3 distribution was found to be non-homogenous throughout the screened tissue section. However, the difference in the wild-type and mutant tissues was evident since Gb3 was hardly visible in wild-type animals (Figure 21F).

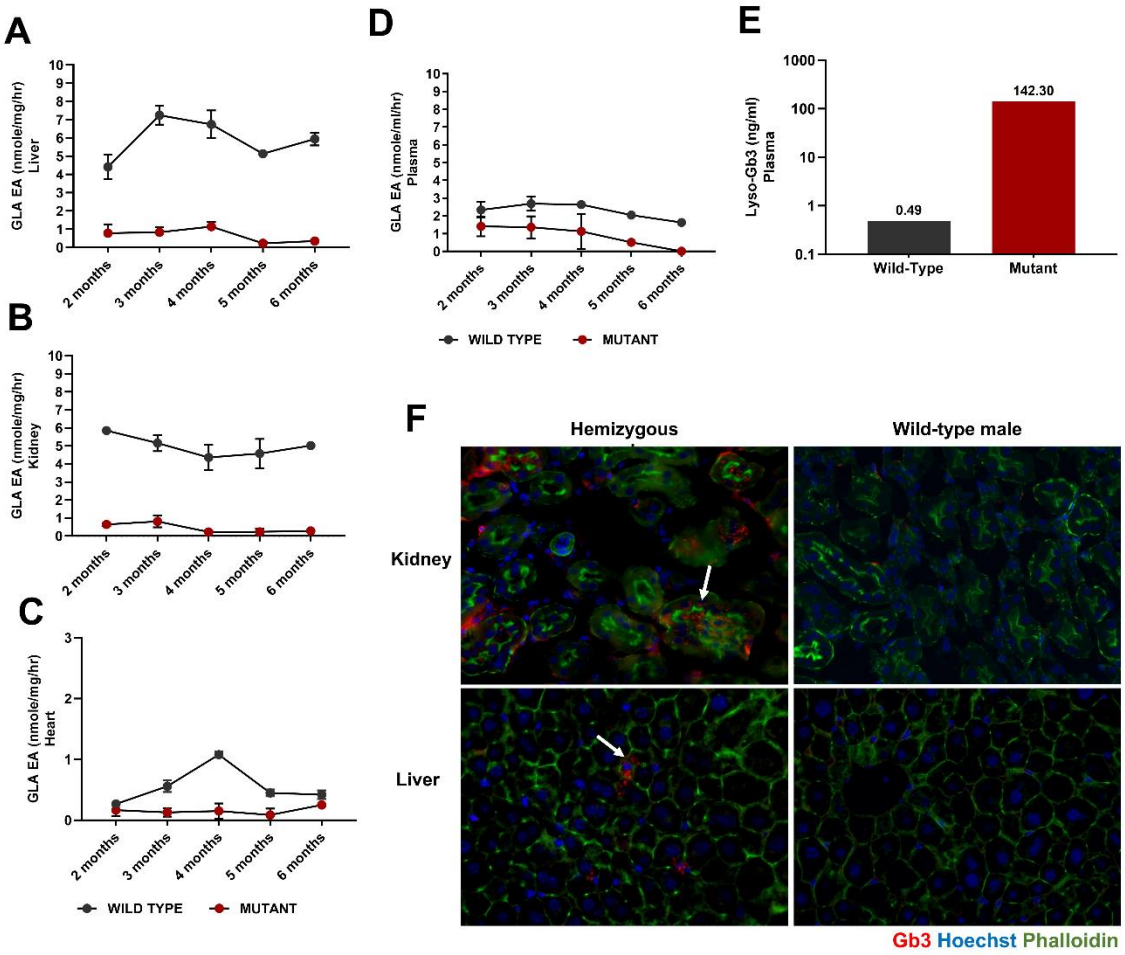

Figure 21. Characterisation of Fabry KO mice. Male Fabry KO animals (n=2) aged 2-, 3-, 4-, 5-, and 6 months were sacrificed, the liver, kidney, and heart were harvested, and blood was collected to extract plasma. Proteins were extracted from the tissue homogenates and GLA enzyme activity assay was done in A) liver B) kidneys and C) heart for all the animals (nmoles/mg/hr). D) GLA enzyme activity was analysed in the plasma isolated from the collected blood (nmoles/ml/hr). E) Lyso-Gb3 accumulation was measured in plasma of 5-months old male hemizygous and wild-type mice (ng/ml) with mass-spectrometric analysis. F) Kidney and liver sections of 5-month-old hemizygous and wild-type male mice were cryopreserved for immunofluorescence with Anti-Gb3 antibody (red), Phalloidin (green) and the nucleus was stained with Hoechst (blue). The white arrows mark the Gb3 accumulation in the hemizygous animals.

4.4 Potential therapy for late-onset Fabry disease

As explained earlier, depending on the onset, Fabry disease can be classified into two variants i.e., the early-onset and the late-onset. In the following studies, experiments have been designed to target the late onset of FD, by keeping in mind the results obtained from 'optimal conditions of gene-based therapies.' 1-month-old (P30) hemizygous male Fabry KO mice were chosen in anticipation of efficient treatment in juvenile mice mimicking late-onset Fabry disease.

4.4.1 AAV-based gene therapy for juvenile Fabry KO mice

Based on previous results obtained by testing different codon-optimized variants of the human GLA gene, hGLA_CO02 proved to be more efficient than wild-type human GLA, therefore all experiments will be done with hGLA_CO02 and the hGLA_WT. In order to obtain proof of principle and a minimum effective dose for a potential therapy for Fabry disease in juvenile mice, AAV-based gene therapy was performed.

4.4.1.1 Minimum effective dose of AAV-based episomal gene therapy

AAV8 vector stocks were prepared in the AAV facility at ICGEB, Trieste using the pSMD2_hAAT-ApoE_hGLA plasmids containing the liver-specific promoter from human Alpha-1 antitrypsin (α-1hAAT), human apolipoprotein E enhancer (ApoE) (Ronzitti et al., 2016) and HBB2 intronic sequence for enhanced expression, flanked by AAV ITRS, nomenclature as, AAV8 pSMD2_hGLA WT and AAV8 pSMD2_hGLA CO02. One-month-old (P30) juvenile hemizygous Fabry KO mice (n=5) were

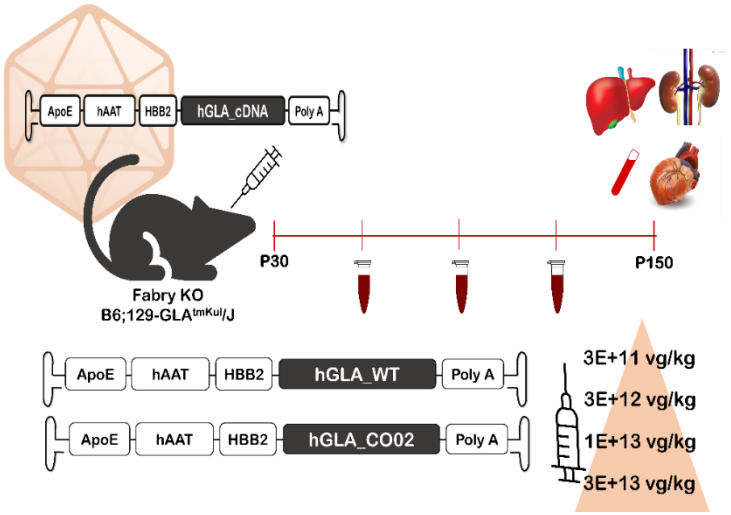

Figure 22. Experimental set-up to study the dose-response of AAV-based gene therapy in Fabry KO mice. Hemizygous male mice (n=5) were treated with either AAV8-pSMD2_hGLA WT or AAV8-pSMD2_hGLA CO02 viral vectors at the dose of 3.0E+13 vg/kg, 1.0E+13 vg/kg, 3.0E+12 vg/kg and, 3.0E+11 vg/kg. Animals were injected retro-orbitally at P30 and sacrificed at 5 months of age. Blood was collected at intermediate time points and at termination along with harvesting the liver, kidneys, and heart for analysis. Age-matched untreated hemizygous males (B6;129-Glatm1Kul/J) and wild type (B6;129sf2/J) were used as controls.

treated with either AAV8 pSMD2_hGLA_WT or AAV8 pSMD2_hGLA_CO02 at four different doses, 3.0E+13 vg/kg, 1.0E+13 vg/kg, 3.0E+12 vg/kg and, 3.0E+11 vg/kg to establish a dose-response in terms of GLA enzyme activity levels and lyso-Gb3 accumulation in tissues and blood plasma. Mice were injected via the retro-orbital route and blood was collected at intermediate time points. Age-matched untreated hemizygous males (B6;129-Gla^{tm1Kul}/J) and wild-type (B6;129sf2/J) animals were used as controls. All the animals were sacrificed after 4 months of treatment at P150. The liver, kidneys, and heart were harvested, and blood was collected for blood plasma analysis (Figure 22).

All the treated and untreated animals were weighed at intermediate time points throughout the timeline of the experiment and no significant changes were observed in either AAV8 pSMD2_hGLA WT (Figure 23A) or AAV8 pSMD2_hGLA CO02 (Figure 23B) compared to untreated mutants or wild-type controls.

AAV viral genome copies were measured in the treated animals in expectation to assess the technical consistency of injections and a dose-dependent response in the viral genome particle (VGP) copies/cell with the decrease in the dose. Genomic DNA extracted from liver homogenates was quantified and used as a template to amplify the promoter region of the AAV8 pSMD2 vector. The measurement of these AAV episomes was done using quantitative RT-PCR as described in the Materials and Methods Section. Figure 23C bars represent the mean of VGP/cell of the groups treated with episomal vector (scale: log 10). The graph indicates a dose-dependent reduction in VGP/cell with the decrease in dosage of the AAV8 episomal vector. No significant changes within hGLA_WT and hGLA_CO02 specific treatments were observed validating the technical consistency.

In order to test the efficiency of AAV-based gene therapy on Fabry KO mice, blood was collected at intermediate time points and at sacrifice as mentioned in the Materials and Methods section. Plasma (2 µl) from blood collected at P45, P60, P90, P120, and P150 from all the treated and untreated animals was assessed for GLA enzyme activity. Figure 24A represents GLA enzyme activity (nmoles/ml/hr) in a logarithmic scale in the blood plasma of AAV8 pSMD2_hGLA WT and AAV8 pSMD2_hGLA CO02 treated at different doses. When compared to the enzyme activity in untreated hemizygotes (black) and wild-type (grey), all the groups reached supraphysiological levels of activity. Observing the trend lines, it is ideal to note that the treatment was stable till the end of the experiment.

For better understanding Figure 24B, focuses on the GLA enzyme activity at 5 months of age i.e., after 4 months of treatment. From the bars, an evident dose-response can be appreciated. Although not significant, hGLA_CO02 (dotted bars) was able to increase enzyme activity more efficiently than hGLA_WT (red bars) with a difference of 3.2x in animals treated at 1.0E+13 vg/kg, 3.8x in 3.0E+12 and 14x in 3.0E+11 vg/kg between the two, except in animals treated at 3.0E+13 vg/kg where a drop in enzyme activity was observed in plasma at the initial timepoints which was later stabilized.

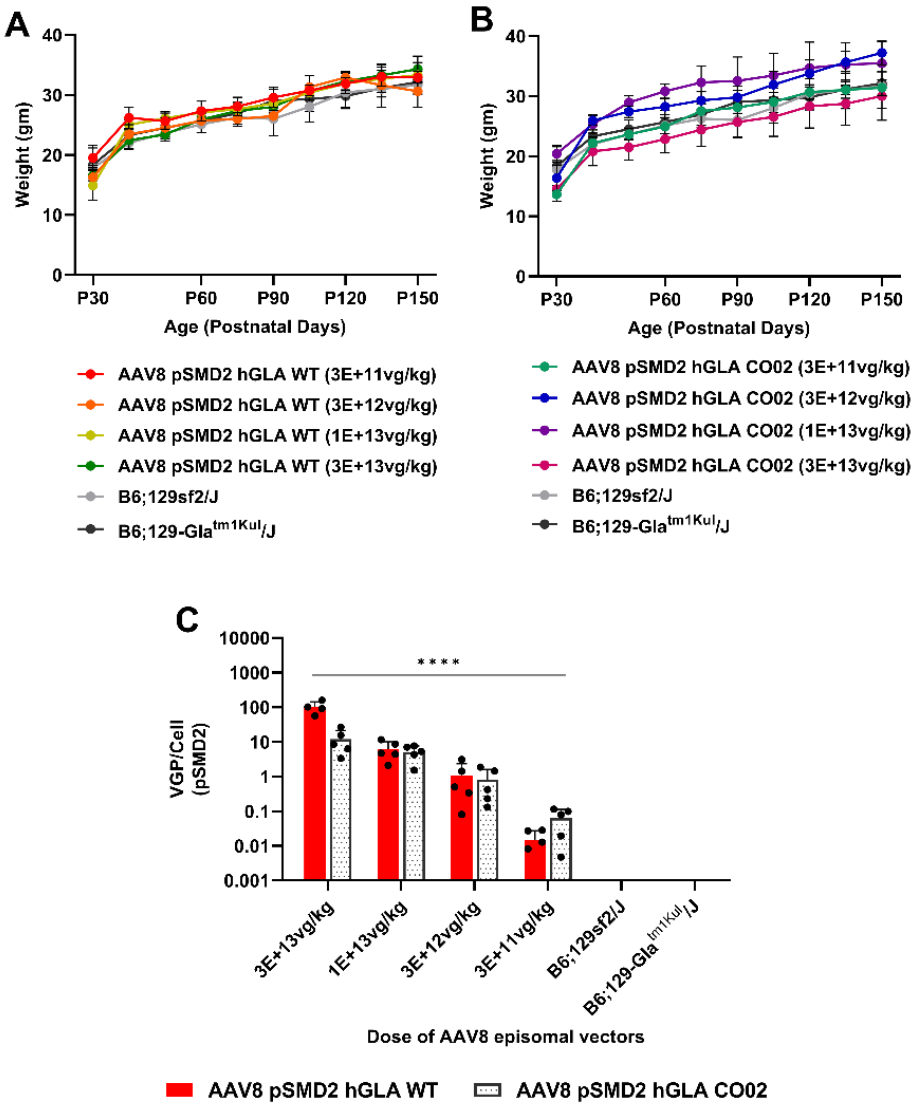

Figure 23. Assessing the effect of a dose study on viral genome copies and weights in Fabry KO mice treated with AAV-based gene therapy. Hemizygous male mice (n=4/5) were treated with either AAV8-pSMD2_hGLA WT or AAV8-pSMD2_hGLA CO02 viral vectors at the dose of 3.0E+13 vg/kg, 1E+13 vg/kg, 3.0E+12 vg/kg and, 3.0E+11 vg/kg. A and B) All the animals were weighed at intermediate time points throughout the experiment along with untreated controls. C) Quantitative RT-PCR was done with genomic DNA extracted from liver homogenated to amplify the promoter region on the AAV8 pSMD2 vector to estimate viral genome copies/cell in the treated animals. The red bars and dotted bars indicate the mean of vgp/cell present in the livers of AAV8 pSMD2_hGLA WT and AAV8 pSMD2_hGLA CO02 treated mice at different doses. Mean±SD, two-way ANOVA (p*<0.05, **<0.001, ***<0.0001).

After the promising GLA enzyme activity results, it was necessary to assess if the therapy was able to rescue the phenotype by evaluating lyso-Gb3 accumulation in plasma. Figure 24C represents the percentage of lyso-Gb3 levels at P45, P60, P90, P120, and P150 in the treated animals, considering the mean of lyso-Gb3 accumulation in untreated hemizygous animals at P150 as 100%. The results are in line with the data acquired from the GLA enzyme assay, with a dose-dependent response to the lyso-Gb3 levels and demonstrating stable substrate reduction over time. Animals treated at 3.0E+13vg/kg

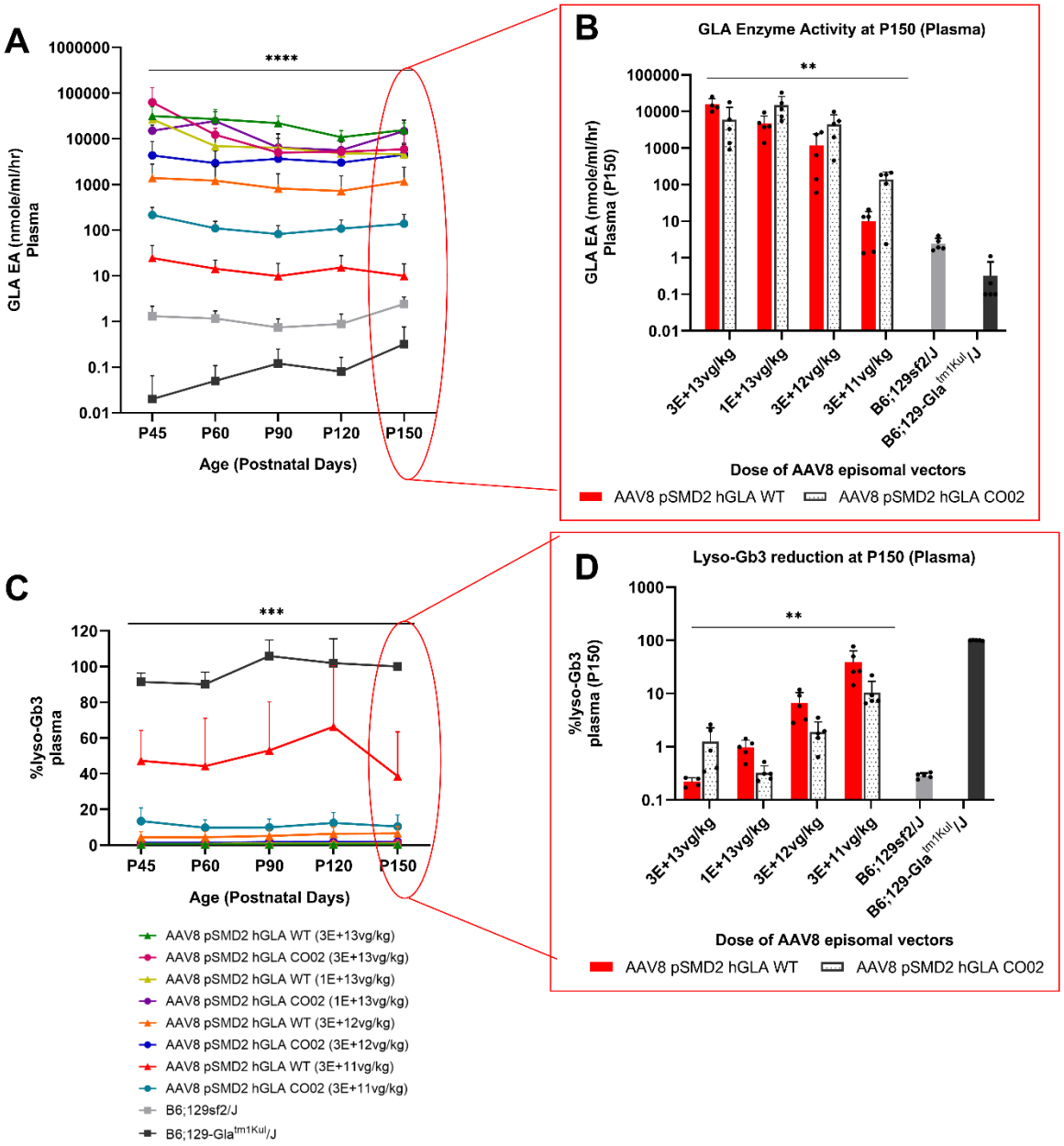

Figure 24. Evaluating FD phenotype in the blood plasma of Fabry KO mice treated with AAV-based gene therapy. Hemizygous male mice (n=4/5) were treated with either AAV8-pSMD2_hGLA WT or AAV8-pSMD2_hGLA CO02 viral vectors at the dose of 3.0E+13 vg/kg, 1E+13 vg/kg, 3.0E+12 vg/kg and, 3.0E+11 vg/kg. A) GLA enzyme activity was measured in blood plasma collected at different time points at P45, P60, P90, P120, and P150 for all treated and untreated animals. The graph demonstrates the mean of the activity (nmoles/ml/hr) at a particular time point. B) Bar graph representation of enzyme activity at P150. C) Lyso-Gb3 levels were measured in blood plasma collected at different time points during the experiment. The lyso-Gb3 levels have been indicated at percentage, considering the mean lyso-Gb3 levels in untreated hemizygous mice as 100%. D) The bar graphs represent lyso-Gb3 at P150. Mean±SD, REML or two-way ANOVA (p*<0.05, **<0.001, ***<0.0001).

and 1E+13vg/kg were able to reduce substrate accumulation by 99-100%. Treatment with 3.0E+12vg/kg reached 96-99% reduction whereas, with the lowest dose of 3.0E+11vg/kg, hGLA_WT, and hGLA_CO02 managed to clear out 61% and 90% lyso-Gb3 in blood plasma respectively at the end of the experiment (P150).

It is interesting to note hGLA_CO02 was more efficient in clearing the lyso-Gb3 accumulation in plasma when compared to its wild-type counterpart by 3x, 3.5x, and 3.7x when dosed at 1.0E+13 vg/kg, 3.0E+12 vg/kg and 3.0E+11 vg/kg respectively. However, animals treated with hGLA_CO02 at 3.0E+13 vg/kg showed 5.7x less clearance than hGLA_WT-treated animals. A similar effect was observed with the GLA enzyme assay. According to the VGP data in figure 23C, there is a noticeable reduction in viral copy numbers in animals treated with hGLA_CO02 at the highest dose, which confirms the compromised efficacy of the codon-optimized construct.

As a hypothesis, this reduction can be explained by the elimination of GLA proteins-containing cells by the induction of immune response caused by endoplasmic reticulum (ER) stress. This ER stress could be generated due to the production of very high levels of GLA proteins in AAV-transduced cells, which is noticed at P45 (GLA enzyme activity, Figure 24A) hence, compromising the overall enzyme activity and lyso-Gb3 reduction efficiency of the hGLA_CO02-treated mice, when compared with hGLA_WT at 3.0E+13vg/kg (Figure 24B and 24D). This hypothesis could be a probable explanation for the phenomenon, which needs to be confirmed.

Due to the secretory nature of the GLA proteins, it was essential to assess the biodistribution and uptake of the GLA delivered through episomal gene therapy. The liver, which is the AAV-target organ, along with kidneys and heart homogenates were prepared for assessments (Figure 25A-C). The enzyme assay done with proteins extracted from the tissues showed elevated activity levels when compared to untreated wild-type controls with an evident dose-response. The animals treated with hGLA_CO02 had ~2-4x higher activity in the kidneys and heart than animals treated with hGLA_WT which confirms the efficient uptake and activity of the codon-optimized version in non-AAV-target organs.

When these tissues were tested for their lyso-Gb3 accumulation, the treatment dosed at 3.0E+13 vg/kg, 1.0E+13 vg/kg and 3.0E+12 vg/kg reduced the substrate by 98-100% regardless of the tissue type (Figure 25D-F). However, the lowest dose with hGLA_WT managed to clear 74.6%, 44.8%, and 47.2% substrate from the liver (Figure 25D), kidney (Figure 25E), and heart (Figure 25F) respectively. On the contrary, 96.5%, 91.3%, and 86% substrate was removed from the later organs with the codon-optimized treatment. This result confirms the higher efficiency of the codon-optimized GLA, able to revert the substrate phenotype even with the lowest dose.

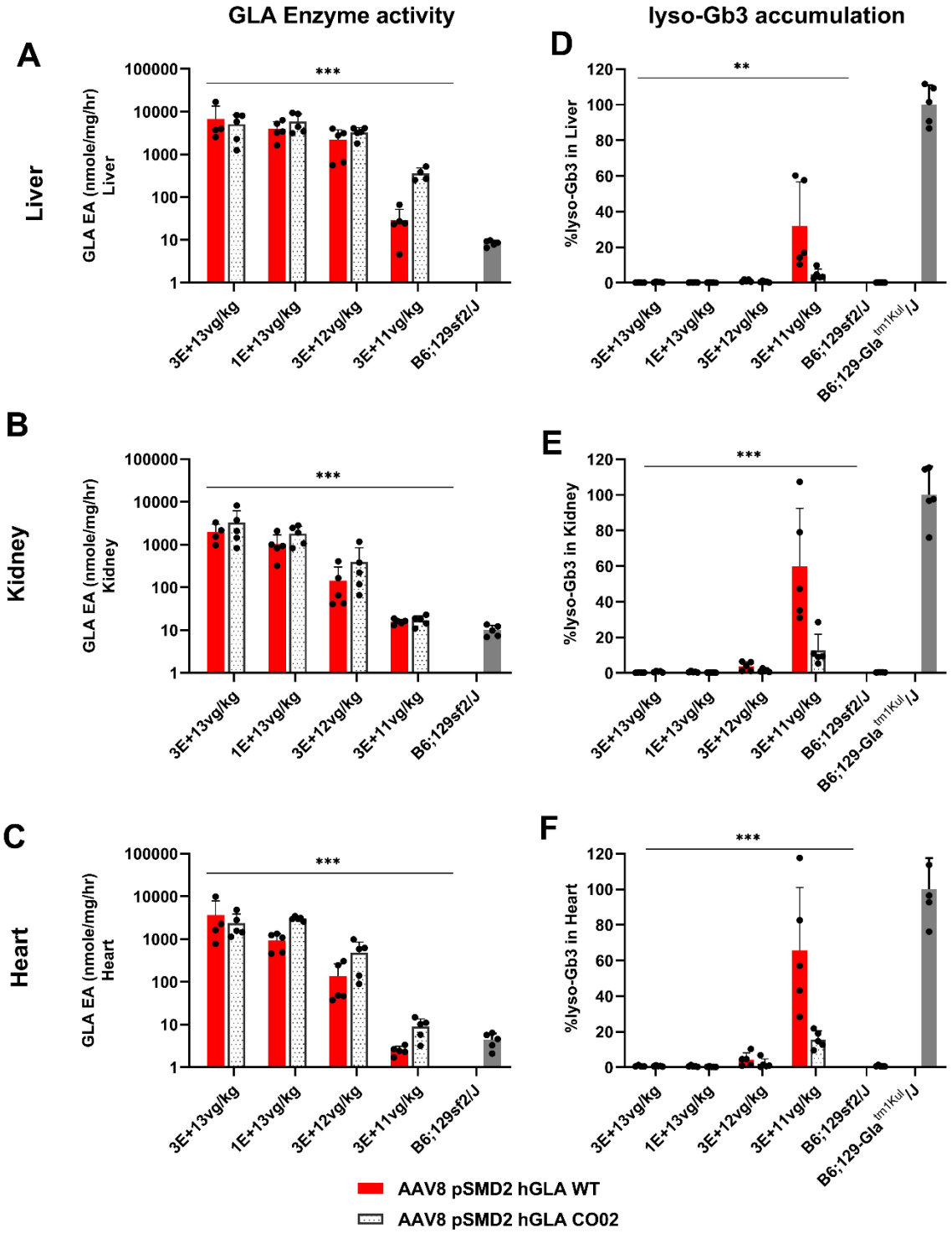

Figure 25. Evaluating biodistribution and phenotype in the tissue of Fabry KO mice treated with AAV-based gene therapy. Juvenile (P30) Fabry KO mice were treated with AAV8-pSMD2_hGLA WT or AAV8-pSMD2_hGLA CO02 viral vectors at the dose of 3.0E+13 vg/kg, 1E+13 vg/kg, 3.0E+12 vg/kg and, 3.0E+11 vg/kg. GLA enzyme activity was measured in proteins extracted from homogenates of A) liver B) Kidney and C) heart. (nmoles/mg/hr). The bars represent the mean of GLA enzyme activity after 4 months of treatment. D) liver, E) kidney and F) heart tissue homogenates were homogenized in water to measure for lyso-Gb3 accumulation. The bars represent the mean percentage lyso-Gb3 levels after 4 months of treatment. Mean±SD Two-way ANOVA (p*<0.05, **<0.001, ***<0.0001).

The GLA protein production levels of the liver as the target organ were measured using a western blot analysis. An anti-GLA antibody was used to detect the GLA-specific bands. The blot in Figure 26 is representative of the GLA expression of the treatment. The reduction in the intensity of the bands with the reduction in the dose is evidence of a dose-dependent response with a clear difference in the higher expression of hGLA_CO02 treated bands when compared to hGLA_WT. For quantitative analysis, the band intensities were quantified and normalized with the HSP70 housekeeping gene and plotted on the bar graph in Figure 26. The mean of the treatments reduced with the dose and confirmed the finding of the GLA enzyme assay and the lyso-Gb3 mass-spectrometric analysis.

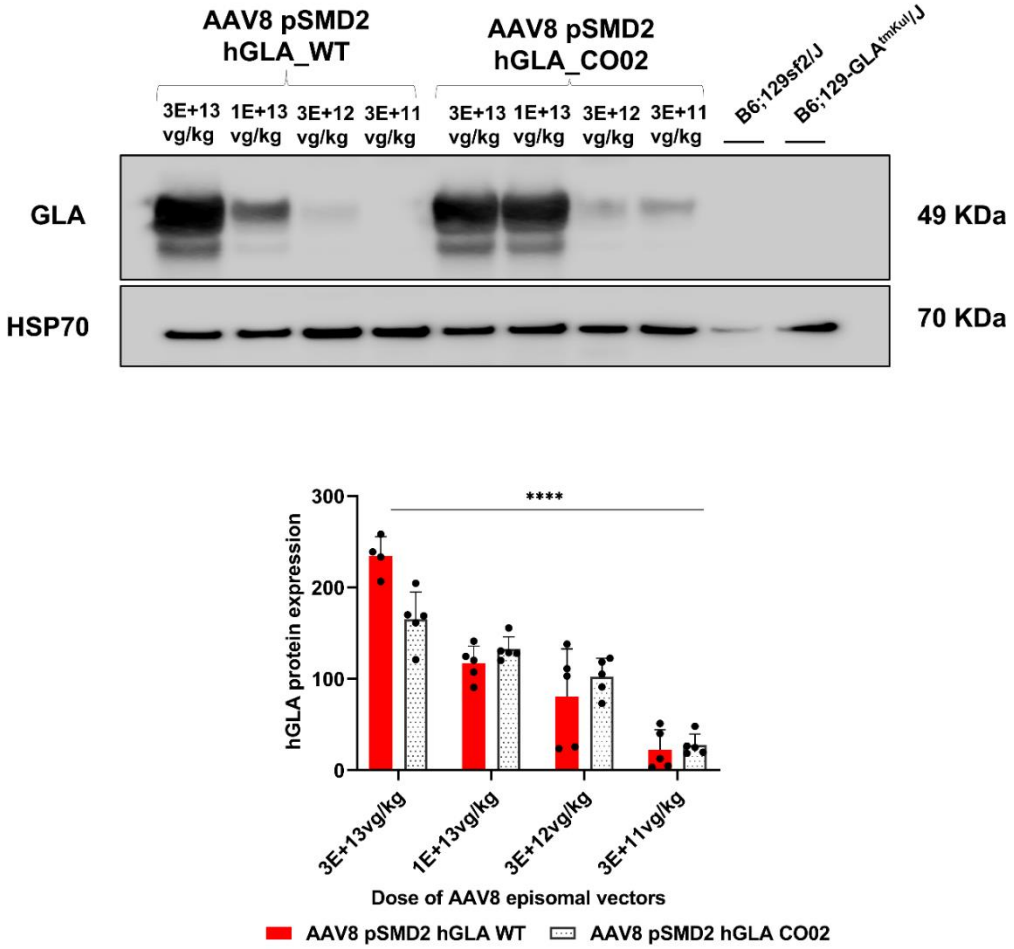

Figure 26. Evaluating GLA protein production in Fabry KO mice treated with AAV-based gene therapy. Hemizygous male mice were treated with either AAV8-pSMD2_hGLA WT or AAV8-pSMD2_hGLA CO02 viral vectors at the dose of 3.0E+13 vg/kg. Proteins extracted from liver homogenates were used to run an SDS-PAGE gel. Western blot analysis was done with the treated animals with Anti-GLA antibody to detect GLA proteins on the blot and HSP70 specific antibody was used as a housekeeping protein. The blot shown is representative of all the treatment groups. The bar graph represents the quantified and normalized values of the bands obtained from all the animals treated at different doses. Mean±SD, Two-way ANOVA (p*<0.05, **<0.001, ***<0.0001).

4.4.1.2 Immune response associated with AAV-based gene therapy

As mentioned above, in the case of animals treated with 3.0E+13vg/kg of AAV8 pSMD2_hGLA CO02 vectors, a reduction in the GLA enzyme activity levels was observed in plasma after 15 days of treatment (P45) which stabilized at later time points. To address this phenomenon, expression levels of immune markers in the liver homogenates harvested after 4 months of treatment with AAV8 pSMD2_hGLA WT and CO02 were studied using quantitative RT-PCR (Figure 27A). TNFα (Tumour Necrosis Factor-alpha), NFκβ (Nuclear factor kappa-light-chain-enhancer of activated B cells), CD86 (Cluster of Differentiation 86), IL6 (Interleukin 6) were measured as markers of innate and adaptive immune response whereas, GRP78 (Glucose-Regulated Protein 78) and CHOP (C/EBP Homologous Protein) were evaluated due to the speculation of potential ER stress. Although statistically insignificant, an increase in TNFα, NFκβ, and IL6 was observed with significant upregulation in CD86.

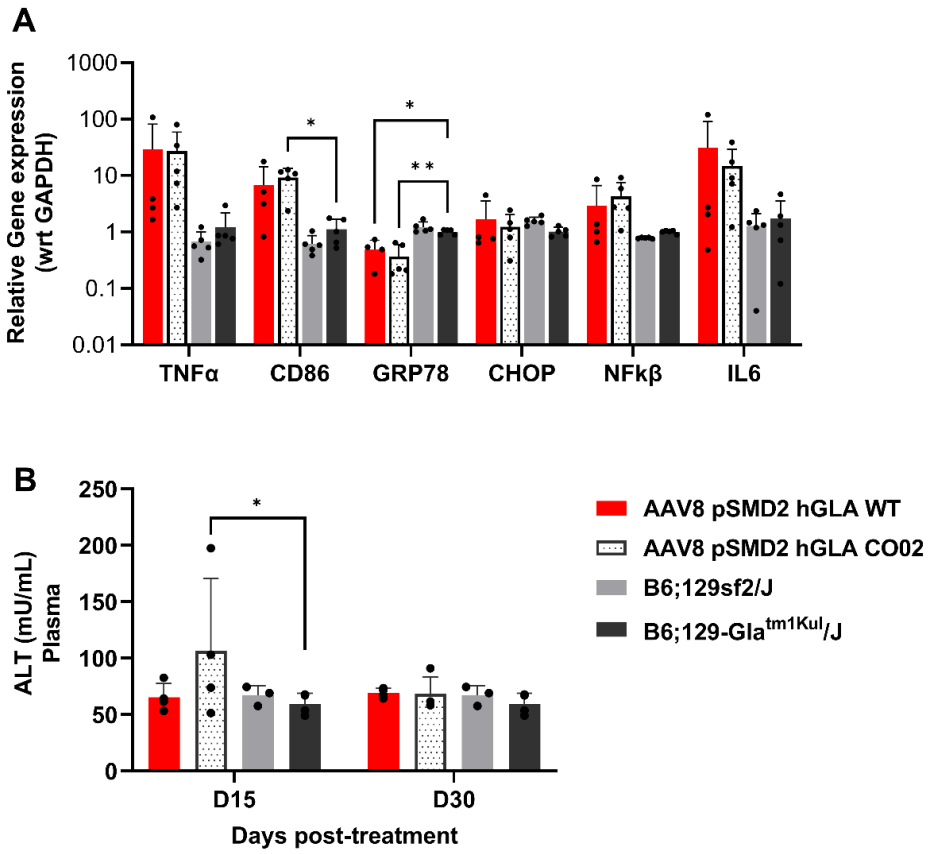

Figure 27. Evaluating immune response markers in Fabry KO mice treated with AAV-based gene therapy. Hemizygous male mice were treated with either AAV8-pSMD2_hGLA WT or AAV8-pSMD2_hGLA CO02 viral vectors at the dose of 3.0E+13 vg/kg. A) RNA was extracted from liver homogenates harvested 4 months post-treatment and later converted to cDNA. Gene expression of different immune response markers (TNFα, NFκβ, CD86 and IL6) and ER stress markers (GRP78 and CHOP) were measured using quantitative PCR and compared to untreated hemizygous and wild-type animals. mGAPDH was used as housekeeping gene to normalize the expression values. The bars represent the mean of the normalized expression levels of treated and untreated mice. B) ALT enzyme assay was done with plasma samples collected at P45 (or D15 and P60 (or D30). The bars represent the mean of the animals in a particular group. Mean±SD, two-way ANOVA (p*<0.05, **<0.001, ***<0.0001).

According to a study in healthy conditions, GRP78 controls the stability of survival pathways like ER signaling molecules and caspases (Miao Wang *et. al.*, 2009). However, under stress conditions, GRP78 is tittered away to unblock these protective pathways. In our study, GRP78 was significantly downregulated indicating an ER-stress environment. CHOP expression was within the normal range in all the treated samples.

To further comprehend the condition, ALT (alanine transaminase) levels were measured in plasma collected from the treated and untreated samples after 15- and 30-days post-treatment. ALT is a liver transaminase that is released into the bloodstream in case of liver damage. Figure 27B shows a statistically significant increase in ALT levels in animals treated with AAV8 pSMD2_hGLA CO02 after 15 days post-treatment compared to untreated hemizygotes, which later drops to a normal range after another 15 days (D30). However, the increase in ALT levels was variable and it was not observed in all the animals of the group.

4.4.2 Gene targeting with AAV vectors containing mALB homology arms in juvenile Fabry KO mice

Genome editing has the potential to overcome the limitations associated with episomal gene therapy by targeting the genome and integrating the transgene, permanently avoiding the reduction of transgene expression due to the loss of AAV episomes. Gene Ride™ (Figure 28) is a genome targeting strategy developed by Mark. A. Kay's team at Stanford in 2015 where a recombinant AAV (rAAV) was used to deliver a promoterless construct containing the human coagulation factor 9 cDNA, with a preceding P2A peptide, flanked by mouse albumin homology arms, to hemophilia B mice (A Barzel et al. 2015). This donor vector targets the albumin locus using the two homology arms at each end. The endogenous albumin promoter controls the production of the albumin and coagulation factor 9 as a chimeric mRNA. The chimeric mRNA then translates into two separate proteins: albumin and Factor 9, with the aid of a P2A peptide executing ribosomal skipping (A Barzel et al. 2015). In another study of our laboratory, Gene Ride™ was used to target the albumin locus of a Crigler-Najjar syndrome type I (CNSI) mouse model with a promoterless therapeutic UGT1A1 cDNA, which led to complete rescue of neonatal lethality and a long-term stable reduction in plasma bilirubin levels (Porro et al. 2017).

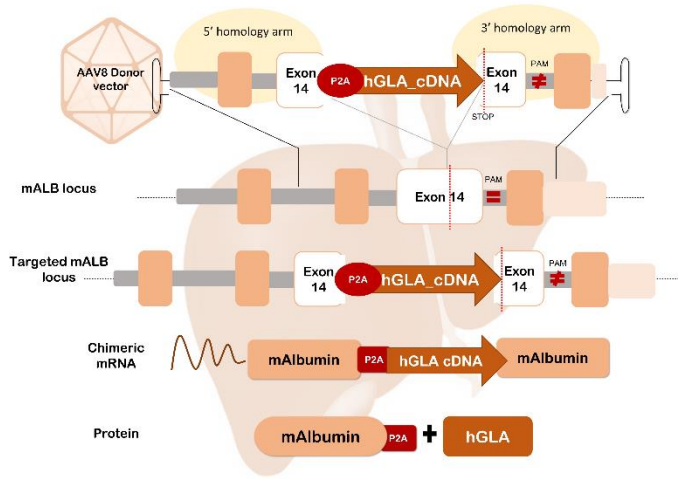

Figure 28. Genome targeting using Gene Ride™ technology. Schematic of the genome targeting construct containing a recombinant transgene with a P2A peptide sequence, flanked by mouse albumin homology at either side.

4.4.2.1 Gene targeting using CRISPR/Cas9 technology

Based on previous evidence supporting the success of genome targeting using Gene Ride technology, an experiment was designed to obtain a potential treatment for late-onset Fabry disease, directed towards the juvenile population of Fabry KO mice. To improve therapeutic efficacy, the donor vector was coupled with CRISPR/Cas9 system to increase the rate of homologous recombination.

Referring to figure 29, AAV stocks were prepared for hGLA_WT and hGLA_CO02 packaged with the donor vector AAV8 pAB 288_mAlb containing mouse albumin homology arms. These donor vectors

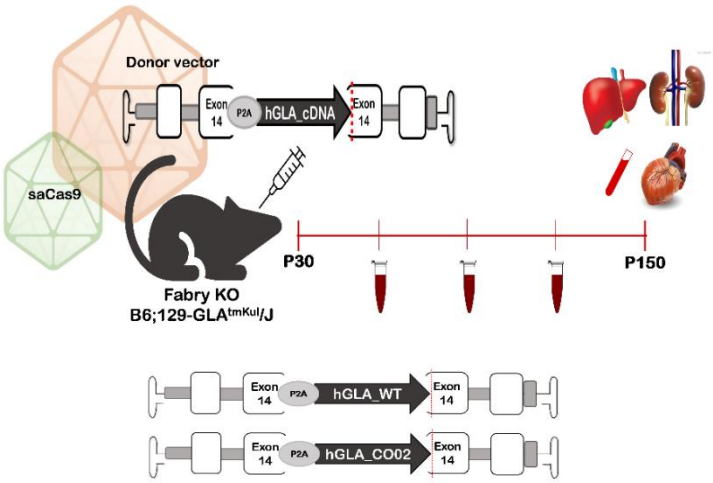

Figure 29. Experimental design for gene targeting using CRISPR/Cas9 technology in Fabry KO mice. Juvenile Fabry KO mice (P30) were treated with a donor vector containing mouse albumin homology arms and *hGLA* transgene (hGLA_WT or hGLA_CO02) via the retro-orbital route of injection. The donor vector was coupled with and without AAV8 pX602_sgRNA, a saCas9 harbouring vector. The experiment lasted for 4 months accompanied by blood collection at intermediate time points. The liver, kidneys, and heart were harvested at sacrifice (P150).

i.e., AAV8 pAB hGLA_WT and AAV8 pAB hGLA_CO02 will also be referred to as the WT Donor vector and CO02 Donor vector. Juvenile Fabry KO male mice (P30) were given WT Donor vector, or CO02 Donor vector at 3.0E+13vg/kg via the retro-orbital route of administration with and without AAV8 pX602_sgRNA vector containing the SaCas9 and single guide RNA (sgRNA).

All the animals were weighed at different time points (Figure 30A) till the termination of the experiment. The treatment had no significant alteration in the weights when compared to the untreated controls. Genomic DNA extracted from the liver homogenates was used to perform a digital droplet PCR (ddPCR) assay to determine the targeting rate. Figure 30B represents the ddPCR analysis in the percentage of homologous recombination in the samples treated with the donor vector only and the donor vector coupled with Cas9. Theoretically, the generation of DSB by CRISPR/Cas9 system increases the homologous recombination rate, however, the results of the ddPCR analysis did not meet the expectations since no difference in the percentage of HR was observed between the animals treated with and without Cas9 at P30.

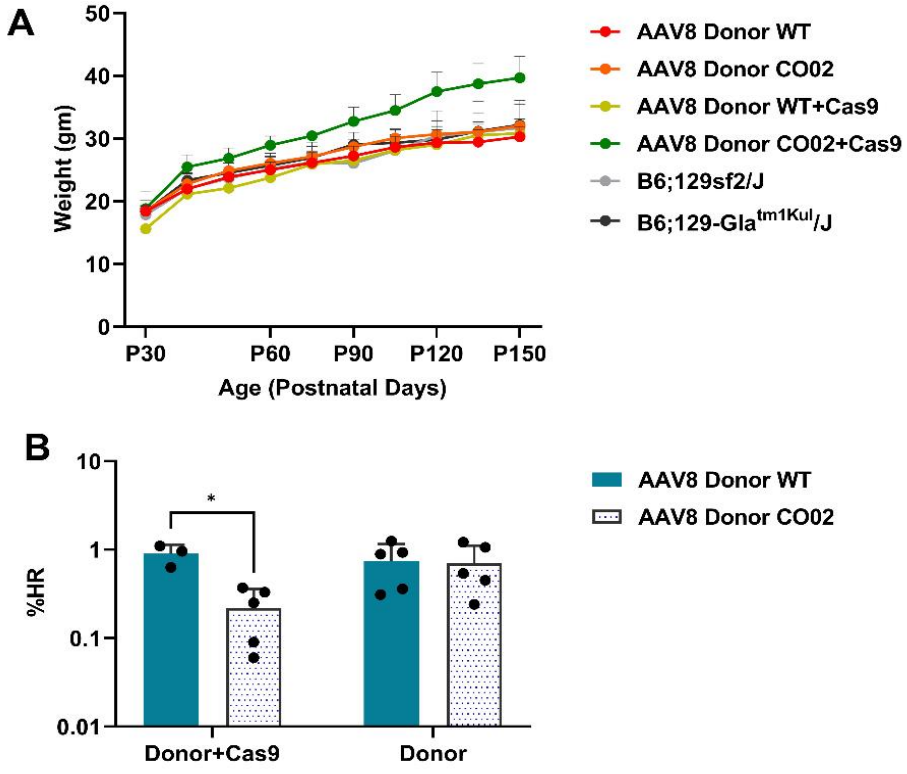

Figure 30. Assessment of the effect of integrative treatment on the weight of Fabry KO animals and evaluating the rate of homologous recombination. A) Weights of all the treated and untreated animals were monitored during the course of the treatment. B) Genomic DNA from liver homogenates was used to perform a ddPCR analysis to evaluate the rate of homologous recombination. The bars represent the mean of the percentage of homologous recombination of the particular treatment. Mean±SD. Two-way ANOVA (p*<0.05, **<0.001, ***<0.0001).

To determine the efficiency of the treatment, plasma isolated from the blood collected at different time points was assessed for GLA enzyme activity and lyso-Gb3 levels. Figure 31A represents the trend that follows post-treatment with hGLA_WT and hGLA_CO02 donor vectors coupled with and without Cas9 (Donor+Cas9). All treated animals showed elevated and stable GLA activity levels till the termination of the experiment. The treatment coupled with Cas9 was able to increase the activity in the plasma by 70x with hGLA_WT and 55x with hGLA_CO02 vector when compared to the treatment with Donor-only treated counterparts. The GLA enzyme activity at P150, plotted as a bar graph in Figure 31B showed 1.2-1.8x higher activity with hGLA_CO02 than with hGLA_WT. Further, to evaluate the effect of the treatment on substrate accumulation, lyso-Gb3 mass-spectrometric analysis was done in the

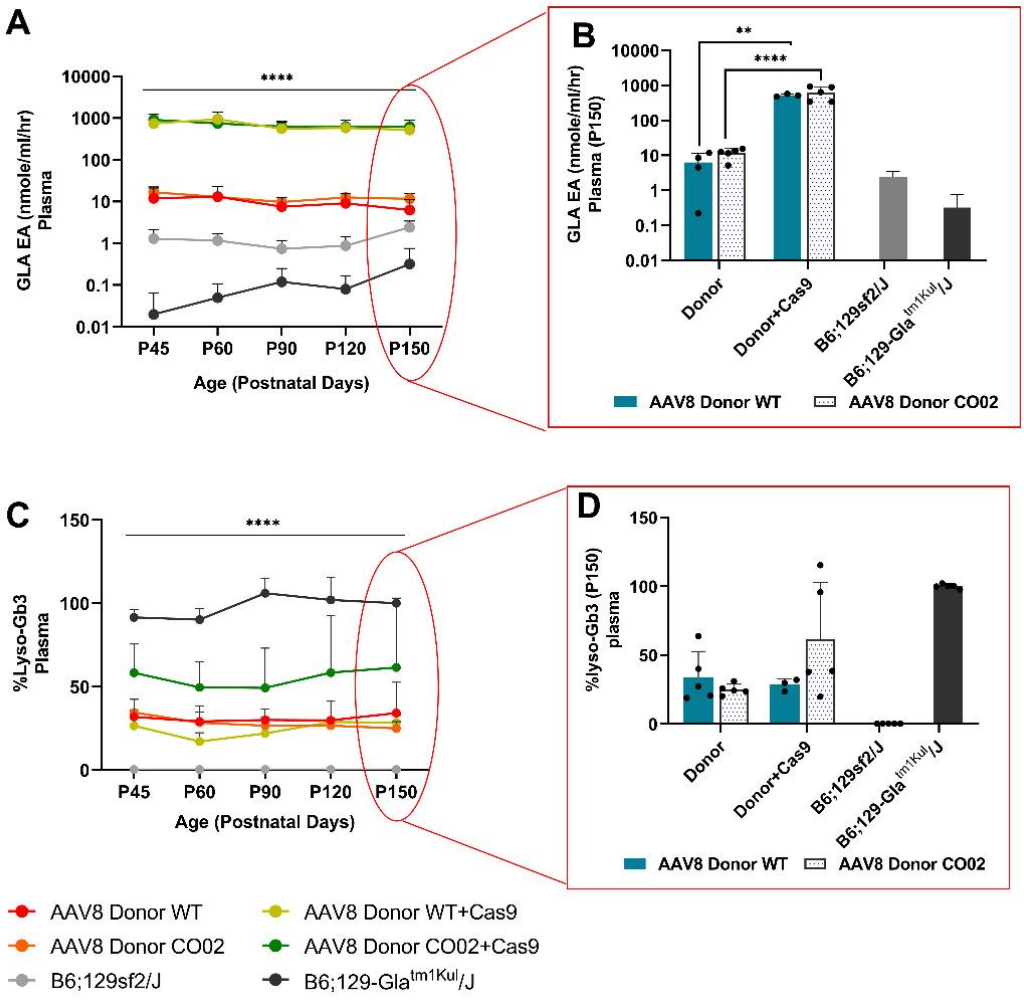

Figure 31.GLA enzyme activity and lyso-Gb3 accumulation in plasma after AAV integrative treatment. Juvenile Fabry KO mice (n=5, Donor WT+Cas9 n=3) were treated with either AAV Donor vector (hGLA_WT or hGLA_CO02 or coupled with Cas9. A) GLA enzyme activity was measured in plasma collected at intermediate time points (nmoles/ml/hr). B) the bars represent the mean of GLA enzyme activity obtained at P150 i.e., after 4 months of treatment. C) Mass-spectrometer was used to measure the lyso-Gb3 accumulation in plasma represented in the percentage of lyso-Gb3 accumulation. D)the bars represent the mean of percentage lyso-Gb3 levels at P150 or 4 months post-treatment. The lyso-Gb3 accumulated in the plasma of untreated hemizygous mice at P150 was considered 100%. Mean±SD, REML or Two-way ANOVA (p*<0.05, **<0.001, ***<0.0001).

plasma samples (Figure 31C-D). The treatments proved to be effective by reducing the accumulation in Fabry KO mice by 66% with Donor WT, 75% with Donor CO02, 72% in Donor WT+Cas9, and 39% with Donor CO02+Cas9 which was sustained until 5 months of age. The treatment with CRISPR/Cas9 system showed higher enzyme activity in the plasma however, it was not able to completely clear substrate accumulation.

The proteins extracted from the liver, kidney, and heart harvested at sacrifice were used to perform a GLA enzyme assay. Figures 32A, B, and C represent the GLA enzyme in the Liver, kidney, and heart respectively. In the case of animals treated with Donor vector+Cas9, there is a supraphysiological increase observed in all the tissues, whereas, in the case of animals treated with only the donor vector the GLA enzyme activity was higher than that of the untreated wild-type animals but did not reach levels high as in Donor+Cas9. In the liver (Figure 32A), Cas9 increased the activity by 58x and 14x with hGLA_WT and hGLA_CO02 respectively. The kidneys (Figure 32B) observed a more impressive increase of 120-144x with the two constructs coupled with the nuclease, similarly, the heart (Figure 32C) had 97-198x higher activity with Donor+Cas9 treatment. However, no specific trend of difference was observed between the wild-type and the codon-optimized GLA constructs.

Similar observations were made when these tissues were tested for lyso-Gb3 accumulation, the donor vector was effective in reducing the accumulated substrate in the liver (Figure 32D) by 84-86% with Donor WT, with and without the use of Cas9. Donor CO02 alone cleared 90% substrate however, with the aid of nuclease it was able to reduce only 55% lyso-Gb3. Figure 32E shows the accumulation percentage in the kidneys with 76% and 68% clearance using Donor WT and Donor WT+Cas9 and, 80% and 36% with Donor CO02 and Donor CO02+Cas9. Similar observations were made in the heart (Figure 32F) with 73%, 67%, and 84% reduction with Donor WT, Donor WT+Cas9, and Donor CO02 treatments respectively, Donor CO02+Cas9 removed 42% lyso-Gb3.

It must be noted that the treatment with donor vector was able to elevate GLA enzyme activity and clear lyso-Gb3 accumulation with and without the use of Cas9, however, the treatment did not meet the expected results. Donor vector coupled with Cas9 presented a supraphysiological level of GLA activity in plasma as well as in tissues but failed to match the lyso-Gb3 levels of untreated wild-type levels. Moreover, there were no significant differences observed between AAV8 pAB_hGLA WT (Donor WT) and AAV8 pAB_hGLA CO02 (Donor CO02) treated animals. Therefore, so far there is no validated evidence of the success of using nuclease to increase the efficacy of the donor vector treatment in this study.

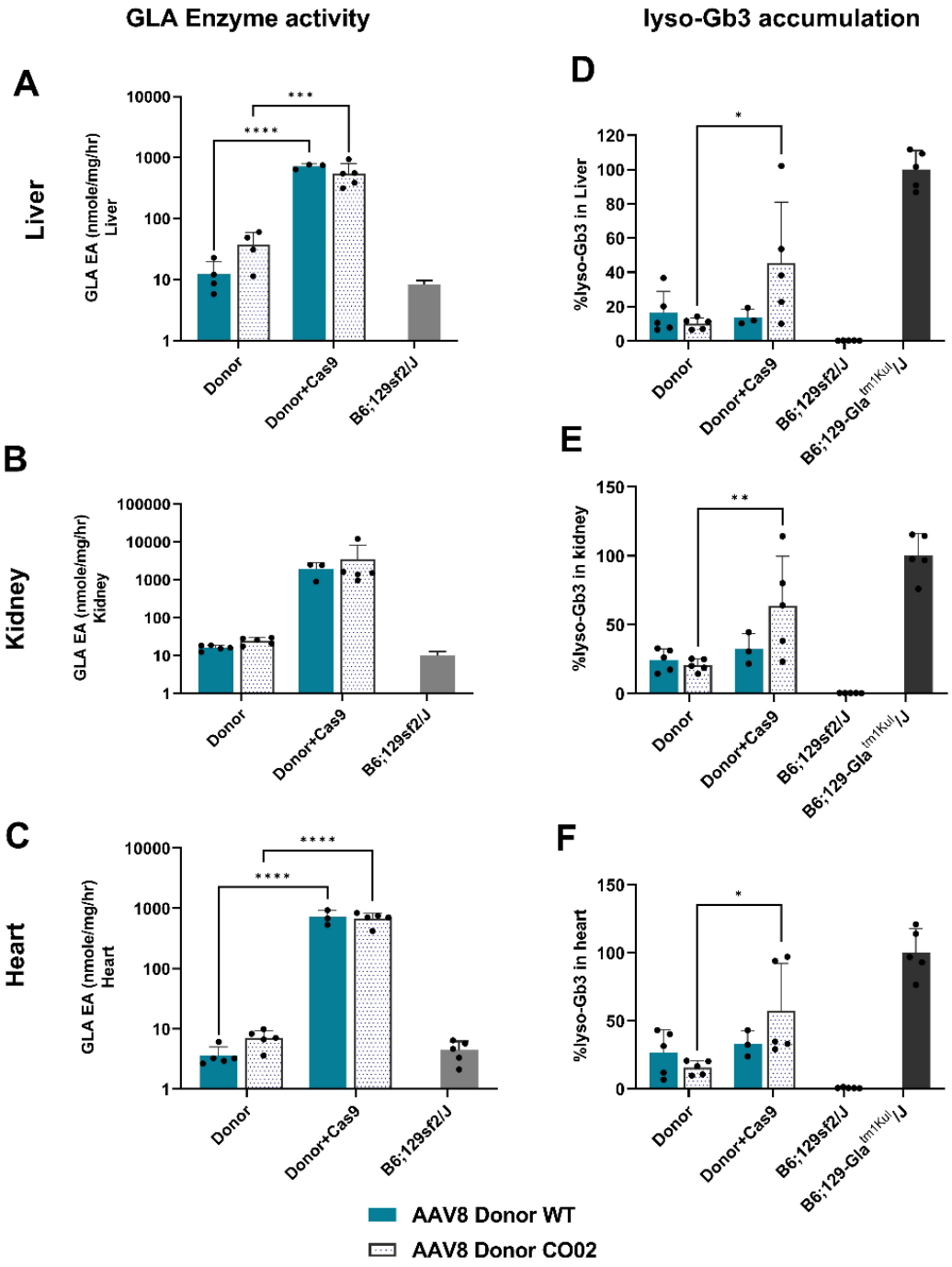

Figure 32. GLA enzyme activity and lyso-Gb3 accumulation in tissues after AAV integrative treatment. Juvenile (P30) Fabry KO mice (n=5, Donor WT+Cas9 n=3) were treated with either AAV Donor vector (hGLA_WT or hGLA_CO02) or coupled with Cas9. GLA enzyme activity was measured in proteins extracted from homogenates of A) liver B) Kidney and C) heart. (nmoles/mg/hr). The bars represent the mean of GLA enzyme activity after 4 months of treatment. Tissue homogenates were used to measure lyso-Gb3 accumulation. The bars represent the mean percentage lyso-Gb3 levels after 4 months of treatment in D) liver, E) kidney and F) heart. Untreated hemizygous tissue levels are considered 100% lyso-Gb3 accumulation. Mean±SD, Two-way ANOVA (p*<0.05, **<0.001, ***<0.0001).

4.4.2.2 Nuclease-free approach to gene targeting

The use of CRISPR/Cas comes along with its pros and cons. The primary risk associated with this technology is the potential off-targeting effect and activation of oncogenes, generating safety concerns. In order to address this issue, a study was designed to replace the Cas9-containing vector with Fludarabine, an FDA-approved drug known to increase the rate of homologous recombination (Tsuji et al. 2022). Fabry KO juvenile (P30) animals were treated with either Donor WT or Donor CO02 vector at 3.0E+13vg/kg. The treatment was coupled with the use of Fludarabine (in the absence of Cas9) and compared with a group of animals without drug exposure. Fludarabine was dosed at 375 mg/kg over the course of three days, by treating the animals intra-peritoneally with 125 mg/kg three times a day for three consecutive days. AAV8 donor vectors were retro-orbitally injected on day 1 (Figure 33).

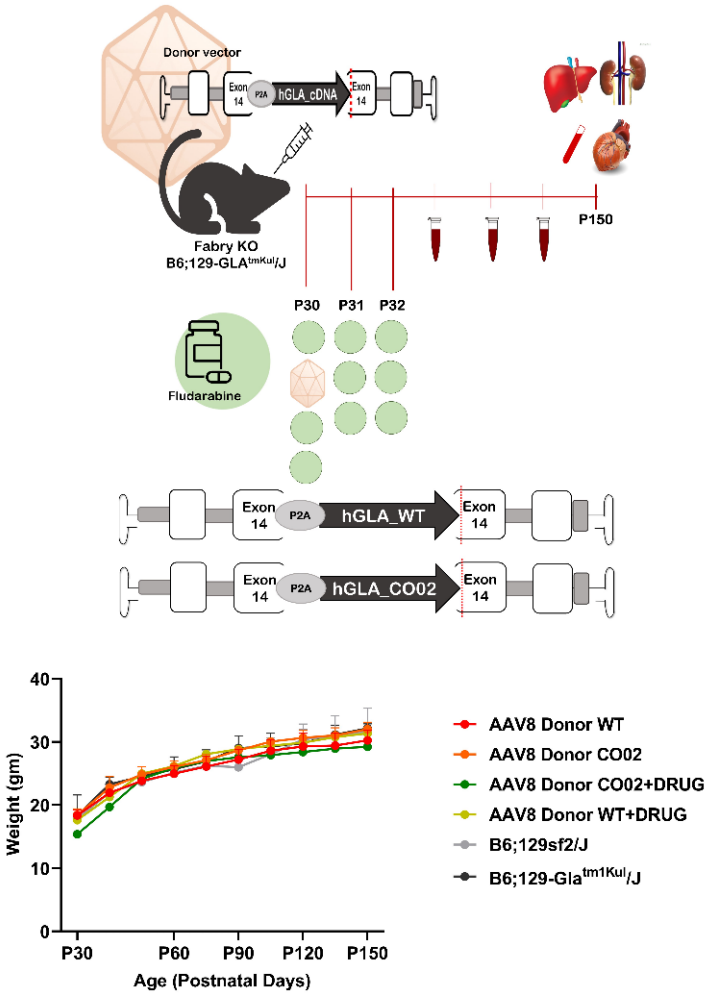

Figure 33. Nuclease-free approach to gene targeting in Juvenile Fabry KO mice. Juvenile (P30) Fabry KO mice (n=5) were treated with AAV Donor vector (hGLA_WT or hGLA_CO02) at 3.0E+13 vg/kg, coupled with Fludarabine at 375mg/kg. This drug was dosed at 125mg/kg per IP injection three times a day for three consecutive days. Intermediate blood was collected, and the animals were sacrificed at P150 or 4 months post treatment. Untreated wild-type and hemizygous Fabry KO males were considered as control animals. The liver, kidney, and heart were harvested for analysis. The weights of all the animals were monitored throughout the course of the treatment Mean±SD.

Untreated wild-type and hemizygous mice were used as controls. The treatment lasted for 4 months, with blood withdrawal at intermediate time points. The mice were sacrificed at P150, harvesting the liver, kidney, and heart. During the course of the treatment, the weight of all the animals was monitored (Figure 33). No significant changes were observed in the weights of the treated animals when compared to the controls.

For the assessment of the efficiency of the treatment, proteins extracted from liver homogenates were used to perform western blot analysis (Figure 34A-B). The blot was incubated with an Anti-GLA antibody to detect the GLA proteins and HSP70 specific antibody was used to detect the housekeeping gene. The quantification of the Western blot analysis after normalization represented in Figure 34B indicates a small increase in protein production of GLA protein when the donor vector was coupled with Fludarabine, however, these minor differences were statistically insignificant. It is also important to observe the 1.08x higher protein production with Donor CO02 when compared to Donor WT.

The liver homogenates were also used to extract genomic DNA which was later used to evaluate the percentage rate of homologous recombination by a digital droplet PCR. Figure 34C demonstrates the quantification of the PCR technique showing no major differences in the homologous recombination efficiency. Although protein production slightly increased due to the use of Fludarabine, the HR rate did not match the expected increase mediated by fludarabine.

Blood collected from the treated and untreated animals at intermediate time points throughout the course of the experiment was evaluated for GLA enzyme activity. Plasma isolated from the blood samples was measured for enzyme activity (nmoles/ml/hr), and represented in Figure 35A, which shows elevated levels of GLA activity when compared to untreated wild-type animals which were stable until the termination of the experiment. From the plasma activity at P150 (Figure 35B), it is clear that Donor+drug treated animals certainly have up to 5x higher GLA enzyme activity with Donor WT and 1.4x higher with Donor CO02 treatment.

Similarly, the plasma isolated was also checked to estimate the lyso-Gb3 accumulation with mass-spectrometric analysis. Figure 35C shows the percentage of lyso-Gb3 in the blood of treated animals when compared to untreated hemizygous males with 100% substrate. The treatment was able to reduce the accumulation by at least 70% in all treated groups which were stable until the end of the experiment.

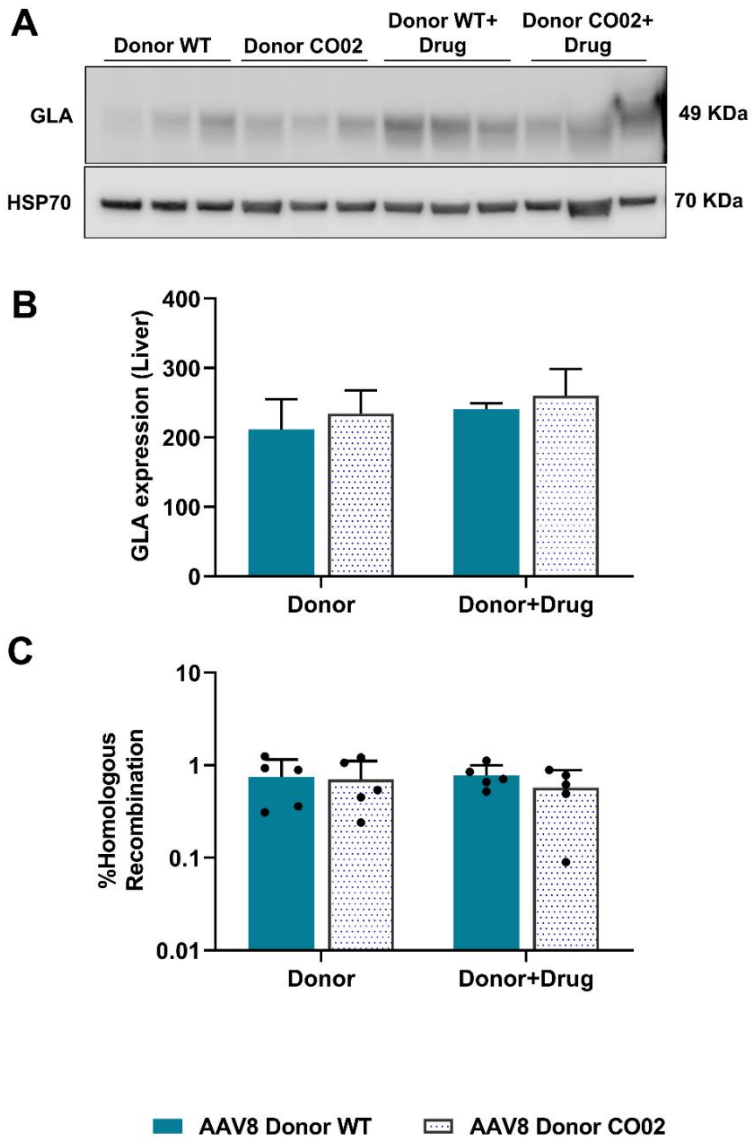

Figure 34. Assessment of Nuclease-free approach to gene targeting on protein production and recombination rate. Juvenile (P30) Fabry KO mice were treated with AAV Donor vector (hGLA_WT or hGLA_CO02) at 3.0E+13 vg/kg, coupled with Fludarabine at 375mg/kg. A and B) Liver homogenates were used to extract proteins to perform western blot analysis (n=3). GLA-specific antibody was used to detect the proteins. HSP70 was used as a housekeeping gene. The bars represent the mean of the normalized intensity observed in the blot. C) Liver homogenates were also used to extract genomic DNA (n=5). The rate of homologous recombination was evaluated in the DNA of treated animals using ddPCR. The bars represent the mean of the percentage HR in a group. Mean±SD, Two-way ANOVA (p*<0.05, **<0.001, ***<0.0001).

Focusing on the values obtained at P150 (Figure 35D), the treatment with Donor WT was able to clear 66% substrate and when coupled with fludarabine the efficiency increased to 85% reduction. Similarly, lyso-Gb3 in the plasma of animals treated with Donor CO02 was reduced by 75% which increased to 81% when the drug was coupled with the treatment. Therefore, it was evident that the drug enhanced the capabilities of the therapy by ~1.2x when compared to donor-only treatment.

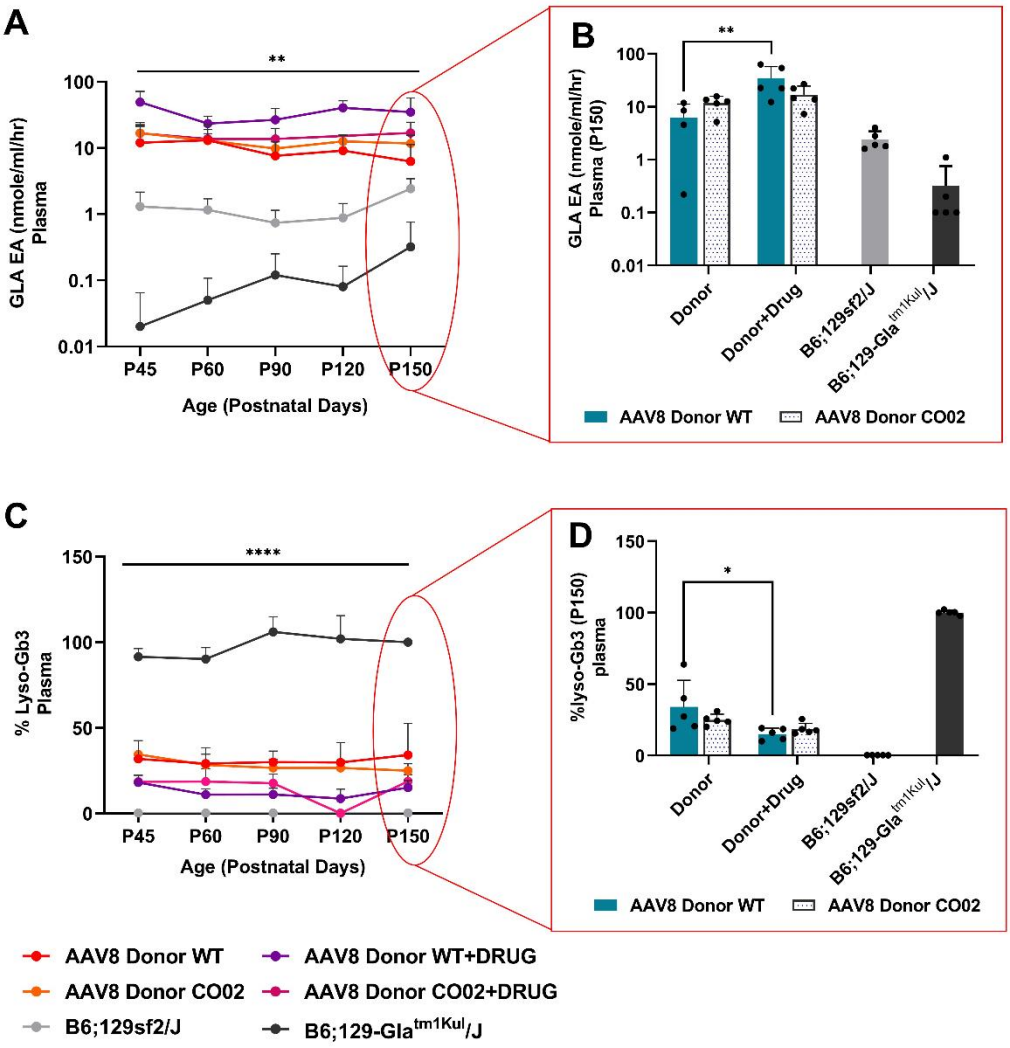

Figure 35. Evaluating GLA enzyme activity and substrate reduction in plasma of Fabry KO mice treated with the nuclease-free approach to gene targeting. Juvenile (P30) Fabry KO mice (n=2) were treated with AAV Donor vector (hGLA_WT or hGLA_CO02) at 3.0E+13 vg/kg, coupled with Fludarabine at 375mg/kg. Plasma samples isolated from the blood collected at different events during the course of the treatment were subjected to evaluation of Fabry disease markers. A) GLA enzyme assay is represented in the XY graph demonstrating the trend of the activity in the plasma from blood collected at different time points. B) The bar graphs represent the mean of the GLA enzyme activity obtained at P150. C) Mass-spectrometry was done to quantify the lyso-Gb3 levels in the blood plasma at different time points. D) the mean percentage of substrate accumulation at P150 is represented in the bar graph. Mean±SD, REML or Two-way ANOVA (p*<0.05, **<0.001, ***<0.0001).

To further investigate the effect of the treatment on Fabry KO mice, a GLA enzyme assay was performed with the liver (Figure 36A), kidney (Figure 36B), and heart (Figure 36C) harvested at sacrifice. The bars represent the mean of the GLA activity obtained by treatment. In the target organ i.e., the liver the results clearly indicate a 12x higher activity in animals treated with Donor WT and

Fludarabine and 1.9x higher activity with Donor CO02 and drug when compared to their counterpart animals treated with the donor vector only.

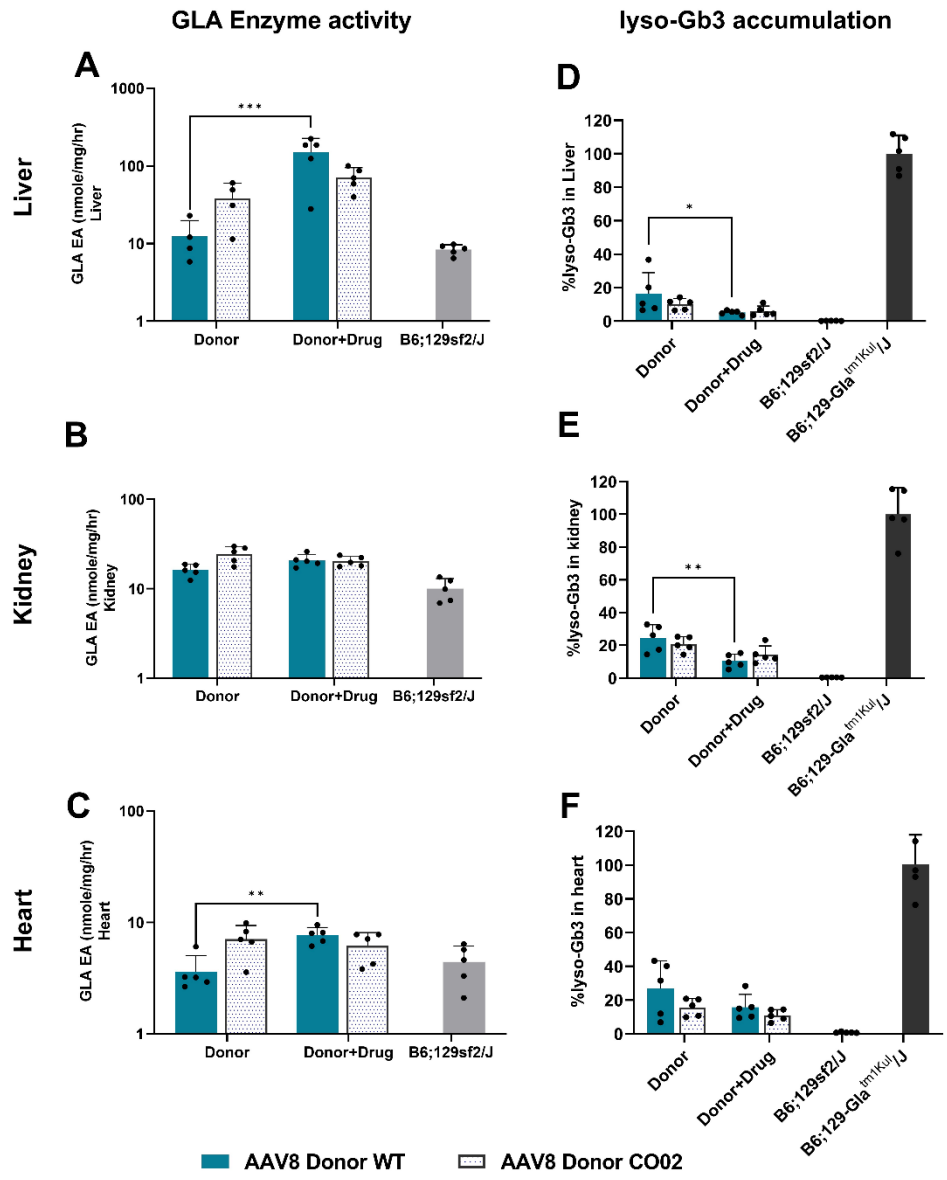

Figure 36. Evaluating GLA enzyme activity and substrate reduction in the tissues of Fabry KO mice treated with the nuclease-free approach to gene targeting. Juvenile (P30) Fabry KO mice were treated with AAV Donor vector (hGLA_WT or hGLA_CO02) at 3.0E+13 vg/kg, coupled with Fludarabine at 375mg/kg. Proteins extracted from the tissue homogenates were used to perform GLA enzyme activity (nmoles/mg/ml) in A) the Liver, B) the kidney and C) the heart. The bar graph represents the mean of the activity obtained by the animals treated. Untreated wild-type animals were considered control. The tissue homogenates were homogenized in water to test for lyso-Gb3 accumulation in D) the liver, E) the kidney and F) the heart. The bar graphs indicate the percentage of substrate accumulation at P150, considering hemizygous make Fabry Ko mice with 100% accumulation. Mean±SD, Two-way ANOVA (p*<0.05, **<0.001, ***<0.0001).

The GLA protein produced in the liver was efficiently biodistributed and taken up by the other organs like the kidney and heart. In Figure 36B, the activity assessment in kidneys shows elevated levels of enzyme activity in the knockout-treated mice that reached wild-type levels. A similar effect was observed in the heart in figure 36C.

After confirming the presence of the GLA protein, its enzyme activity, and its uptake, the tissues were evaluated for lyso-Gb3 substrate accumulation. Figures 36D, E, and F represent the lyso-Gb3 accumulation values in the liver, kidney, and heart respectively. The bar graph plots the substrate accumulation in percentage, compared to untreated hemizygous male Fabry KO mice accumulating 100% lyso-Gb3 in their organs. The results show a clearance of the substrate in all the organs. In the liver, the treatment coupled with the drug was able to clear 94% of the substrate which is higher than when the animals were treated with the only-donor WT (84%) or Donor CO02 (90%). Similarly, the donor-only constructs removed 76-80% substrate from the kidneys, which increased to 86-90% when coupled with the drug. In the heart, the 73-84% reduction was observed with the donor vectors which increased to 85-90% under the influence of the drug. The reduction was always ~10% higher than the animals treated with only the donor vector.

The nuclease-free approach proved to be effective and more efficient than treatment with the gene-targeting AAV vector alone. By eliminating the use of the CRISPR/Cas system, genome editing has the potential to be safer due to the absence of off-target sites leading to tumorigenesis.

4.5 Potential therapy for early-onset Fabry disease

Following the previous experiment in which mice were treated at P30, the tested treatment was tested in mice at early stages since it was shown higher rate of targeting with AAV-based genome editing. Thus, we treated neonatal Fabry KO mice with AAV-based gene targeting as a potential therapy for the early onset of Fabry disease.

4.5.1 AAV-based gene-targeting in neonatal Fabry KO mice using CRISPR/Cas9 technology

An experiment was designed to target Fabry KO neonatal mice (P5) with AAV8 pAB hGLA_WT or AAV8 pAB hGLA_CO02 donor vectors coupled with AAV8 pX602_sgRNA Cas9 vector (1:5) at two different doses retro-orbitally. 3.0E+13vg/kg of donor vector with 6E+12vg/kg Cas9 was initially given as the normal dose used throughout this study. Later a higher dose of 3.0E+14 vg/kg of donor vector coupled with 6E+13vg/kg of Cas9-containing vector was used to test the efficacy of the treatment. Untreated age-matched wild-type and hemizygous male mice were used as control animals. All the animals were sacrificed at the age of 5 months harvesting the liver, kidneys, and heart. The animals

were intermittently bled for blood plasma and their weights were monitored which remained unchanged between the treated and untreated groups (Figure 37).

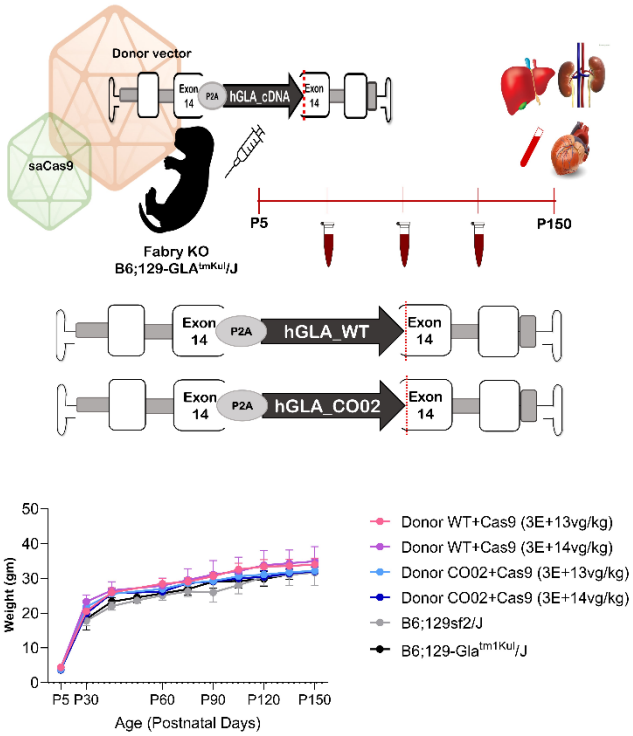

Figure 37. Schematic diagram of gene targeting in neonatal Fabry KO mice. Neonatal (P5) Fabry KO mice (n=5) were treated with AAV Donor vector (hGLA_WT or hGLA_CO02) at 3.0E+13 vg/kg or 3.0E+14 vg/kg, coupled with AAV8 pX602_sgRNA at 6E+12vg/kg or 6E+13vg/kg respectively. Untreated age-matched wild-type and hemizygous male mice were treated as control. Blood was collected at intermediate time points and the weights of all the animals were monitored. All the animals were sacrificed at 5 months of age harvesting the liver, kidney, and heart.

Proteins were extracted from liver homogenates to evaluate protein production. Proteins (15 µg) were run on an SDS PAGE gel to perform Western blot analysis (n=3). Anti-GLA antibody was used to detect GLA proteins and HSP70 was used as a housekeeping protein (Figure 38A). The intensity of the bands confirms a dose-response effect, the higher dose of 3.0E+14vg/kg displays more intense bands than in animals treated with 3.0E+13vg/kg for both Donor WT as well as Donor CO02. Quantification of the band intensities suggests 9x and 5x higher protein levels in the case of animals treated with 3.0E+14vg/kg Donor WT and Donor CO02, respectively, compared to the lower dose (Figure 38B). Importantly, expression levels of the CO02 were 2.4x to 4x higher than that of the WT construct with higher and lower doses respectively.

Genomic DNA was isolated from the liver homogenates to evaluate the rate of homologous recombination (HR) by digital droplet PCR. Figure 38C shows the quantification of the ddPCR results.

There is a statistically significant increase in the percentage of HR in the albumin locus when the animals were treated with a higher dose, ranging from 8.5 to 8.1% HR in neonatal mice treated with 3.0E+14vg/kg to 0.21-0.85% in those treated with 3.0E+13vg/kg.

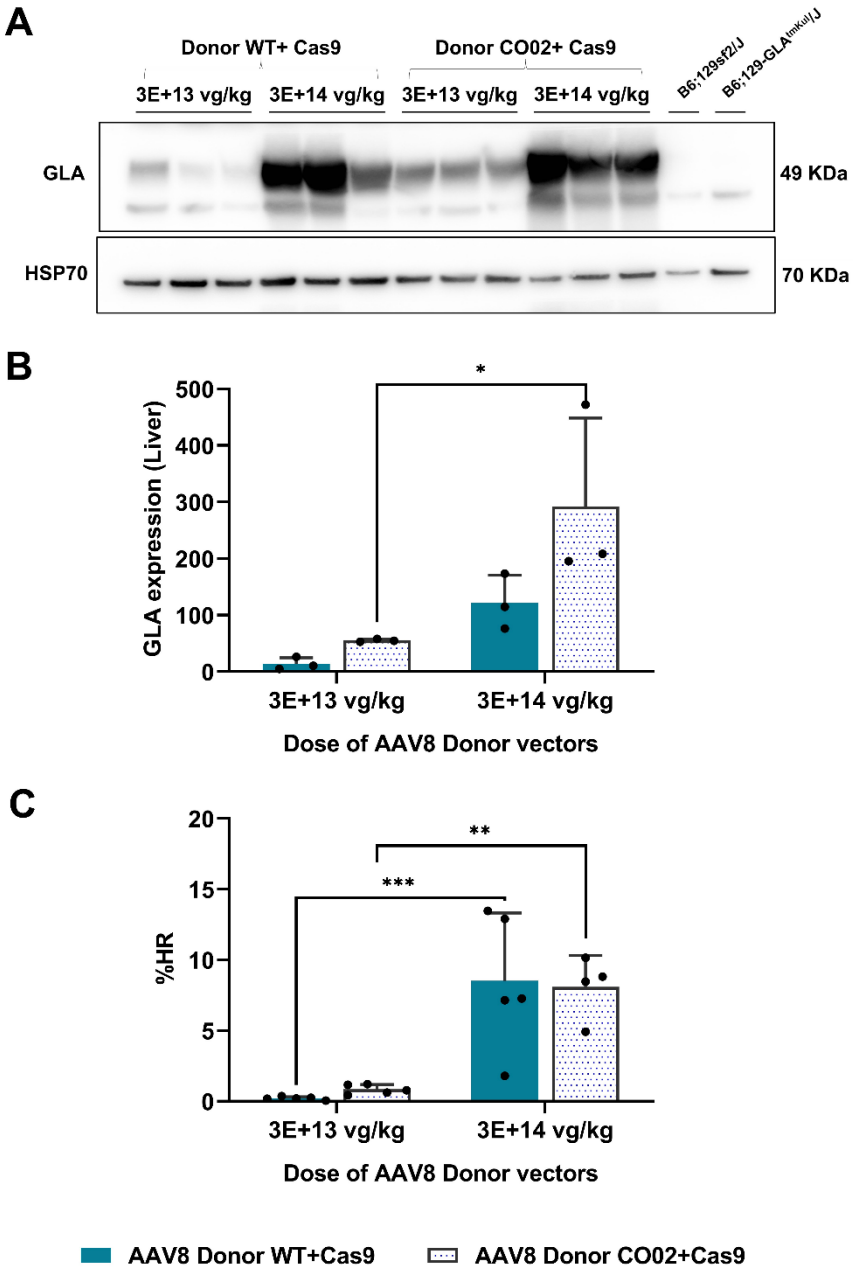

Figure 38. Assessment of protein production and recombination rate in neonatal Fabry KO mice treated with AAV-based gene targeting. Neonatal (P5) Fabry KO mice were treated with AAV Donor vector (hGLA_WT or hGLA_CO02) at 3.0E+13 vg/kg and 3.0E+14vg/kg, coupled with Cas9 (1:5). A and B) Liver homogenates were used to extract proteins to perform western blot analysis. GLA-specific antibody was used to detect the proteins. HSP70 was used as a housekeeping gene. The bars represent the mean of the normalized intensity observed in the blot. C) Liver homogenates were also used to extract genomic DNA. The rate of homologous recombination was evaluated in the DNA of treated animals using ddPCR. The bars represent the mean of the percentage homologous recombination (HR) in a group. Mean±SD, Two-way ANOVA (p*<0.05, **<0.001, ***<0.0001).

To further investigate the effects of the treatment, plasma was isolated from the blood collected at intermediate time points and at the time of sacrifice. This blood plasma containing the GLA proteins was tested for enzyme activity. Figure 39A shows the GLA enzyme activity plotted at different time points for all the treated and untreated animals. The trendlines suggest a supraphysiological increase in the activity in the treated animals which was stable till the termination of the experiment at 5 months of age. The GLA enzyme activity obtained at P150 was plotted on a bar graph shown in Figure 39B. An increase of 105x was observed in animals treated with Donor WT+Cas9 at 3.0E+14 vg/kg when comparing the treatment at 3.0E+13 vg/kg. Similarly, a 15x increase with the higher dose was noticed in the case of Donor CO02 treatment. It is also interesting to note that the treatment with Donor CO02+Cas9 was able to elevate the enzyme activity more than that of Donor WT+Cas9 at both doses.

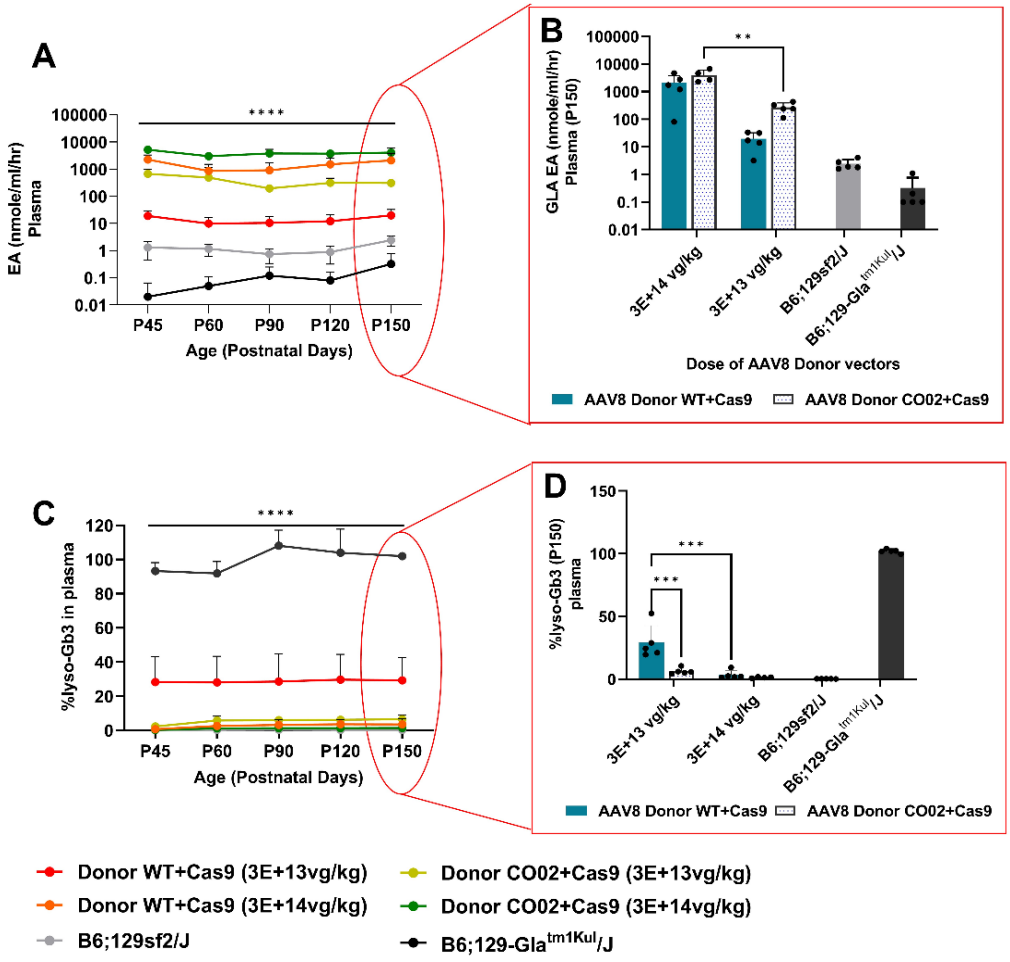

Figure 39. Evaluating GLA enzyme activity and substrate reduction in plasma of Fabry KO mice treated with the nuclease-free approach to gene targeting. Neonatal (P5) Fabry KO mice were treated with AAV Donor vector (hGLA_WT or hGLA_CO02) at 3.0E+13 vg/kg and 3.0E+14vg/kg, coupled with Cas9 (1:5). Plasma samples isolated from the blood collected at different events during the course of the treatment were subjected to evaluation of Fabry disease markers. A) GLA enzyme assay is represented in the XY graph demonstrating the trend of the activity. B) The bar graphs represent the mean of the GLA enzyme activity obtained at P150. C) Mass-spectrometry was done to quantify the lyso-Gb3 levels in the blood plasma at different time points. D) the mean percentage of substrate accumulation at P150 is represented in the bar graph. Mean±SD, REML or Two-way ANOVA (p*<0.05, **<0.001, ***<0.0001).

Mass-spectrometry was done to test substrate accumulation in plasma samples collected from the treated and untreated animals. Figure 39C shows the results obtained from the assay in the percentage of lyso-Gb3 accumulation, considering that untreated hemizygous Fabry KO males have 100% accumulation at P150. The treatment with both doses was able to clear lyso-Gb3 accumulation since the initiation of the experiment and was stable till the termination. Looking closely at the data obtained at sacrifice or P150 (Figure 39D) shows that the plasma of treated hemizygous mice presented almost similar lyso-Gb3 levels as the healthy wild-type animals. The Donor WT at 3.0E+14 vg/kg cleared 97% substrate compared to the lower dose (71%), similarly, the highest dose of Donor CO02 reduced the lyso-Gb3 by 99% and the lower dose by 94%. This result confirms the efficacy of the treatment even at a dose of 3.0E+13 vg/kg with hGLA_CO02 vectors.

GLA enzymes produced by targeting the liver were found to be in supraphysiological levels in the blood plasma confirming the outflow of abundant GLA from the liver to the bloodstream. To confirm the uptake of this enzyme by other target organs, the kidney, and heart, together with the liver, were used to perform a GLA enzyme assay. In the liver (Figure 40A), the enzyme activity reached 2826.2 nmoles/mg/hr with the highest dose of Donor WT which is 19x higher than the lower dose (147 nmoles/mg/hr), likewise, the activity is elevated to 9129.6 nmoles/mg/hr with Donor CO02 at 3.0E+14 vg/kg which is 15x higher than that achieved by 3.0E+13 vg/kg. It is important to note that despite the clear differences in the activity with the dose, a 3-4x higher activity was observed with hGLA_CO02 codon-optimized vectors than with hGLA_WT in the liver. Also, in the kidneys (Figure 40B) and heart (Figure 40C) 52x and 4x higher activity was observed with Donor CO02 with the higher dose respectively when compared to Donor WT. The dose-response was evident with the enzymatic assay.

To further check whether the increase in GLA enzyme activity had an effect on substrate accumulation, tissue homogenates were analyzed by mass spectrometry. Figures 40D-F represent the percentage of lyso-Gb3 present in the liver, kidneys, and heart, post-treatment with AAV8 genome targeting donor vectors after 5 months of injection. Associating untreated hemizygous mice at P150 with 100% lyso-Gb3 accumulation, in the liver, the Donor WT dosed at 3.0E+13vg/kg was able to reduce the accumulation to 89% whereas Donor CO02 cleared 98% substrate. At the higher dose of 3.0E+14vg/kg, both the Donor vector (WT and CO02) were able to completely clear the substrate reversing the lyso-Gb3 phenotype completely. In the case of the kidneys, animals dosed at 3.0E+13vg/kg reduced substrate by 85% with Donor WT and 95% with Donor CO02. The kidneys of animals treated with the higher dose were able to eliminate any accumulating substrate. A very similar situation was observed in the heart, where the animals given the vector at 3.0E+13vg/kg reduced lyso-Gb3 by 89% and 94% with Donor WT and Donor CO02, whereas 97% and 99% with the higher dose. Clearance of lyso-Gb3 was in all cases more effective with the CO02 than with the WT GLA cDNA.

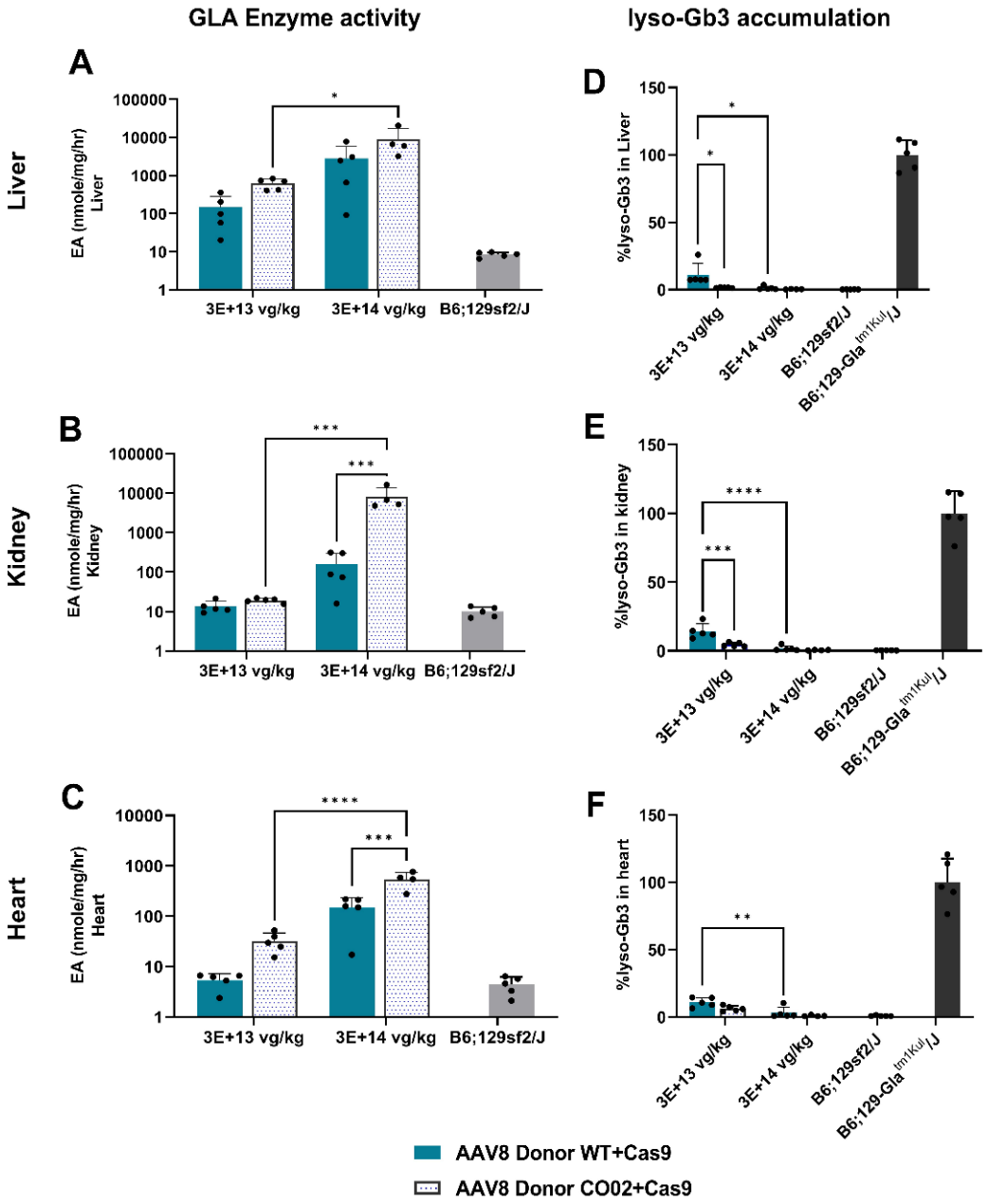

Figure 40. Evaluating GLA enzyme activity and substrate reduction in the tissues of neonatal Fabry KO mice treated with AAV-based gene targeting. Neonatal (P5) Fabry KO mice were treated with AAV Donor vector (hGLA_WT or hGLA_CO02) at 3.0E+13 vg/kg and 3.0E+14vg/kg, coupled with Cas9 (1:5). A-C) Proteins extracted from the tissue homogenates were used to perform GLA enzyme activity (nmoles/mg/ml) in A) the Liver, B) the kidney and C) the heart. The bar graph represents the mean of the activity obtained by the animals treated. Untreated wild-type animals were considered control. D-F) The tissue homogenates were homogenized in water to test for lyso-Gb3 accumulation in D) the liver, E) the kidney and F) the heart. The bar graphs indicate the percentage of substrate accumulation at P150, considering hemizygous make Fabry Ko mice with 100% accumulation. Mean±SD, Two-way ANOVA (p*<0.05, **<0.001, ***<0.0001).

4.5.2 Optimization of Nuclease-free approach to gene targeting in C57BL/6 WT neonatal mice.

After the positive results obtained from the gene-targeting approach in Fabry KO neonatal mice using CRISPR/Cas9, it was necessary to optimize a protocol for a genome-targeting therapy coupled with fludarabine in neonatal mice since the toxic effect of a high dose of the drug on pups was still undetermined. Therefore, a study was designed in C57BL/6 WT neonatal mice (n=3). A donor vector containing EGFP transgene and mouse albumin homology arms (AAV8 pAB_EGFP) was retro-orbitally injected at 3.0E+13vg/kg at P5 (Figure 41). The treatment was coupled with fludarabine at two different doses of 190mg/kg and 95mg/kg with varying booster frequency intra-peritoneally. Group 1 was given the donor vector with EGFP only. Group 2 was dosed with donor vector and 190 mg/kg of fludarabine once per day for two consecutive days (total of 380 mg/kg). Group 3 was dosed with the donor vector and 95 mg/kg of the drug was given twice per day for two consecutive days (a total of 380 mg/kg). Lastly, group 4 was given the donor vector and an increment of fludarabine by treating the animals with 190 mg/kg twice a day for two consecutive days (a total of 760 mg/kg). An age-matched untreated mouse was used as a control. All the treated and untreated animals were sacrificed after 15 days of treatment at P20 collecting the blood and harvesting the liver.

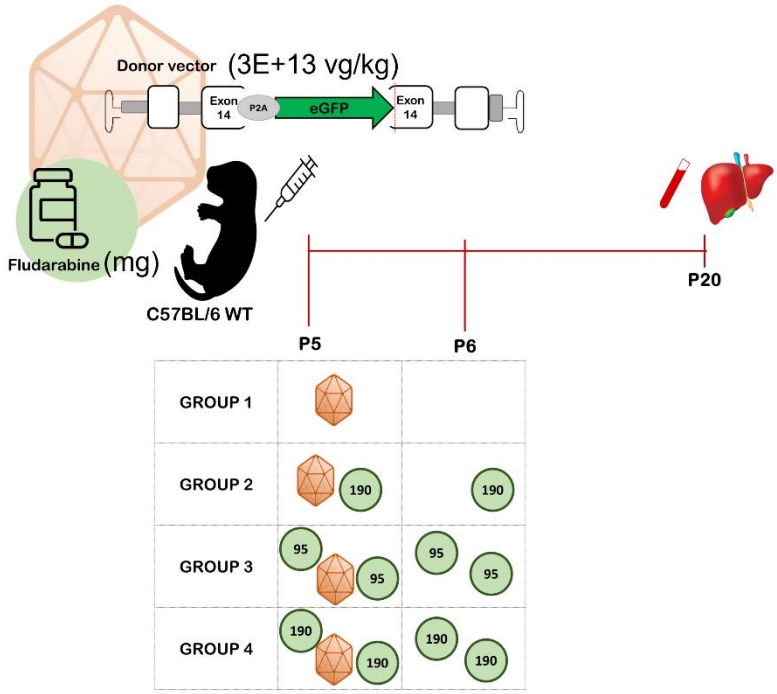

Figure 41. Experimental design to optimise the nuclease-free approach to gene targeting in C57BL/6 WT neonatal mice. Neonatal (P5) C57BL/6 WT mice were treated retro-orbitally with AAV8 pAB_EGFP vector containing mouse albumin homology arms and EGFP transgene at 3.0E+13vg/kg with and without Fludarabine (n=3). The drug was given at different concentrations of 190mg/kg or 95mg/kg with different frequencies of booster doses as can be seen in the figure. Age-matched untreated WT mice were used as a control. All the treated and untreated mice were sacrificed at P20 after 15 days of treatment. The liver was harvested for analysis.

Proteins extracted from the liver homogenates were used to perform an SDS-PAGE. Western blot was done to detect EGFP proteins using an Anti-EGFP antibody and HSP70 was used as housekeeping control (Figure 42A). A bar graph was plotted with the relative EGFP expression obtained after quantification and normalization of the western blot (Figure 42B). There is a minor non-statistically significant difference observed after quantification of the intensities, where Group 4 with the highest dose of the drug had the highest EGFP expression level as represented in the bar graph.

To determine the levels of fused mALB+EGFP expression, a quantitative RT-PCR was performed to amplify the region between the EGFP transgene and exon 12 on the endogenous albumin (Figure 42C). The qRT-PCR analysis indicates the relative expression of the fused mALB+ EGFP represented in bars as the mean of the expression of all animals in the group. When compared to the animals treated with the donor vector only (Group 1), the animals with a single dose of 190 mg/kg drug given for two days (Group 2) showed 2.3x more fused mRNA expression, whereas Group 3 with two doses of 95 mg/kg drug for two days express 1.6x more fused mALB+ EGFP. Group 4 with the highest dose of fludarabine with 190 mg/kg twice a day for two days was significantly able to increase the expression by 4.3x.

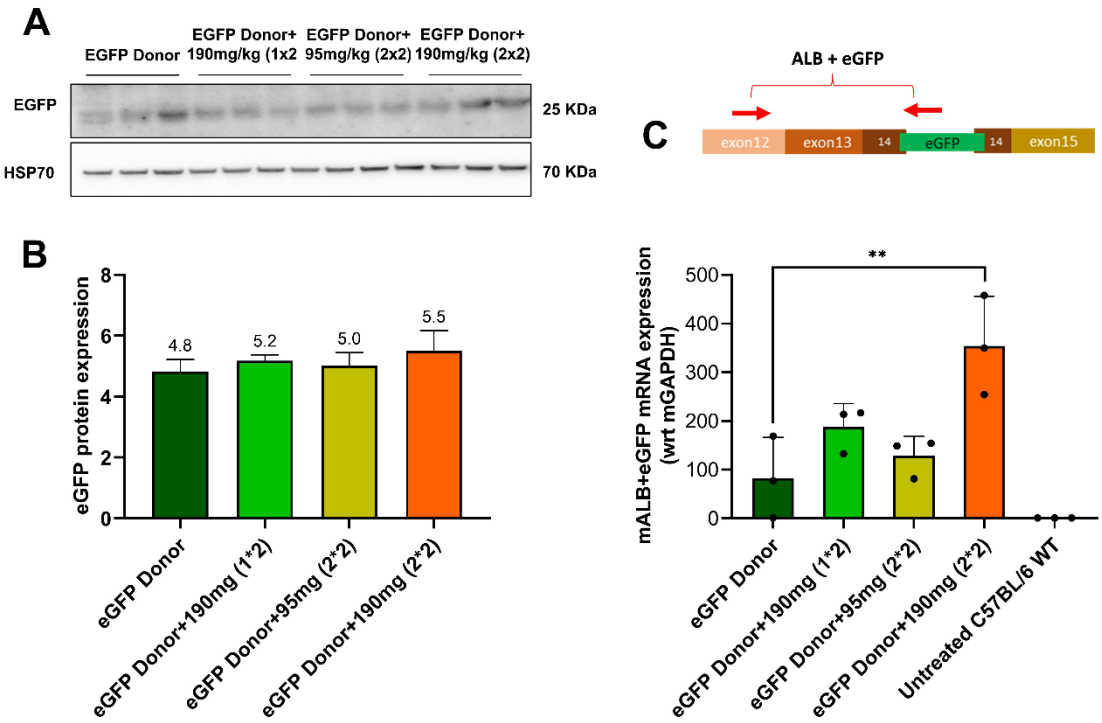

Figure 42. Protein and mRNA expression analysis of the nuclease-free approach to gene targeting in C57BL/6 WT neonatal mice. Neonatal (P5) C57BL/6 WT mice were treated retro-orbitally with AAV8 pAB_EGFP vector containing mouse albumin homology arms and EGFP transgene at 3.0E+13vg/kg with and without Fludarabine (n=3). A) Western blot was done with proteins extracted from liver homogenates using EGFP-specific antibody and HSP70 as a housekeeping protein. B) Quantification of the western blot where bars represent the mean of relative GFP expression of the animals in the group. C) A qPCR was done to amplify the cDNA between the EGFP transgene and the exon 12 in the endogenous albumin locus. The bars represent the fused mALB+ GFP expression obtained after normalization with mGAPDH. Mean±SD, One-way ANOVA (p*<0.05, **<0.001, ***<0.0001).

Moreover, liver cryosections were prepared and counter-stained with DAPI (nuclear dye) as mentioned in the Materials and Methods section. Figure 43 shows the liver sections as seen under a fluorescent microscope where the green signal indicates EGFP expression and the nucleus is stained in blue. After quantifying the sections for EGFP-positive cells, it was concluded the highest dose of fludarabine increased the percentage of EGFP-positive cells by 2.5x, although non-significant statistically.

These analyses are inclined towards the use of the conditions mentioned in Group 4 with the highest dose of fludarabine to achieve optimum results in neonatal animals.

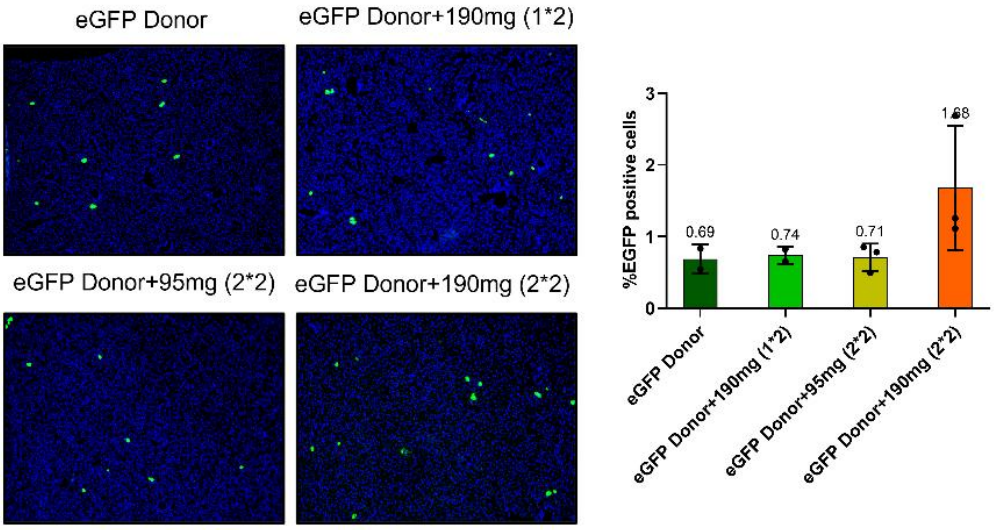

Figure 43. EGFP expression in the liver section of C57BL/6 WT neonatal mice treated with a nuclease-free approach to gene targeting. Liver sections from animals treated with AAV8 pAB_EGFP with and without the drug were counter-stained with DAPI. The green signal indicated the GFP expression whereas the nuclease is stained in blue (DAPI). The quantification of the GFP positive cells is plotted as a bar graph representing the mean percentage positive cells of the treated animals in the group. Mean±SD, One-way ANOVA (p*<0.05, **<0.001, ***<0.0001).

4.6 A comparative study with Enzyme replacement therapy in Fabry KO mice

Enzyme replacement therapy is the standard treatment used for Fabry patients currently. It was necessary to compare the strategies developed in this study with the available treatment. For this, an experiment was designed using Replagal or Agalsidase alpha which is the enzyme replacement drug from Takeda pharmaceutical. Replagal (1 mg/kg) was given to 3-month-old (P90) Fabry KO male (n=5) mice via tail vein injections every week for two months, making a total of eight infusions. All the

animals were sacrificed at P150 harvesting the liver, kidney, and heart. Blood was collected 24 hours post-injection for plasma extraction at intermediate time points during the experiment (Figure 44A).

Enzyme activity analysis was done using the blood plasma and the tissues harvested. Figure 44B shows GLA activity in plasma, where the activity of Fabry knock-out mice treated with ERT levels resembles

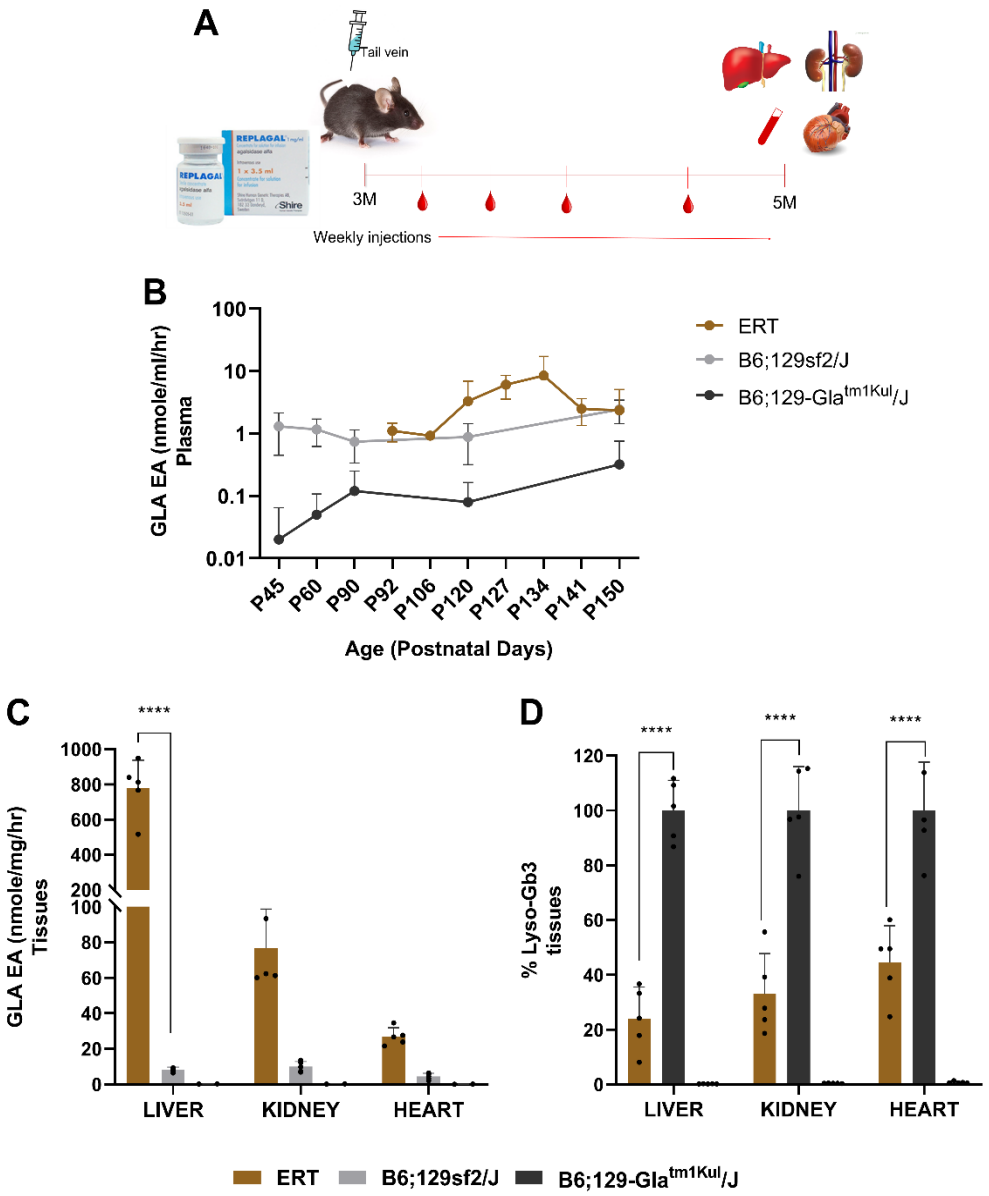

Figure 44. ERT treatment in Fabry KO mice. A) Hemizygous Fabry KO male mice (n=5) at P90 were treated with Replagal (1mg/kg) every week via tail vein injection for 2 months. Age-matched untreated hemizygous and wild-type animals were treated as control. All the animals were sacrificed at 5 months of age harvesting the liver, kidneys and heart. Blood was collected at intermediate time points. B) GLA enzyme assay was done in plasma isolated from the blood collected. The trendlines with the dots show the mean of activity at different time points in nmoles/ml/hr. C) GLA enzyme activity was done in tissues. The bars represent the mean activity of all the animals in the different treated and untreated groups in the liver, kidney, and heart (nmoles/mg/ml) C) Lyso-Gb3 was measured using LCMS analysis in the tissues. The bars represent the mean percentage of substrate in the liver, kidney, and heart of treated and control animals. The substrate accumulation in the untreated hemizygous males at P150 was considered 100%. Mean±SD, Two-way ANOVA (p*<0.05, **<0.001, ***<0.0001).

that of untreated wild-type enzyme activity levels. Whereas figure 44C shows GLA activity in tissues, reaching supraphysiological levels of 777 nmoles/mg/hr in the liver, 77 nmoles/mg/hr in kidneys, and 27 nmoles/mg/hr in the heart which is 100x (liver), 8x (kidney) and 6x (heart) higher than untreated wild-type animals. The elevated level in the tissues is evidence of the efficiency of the enzyme replacement therapy, however, it was necessary to assess substrate reduction in these tissues. Figure 44D shows the percentage of lyso-Gb3 in the different organs, a reduction of 76% in the liver, 67% in the kidneys, and 56% in the heart was observed in hemizygous animals treated with ERT. These results indicate the effective release of GLA enzyme from the liver and uptake in the different organs with Replagal.

4.7 Determination of translatability of gene targeting therapy

The data obtained in juvenile as well as neonatal Fabry KO animals showed promising results with the integrative approach using vectors containing mouse albumin homology arms. The next step forward is to construct the integrative vectors suitable for human transduction for translational purposes and test them *in vitro* and *in vivo* in humanized mice, these are immunocompromised animals that have had their liver cells replaced with human hepatocytes.

4.7.1 Construction of human ALB homology arms containing donor vector

The first step in the construction of human albumin homology arms containing integrative vectors is to study the human ALB gene. It has been reported in literature sourced from the '1000 Genomes project' that in the human population there are several haplotypes of albumin genes considering single nucleotide polymorphism at different positions. Focusing on the hALB locus and the region of interest there are 7 variants of the human albumin gene, considering the six SNP positions (Table 6). Amongst

POSITION	ID	HAP1	HAP2	HAP3	HAP4	HAP5	HAP6	HAP7
74285239	rs962004	T	C	C	C	C	T	C
74285552	rs4076	A	G	A	A	A	G	G
74285567	rs962005	C	A	C	C	C	A	A
74285758	rs2236766	G	T	T	G	G	T	T
74285823	rs2236767	G	A	G	G	G	A	A
74287403	rs4429703	C	T	T	C	T	T	C
Frequency		50.14%	44.69%	2.15%	1.51%	1.37%	0.09%	0.05%

Table 13. Haplotypes of human albumin locus. According to the 1000 genomes project, there are several variants or haplotypes considering the single nucleotide polymorphisms (SNPs). Haplotype 1 and haplotype 2 are predominantly available in the human population with a frequency of 50.14% and 44.69% respectively.

these variants, haplotype 1 (Hap1) and haplotype 2 (Hap2) can be found predominantly in the human population having a frequency of 50.14% and 44.69% respectively.

Taking into consideration this information, two different albumin homology arm constructs were created with the SNPs at the positions mentioned in Table 6 corresponding to haplotype 1 and haplotype 2. The right homology arm (1401 base pair) starts at the stop codon in exon 14 and ends with the locus whereas the left arm corresponds to 1302 bases upstream of the latter. A 2A peptide and EGFP transgene sequences were added upstream to the stop codon in the exon 14, flanked by the two homology arms.

These two sequences, containing the human albumin homology arms (Hap1 or Hap2), the 2A peptide sequence, and the EGFP transgene, were cloned into an AAV ITR containing pAB 288 plasmid replacing the original mouse albumin regions to form pAB hALB Hap1_EGFP and pAB hALB Hap2_EGFP. AAV viral stocks were made by packaging these plasmids with a plasmid containing the serotype AAV LK03. AAVLK03_pAB_hALB_Hap1_EGFP and AAVLK03_pAB_hALB_Hap2_EGFP were purified and tittered.

Alongside, in order to assemble a SaCas9 and human albumin-specific sgRNA containing plasmid, a PAM site (TTGAAT) downstream of the albumin stop codon was identified using the CHOPCHOP tool (https://chopchop.cbu.uib.no/). This PAM site was then modified to avoid self-cleavage by changing the guanine to adenosine and the terminal thymine to cytosine (TTAAAC). The preceding 21 bases to the PAM site were identified as the guide RNA (5' AGCATCTCAGGTAACTATATT 3'). This guide RNA was cloned into an AAV ITR and saCas9 containing plasmid (px602_hsgRNA). Later this plasmid was packaged with AAV LK03 serotype and viral stocks were prepared.

The cleavage efficiency of the CRISPR/Cas9 vector was tested *in vivo* in HuH7 liver-derived human cells, using TIDE (Tracking of Indels by Decomposition) analysis. HuH7 cells were transfected with the pX602_hsgRNA plasmid. The transfected and mock untreated cells were collected post-transfection. Genomic DNA isolated from these cells was used to amplify the albumin region around the CRISPR target site using a PCR followed by sequencing. The raw data were analyzed using the TIDE web tool (https://tide.nki.nl/). Figure 45A shows the expected break site and the areas of alignment and decomposition. Figure 45B shows the percentage of Indels generated using the guide RNA targeting the human albumin locus with a total efficiency of 34.1%.

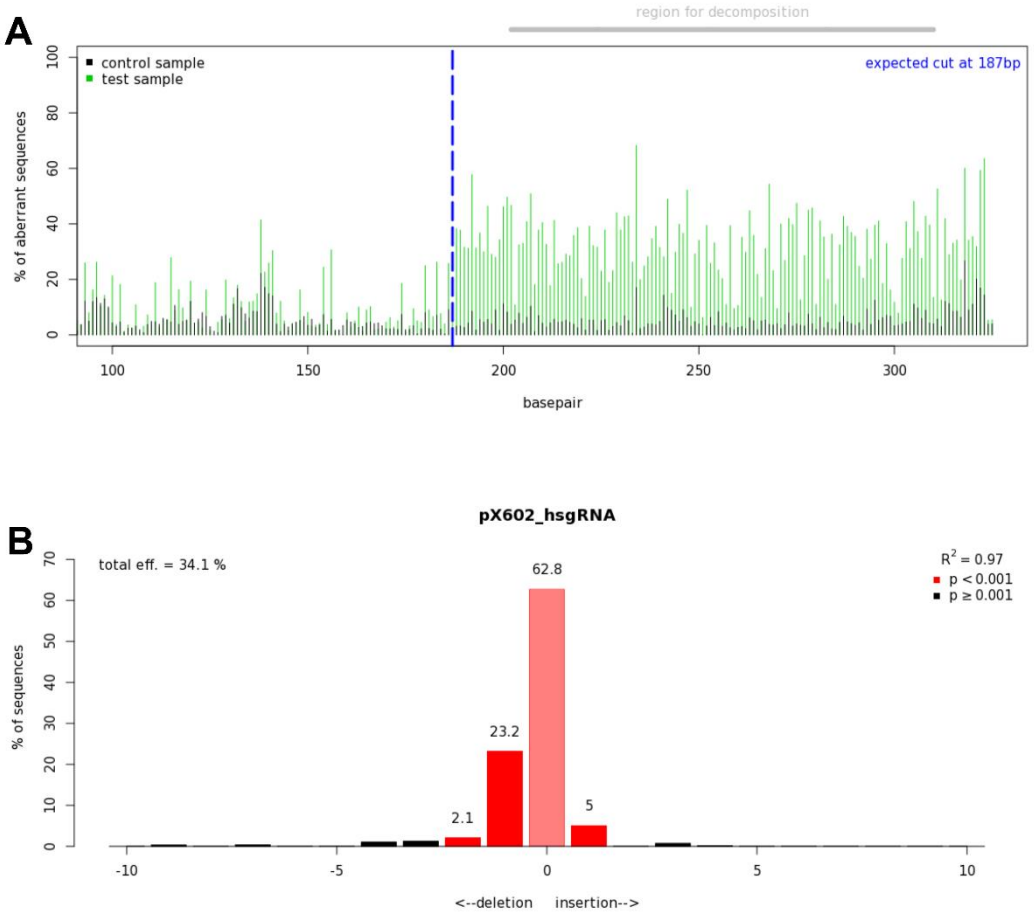

Figure 45. TIDE analysis. A TIDE (Tracking of Indels by Decomposition) analysis was done for guide RNA designed to target the human Albumin locus. A) The quality control chart shows the expected break site as a dotted blue line. The wild-type control signals can be observed in black whereas the region of decomposition is evident in green signals. B) The bar graphs represent the spectrum of expected Indels and their frequencies and efficiency.

4.7.2 *In vitro* testing of human ALB homology donor vector

The human donor vectors AAVLK03_pAB_hALB_Hap1_EGFP (AAV_Hap1_Donor) and AAVLK03_pAB_hALB_Hap2_EGFP (AAV_Hap2_Donor) were tested *in vitro* in HuH7 cells. HuH7 cells were plated in a 96-well cell culture plate and transduced with AAV LK03 donor vectors at 500,000 MOI. To confirm the effect of Cas9 on homologous recombination, the donor vectors were coupled with AAV LK03_px602_hsgRNA. This Cas9 and guide RNA-containing vector was transduced at 100,000 MOI in a mix containing donor vector (1:5). The experiment was performed to test the donor vector in the nuclease-free approach to gene editing with the use of Fludarabine. The drug

was dosed at 100 µM 16 hours before transduction of the donor vectors. Untreated cells were considered mock control. After 72 hours of infection, cells were collected with trypsin, washed with PBS, and plated into a 24-well plate for another 72 hours. Post 72 hours the same procedure was repeated, and the cells were transferred into a 12-well plate, followed by transfer to a 6-well plate, and finally into a 100 cm^2 dish (Figure 46). This was done to allow the cells to duplicate and expand so as to maximize EGFP expression at the end of the experiment. After a total incubation of 12 days cells were harvested and DNA and RNA were extracted using protocols mentioned in the Methods and Materials section. Cells were also imaged under a fluorescent microscope to see evidence of green fluorescent proteins.

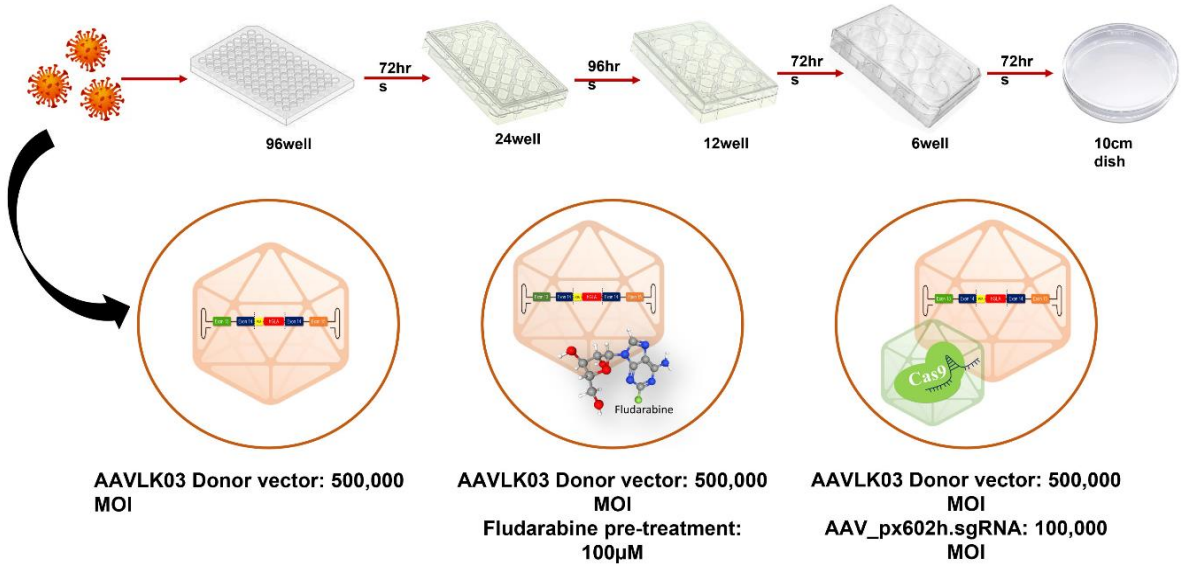

Figure 46. Experimental design for testing human albumin donor vectors *in vitro* in HuH7. HuH7 cells plated in a 96-well plate were infected with either AAV LK03_donor Hap1_EGFP or AAV LK03_donor Hap2_EGFP at 500,000 MOI. The treatment was coupled with either fludarabine or AAV LK03_pX602_sgRNA (100,000 MOI). 72 hours post infections the cells were trypsinized and plated in a 24-well plate to expand for 72 hours. Followed by transfer into a 12-well plate and then to a 6-well plate each incubation lasting at least 72 hours. Finally, the cells were expanded in a 10cm^2. Mock untreated cells were used as control. After the termination of the experiment, the cells were imaged under a fluorescent microscope and collected to extract RNA and DNA.

The RNA extracted from the cells was used to run a quantitative PCR reaction with primers amplifying the region between the EGFP sequence and exon 12 of the endogenous albumin, which is located outside of the homology region present in the donor vector (Figure 47A). The quantification of the amplification cycles normalized with the human GAPDH gene is represented in the bar graph, showing an increase in the fused hALB+EGFP expression when the AAVLK03 donor vectors were coupled with the drug and the Cas9-containing AAV vector. In the case of Hap1 Donor vector treatment the drug increased the expression by 3.3x and Cas9 by 2.2x, whereas in the cells treated with Hap2 Donor vector, the drug and Cas9 elevated the expression level by 2.4x and 2.8x respectively. It is also important to

note the difference between the expression levels in the case of treatment with AAV LK03_Donor Hap1 and AAV LK03_Donor Hap2. Hap2 Donor treated cells have 6x higher expression than Hap1 Donor vector treated cells, similarly, Hap2 Donor+drug and Hap2 Donor+Cas9 have 4x and 7x elevated expression levels compared to their Haplotype 1 counterparts. Haplotype 2 seems to be more amenable to homologous recombination. This is due to the fact that the HuH7 cells used for the analysis are positive for haplotype 2 (see next section). Figure 47B shows the cells as seen in a fluorescent microscope. The bright green in the cells indicates the expression of green fluorescent proteins (EGFP). These results confirm the importance of haplotype specificity in events of homologous recombination.

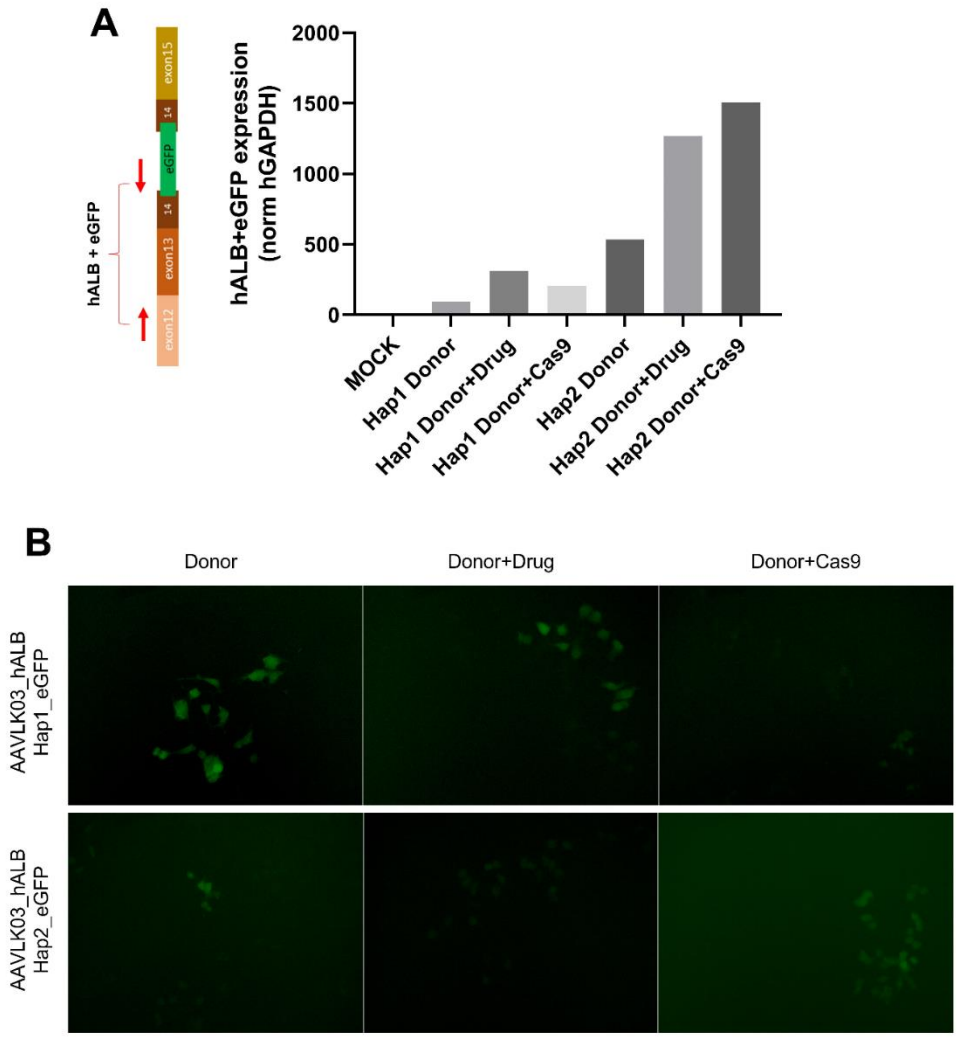

Figure 47. Tests to check homologous recombination in HuH7 cells infected with human albumin arms containing donor vectors. HuH7 cells were infected with either AAV LK03_donor Hap1_EGFP or AAV LK03_donor Hap2_EGFP at 500,000 MOI coupled with either fludarabine or AAV LK03_pX602_sgRNA (100,000 MOI) were harvested. A) RNA isolated from the cells was converted into cDNA and used to run a quantitative PCR to amplify the region between GFP and endogenous human albumin exon 12. Human GAPDH was used as a housekeeping gene to normalize the observed expression. B) The panel shows the cells as seen in a fluorescent microscope. The bright green in the cells indicates the expression of green fluorescent proteins.

4.7.3 SNP genotyping of the human albumin gene

As mentioned earlier, the region of interest for the donor vector containing albumin homology arms can be classified into seven haplotypes based on single nucleotide polymorphisms (SNPs) in six positions. Also, in order to understand the increase in expression of fused hALB+EGFP due to higher homologous recombination in the case of cells treated with AAV LK03_Hap2 Donor, it was necessary to check the genotype of the cells used. TaqMan predesigned SNP genotyping assay from Thermofisher Scientific was used to genotype the SNP ID rs962004, using fluorophores for Haplotype 1 (FAM/ TTGTTGAGCTT) and Haplotype 2 (VIC/ TTGTTGAGCTC). Genomic DNA was isolated from untreated HuH7 and four different human blood samples to increase confidence in the genotyping assay. Water was used as the negative control. According to the results shown in Figure 48, three out of four blood samples were heterozygous to the SNP whereas one was homozygous for Haplotype 1. HuH7 cells were also homozygous for Haplotype 2. This genotyping confirmed the importance of haplotype with the donor DNA in the events of homologous recombination.

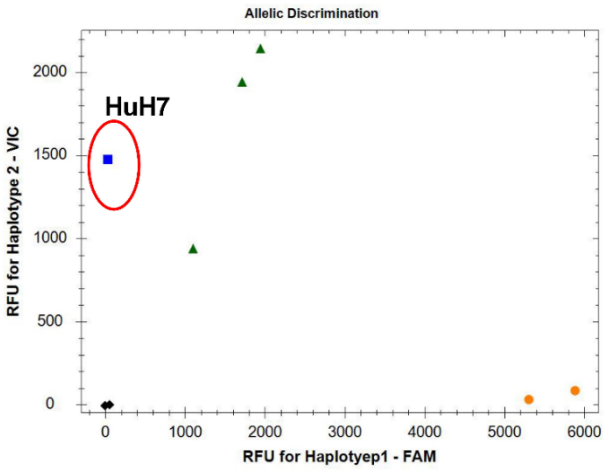

Haplotype	Fluorophore	Allele	Sequence SNP
Haplotype 1	FAM	Allele 1	TTGTTGAGCTT
Haplotype 2	VIC	Allele 2	TTGTTGAGCTC

SAMPLE	SAMPLE TYPE	GENOTYPE
HuH7	Human hepatocyte cell line	Haplotype 2
Sample A	Human blood	Haplotype 1
Sample B	Human blood	Heterozygote
Sample C	Human blood	Heterozygote
Sample D	Human blood	Heterozygote
Water	Negative control	NA

Figure 48. SNP genotyping of the human albumin gene. Optimization of single nucleotide polymorphism in human albumin gene using HuH7 cells and human blood samples.

For translational purposes, AAV viral stocks for vectors containing the human albumin arms have been prepared and efficiency has been evaluated in HuH7 cells. Further, these constructs will be tested in primary cultures of human hepatocytes and in chimeric mice containing humanized liver to validate the applicability of the AAV-based gene-targeting strategy for use in the clinics.

Discussion

5.1 Liver-directed gene-based therapies using AAV vectors

AAV-based liver-directed episomal gene therapy is an active area of research and has proved to be an emerging tool for the treatment of many monogenic disorders. Recently in 2022, new therapies for Haemophilia A and B were approved using AAV5, Roctavian (BioMarin) for adults with severe hemophilia A (Blair 2022), and Hemgenix (UniQure) for Haemophilia B (Sachin Navale et al. 2022). Before that, Luxturna was approved by Spark Therapeutic for rare inherited retinal dystrophy in 2017 and Zolgensma for Spinal Muscular Dystrophy was approved in 2019 by Novartis. The first gene therapy product Glybera approved for hereditary lipoprotein lipase deficiency dates back to 2012.

However, AAV-based liver-directed episomal gene therapy presents important limitations in neonatal and pediatric settings. The vector DNA is mainly present in the form of extrachromosomal episomes (Hiroyuki et al. 2001), and therefore, even though episomal gene therapy is seeing success in adults, serious concerns are present for the treatment in the pediatric setting. In fact, AAV episomes are lost in the growing livers of pediatric patients due to hepatocyte duplication, resulting in the loss of therapeutic efficacy (Cunningham et al. 2013). Loss of viral DNA and therapeutic efficacy may also occur in adult patients, associated with liver damage, in addition to a minor loss associated with the naturally low rate of hepatocyte duplication in a healthy liver. Regrettably, vector re-administration is not possible due to the presence of anti-AAV neutralizing antibodies raised after the first vector administration. Therefore, vector dilution and loss in both pediatric and adult settings remain a major challenge of AAV-based episomal gene therapy.

To address this issue, several strategies are being studied, one of them consists in the permanent modification of the genome, so the therapeutic transgene is transmitted to daughter cells upon duplication. The integrative approach used in this study is based on the delivery of a promoterless sequence containing a transgene cDNA flanked by albumin homology arms which undergoes spontaneous integration into the albumin locus. This genome targeting strategy is a promising approach for gene transfer in pediatric settings. This strategy has been successful in preclinical settings with a severe mouse model of Crigler-Najjar (CN) syndrome rescuing lethality (Porro et al. 2017), methylmalonic acidaemia (MMA) mouse model (Chandler et al. 2021) and also in treating hemophilia B mice (A Barzel et al. 2015).

In order to confirm the differences between episomal and integrative approaches, C57BL/6 WT mice were treated at different time points with an episomal AAV8 vector (ranging from neonatal to juvenile) containing an EGFP transgene and a liver-specific promoter (AAV8-pGG2-AAT-EGFP; episomal treatment) or with AAV8 donor vectors containing the eGFP transgene flanked by mouse albumin homology arms (AAV8-pAB288-ALB-EGFP) coupled with a Cas9 and guide RNA containing AAV

vector to test the integrative gene targeting strategy. Coupling the donor vector with the CRISPR/Cas9 system to increase the rate of homologous recombination was previously tested and yielded the complete correction of the phenotype in CN neonatal mice consequent to an increase in transgene recombination rate (De Caneva, Porro, Bortolussi, Sola, Lisjak, Barzel, Giacca, Mark A Kay, et al. 2019). The results of the experiment confirmed the principle behind gene therapy and the age of treatment. The liver of neonatal mice undergoes rapid hepatocyte duplication which led to AAV episome loss and an almost complete loss of EGFP expression after 2 months of treatment, whereas, genome editing with Cas9 was able to integrate EGFP in the hepatocytic genome which passed to the daughter cells in the animals treated between the postnatal days of P1 and P10 when the liver growth is at its peak, and reached maximum transgene expression which was observed at 2 months of age. On the contrary, when juvenile animals were treated with episomal gene therapy, the expression was more stable and prominent at 2 months of age, whereas there was a significant reduction in EGFP expression in juvenile animals treated with integrative AAV donor vector compared to the treatment done in neonatal ages. These results explicitly verify the importance of liver growth and hepatocyte duplication in gene transfer.

Therefore, gene therapy can be applied to adults but serious concerns regarding the loss of efficacy of the transgene are present for its application in children due to vector loss over time, which eventually creates the need for re-administration. Different approaches are being tested to allow AAV re-administration a reality, ranging from immunomodulation to plasmapheresis and the use of antibody-cleaving proteases to target the issue of pre-existing neutralizing antibodies against AAVs (Meliani et al. 2018) (Earley et al. 2023) (Chu and Ng 2021) (Bertin et al. 2020) (Elmore et al. 2020), but these methods are still in a pre-clinical phase and need further experimentation. The targeted modification of the genome is a promising approach giving pediatric patients the opportunity to receive a permanent cure.

5.2 Fabry knock-out mouse model

Fabry knock-out mice B6;129-Gla^{tm1Kul}/J, were brought to the ICGEB animal facility from Jackson laboratory (Cat no#003535). Also known as α-Gal A KO (*α-Gal A*$^{-}$), this model was developed by Dr Ashok B Kulkarni, by replacing a 1kb region from the exon 3 and intron 3 region with a neomycin resistance cassette (Oshima T et. al, 1997). These mice have a complete deficiency of Alpha-Galactosidase A enzyme due to which they develop the Fabry disease.

The GLA protein and lyso-Gb3 levels were used as disease markers to characterize FD mice. GLA proteins were tested by measuring the enzymatic activity in plasma and tissues (nmoles/ml/hr or nmoles/mg/hr). The GLA enzyme activity of a 5-month-old hemizygous mice was assessed in the liver

(0.22 nmoles/mg/hr), kidney (0.23 nmoles/mg/hr), heart (0.085 nmoles/mg/hr), and plasma (0.51 nmoles/ml/hr) confirming the lack of GLA enzyme activity. Wild-type animals (5-month-old) on the other hand had 5.1 nmoles/mg/hr in the liver, 4.58 nmoles/mg/hr in the kidneys, and 0.45 nmoles/mg/hr in the heart. Plasma enzyme activity reached up to 2.05 nmoles/ml/hr.

When the lyso-Gb3 levels were measured in these animals, hemizygous males accumulated 142.30ng/ml of substrate in the plasma whereas age-matched wild-type male mice had a nearly negligible substrate accumulation (0.49ng/ml). This difference in the lyso-Gb3 levels of the diseased and healthy mice proved to be a useful tool in the assessment of the treatments in Fabry KO mice in this study (Ohshima, Gary J. Murray, et al. 1997). Considering these observations made during the characterization of the FD mouse model, it was decided that regardless of the age of treatment, the experiments should be designed to last at least up to 5 months of age in order to observe significant changes and effects on the phenotype due to the progressive accumulation of substrate in the tissues and fluids which can be compared to late-onset FD in patients as discussed in a study by Dinesh Bangari *et. al.* (Bangari et al. 2015).

Despite the mild phenotype and no physical evidence of the disease, this model proved to be useful and effective in replicating Fabry disease conditions and evaluating the efficacy of the treatments using the disease markers. This Fabry KO model has been extensively used for research with Fabry disease and proved valuable in preclinical data generation (Zhu et al. 2019) (Biferi et al. 2021).

5.3 Liver-directed gene therapy is a promising tool for genetic disorders

Gene therapy using AAV vectors has been successfully applied in genetic disorders like hemophilia, retinal dystrophy, and Spinal Muscular Dystrophy (SMD) targeting the adult population as mentioned earlier (Blair 2022) (Sachin Navale et al. 2022). The accelerated research in lysosomal storage disorders is also fuelling gene therapy interests and its global market in general. In a report published in 2021 in Biopharma Dive, according to Cowen investment bank, around 23% of the gene therapies in the pipeline globally comprised lysosomal storage disorders (https://www.biopharmadive.com/news/gene-therapy-lysosomal-storage-disorders-fabry/594991/).

Talking about Fabry disease, AAV-based interventions by Sangamo therapeutics (ST-920; NCT05039866) (Ganesh et al. n.d.), and Freeline therapeutics (FLT190; NCT04455230) (Jeyakumar et al. 2023) proved potential in phase 1 and phase 2 and are now being observed for their long-term follow-up results. Fabry disease is a lysosomal storage disorder giving rise to systemic clinical manifestation due to the lack of alpha-galactosidase A enzyme, destined to degrade Gb3 and lyso-Gb3 molecules in the lysosomes (Germain 2010). Enzyme replacement therapy with Fabrazyme and Replagal is the

standard method of care, however according to a recent study the average annual cost for ERT per patient/year was €199,452 (Fabrazyme) and €200,503 (Replagal), accompanied by depreciation in the quality of life of the patients (Katsigianni and Petrou 2022) (Rombach et al. 2013). Gene therapy with AAV is the promise of a hopeful future for LSDs as it is expected the long-term duration of a one-time treatment.

Constant developments in the field of gene therapy aimed at understanding and increasing therapeutic efficiency and safety. One aspect of achieving the desired competence is by designing novel AAV serotypes that have enhanced tissue-specific or species-specific transduction efficiencies. AAV8 is a naturally occurring AAV serotype known for its transduction abilities in pre-clinical studies (Collaud et al. 2019) (Wang et al. 2012) (Jeyakumar et al. 2023) and has a definite advantage over other natural serotypes due to its liver-tropism and rapid capsid uncoating capabilities (Gao et al. 2002) (Gonçalves 2005b) (Thomas et al. 2004). Alternatively, AAV-DJ is a hybrid vector made by DNA shuffling of eight different AAV serotypes which resulted in better transduction abilities in the mouse liver tissues (Dirk et al. 2008). Another synthetic vector AAV-LK03 was developed by shuffling five AAV serotypes and has proved efficient in specie-specific transduction in human hepatocytes (Lisowski et al. 2014).

Other than opting for the favorable AAV serotype, designing the optimum construct aids in the efficiency of the therapy. A typical AAV vector genome comprises ITR overhangs, a transgene, and a mammalian promoter (Naso et al. 2017). The promoter facilitates and manages the expression of the transgene as well as the site of expression. For example, in the case of systemic expression ubiquitous promoters like human elongation factor 1α-subunit (EF1α), cytomegalovirus (CMV), chicken β-actin (CBA), and ubiquitin C (UBC) can be used to promote expression in all cell types (Naso et al. 2017) (Powell, Rivera-Soto, and Gray 2015). However, in cases of liver-targeted gene therapy, the α1-antitrypsin (hAAT) (Cunningham et al. 2008) and the thyroxine-binding globulin (TBG) (Yan, Yan, and Ou 2012) promoters have been thoroughly tested for expression restricted to the liver with minimum or null expression in other tissues.

Optimizing the transgene is another way to achieve an enhanced and optimum expression. Codon-optimization is done by altering the codons in the transgene sequence using the biasing strategy and manipulating cryptic splice sites, CpG islands, and using optimal open reading frames. In this study, transcript 201 of the human Alpha Galactosidase A (*hGLA*) gene was used to perform gene-based therapies in Fabry knock-out mice. Prior to the treatments, the *hGLA* WT cDNA was codon-optimized to generate four different variants of the gene hGLA_CO01, hGLA_CO02, hGLA_CO03, and hGLA_CO04. These variants were tested *in vitro* in HuH7 cells and *in vivo* in C57BL/6 WT mice to evaluate the efficiency of the cellular as well as the secretory GLA enzyme activity and protein production. The enzyme activity of hGLA_CO02 was 4.5x and 3.4x higher in growth medium and blood plasma respectively whereas, 2x in HuH7 cells and liver homogenates when compared to

wildtype *hGLA* cDNA. Even in terms of protein production, this construct performed better. The codon-optimized construct (hGLA_CO02) with the optimal performance was selected for all the experiments alongside hGLA_WT.

Liver-directed gene transfer is an ambitious strategy to target genetic disorders like lysosomal storage diseases in adults. A potent therapy can be achieved by optimizing the AAV serotype selection to achieve high transduction efficiency and designing the optimal vector genome to obtain a long-term high expression of the therapeutic transgene.

5.4 AAV-based episomal gene therapy for late-onset Fabry disease

There are a number of gene therapy studies ongoing for Fabry disease. However, in an attempt for a more effective strategy, this study was designed to convert the liver into a factory that produces GLA enzyme which can be up taken by other organs from the blood stream. An episomal AAV8 vector was used containing hAAT strong liver-specific promoter (Cunningham et al. 2008), a human apolipoprotein E enhancer (ApoE) (Ronzitti et al., 2016), and HBB2 intronic sequence for enhanced expression, flanked by AAV ITRs required for AAV generation (De Sabbata et al. 2021). The vector contained the human GLA WT, or codon-optimized cDNA previously (AAV8 pSMD2_hGLA WT/ AAV8 pSMD2_hGLA CO02) packaged in AAV8.

Ideally, a more effective strategy means efficient transgene expression with the minimum dose possible. Therefore, a dose-escalation study was conducted with the two episomal vectors using four intermediate doses with 3E+13vg/kg being the highest dose, and 3E+11vg/kg being the lowest. Fabry KO juvenile mice (P30) were chosen for the study considering the results obtained in the previous experiment that determined a stable expression of episomal EGFP vectors at P30. Treating juvenile mice at the age of 1 month was a balanced compromise considering late-onset Fabry disease which is characterized by a residual 3-30% GLA activity in humans and symptoms evident after the second decade of life (Michaud et al. 2020), and the stable AAV episomal transgene expression. The enzyme assay showed an evident dose-dependent increase in the plasma GLA enzyme activity levels with the increase in the dose of the AAV vectors, however, all the doses reached supraphysiological levels of activity when compared to untreated healthy wild-type animals or untreated knock-out animals. The experiment was followed up to 5 months of age with significantly stable GLA expression.

Since it was vital to see if the enzyme was able to degrade the substrate accumulation in the plasma, lyso-Gb3 amounts were measured. Animals treated at 3E+13vg/kg and 1E+13vg/kg were able to reduce substrate accumulation by 99-100%. Treatment with 3E+12vg/kg reached 96-99% reduction. Even with the lowest dose of 3E+11vg/kg, hGLA_WT removed 58% and hGLA_CO02 proved its advanced

abilities by clearing out 91% lyso-Gb3 in blood plasma. This validates the efficiency of the treatment in Fabry KO mice. The reduction in the substrate can be noticed with the first time point evaluated and lasts until the termination of the experiment.

Due to its secretory as well as cellular nature, it was expected from the GLA observed in the bloodstream to reach and be up taken by the organs. Therefore, GLA enzyme activity and lyso-Gb3 accumulation were measured in the liver, the kidneys, and the heart. Due to the severity of the clinical manifestation observed in the kidney and heart, FD is also classified as the renal FD variant and the cardiac FD variant (Michaud et al. 2020). The GLA enzyme assay and the measure of the accumulated lyso-Gb3 substrate were in line with the dose-dependent effect seen in the blood plasma in the tissues.

An experiment conducted by Sangamo therapeutics in Fabry mice showed <70% reduction of lyso-Gb3 in the kidneys and <80% in the liver and plasma when treated with an AAV2/6 vector containing a codon-optimized GLA cDNA at 2E+12 vg/kg and only 40% clearance in the plasma and tissues with a dose of 2.5E+11 vg/kg (Yasuda et al. 2020). This drug developed by the pharmaceutical company has been granted the fast-track designation by the US FDA in May 2023 for their phase 3 trials in Fabry patients. When comparing this existing therapy with the results obtained in this study, a proof of the advanced performance is established. Even with the lowest dose of 3E+11vg/kg AAV8 pSMD2 hGLA_CO02 episomal vector reduced 95% substrate in the liver, 87% in the kidneys, and 85% in the heart. This data is indicative of the potential of the vector design and the codon-optimized construct.

However, it is interesting to note that the plasma GLA levels in mice treated at the highest dose of AAV8 pSMD2_hGLA CO02 vectors experienced a drop in the activity level during the first-month post treatment which later stabilized until the termination of the experiment. As a hypothesis, this reduction can be explained by the elimination of GLA proteins-containing cells by the induction of immune response spawned due to the endoplasmic reticulum (ER) stress. This ER stress could be generated due to the production of very high levels of GLA proteins, hence, compromising the efficiency of the hGLA_CO02-transduced hepatocytes, when compared with hGLA_WT-transduced ones, at the highest dose of 3E+13vg/kg. When the gene expression of inflammation markers was measured, a statistically insignificant, increase in TNFα, NFκβ, and IL6 and a significant upregulation of CD86 was observed. GRP78 which is an ER stress marker was also measured which is responsible for the stability of survival pathways like ER signaling molecules and caspases and is reduced under stress conditions to unblock these protective pathways (Miao Wang *et. al.*, 2009). The expression of this marker was found to be significantly reduced, which was indicative of increased ER stress in these animals. The supraphysiological production of GLA proteins may create this stress, therefore, lowering the dose of the vector should be considered, being more evident in hGLA_CO02-transduced cells due to the increased translatability of this cDNA and consequent higher GLA production levels.

The expression of the GLA gene by gene transfer through AAV-based gene therapy was able to ameliorate the phenotype of the disease in juvenile mice. The expression also lasted for 4-months until the termination of the experiment, however, concerns like unregulated expression (Nathwani et al. 2011) (Russell & Kay 1999), random integration (Hendrie, Hirata, et al. 2003), and even increased oncogenic (Garrick, Fiering et al. 1998) risks persist. Moreover, it is unclear whether or not there will be a loss of efficacy in the long term due to AAV episome dilution and loss. This is a situation that lists as a major drawback of AAV-based episomal gene therapy. In the case of adults with fully developed livers, though the majority of the hepatocytes are in the quiescent state, <1-2% of hepatocytes are always duplicating at any given time although the turnover takes place over 200 to 300 days (Duncan, Dorrell, and Grompe 2009) (Kattenhorn et al. 2016). Hepatocyte regeneration in response to toxic injury is also an evident phenomenon also confirmed by partial hepatectomy (Taub 2004). Hepatocytic diseases can occur in case of hepatitis infections, cirrhosis, non-alcoholic fatty liver disease (NAFLD) drug overdose, poisoning, obesity, and also following a lifestyle involving alcohol consumption (Van Haele, Snoeck, and Roskams 2019). Therefore, after undergoing gene therapy, there is a constant risk of episomal vector loss and dilution in case a repair response is triggered in the liver and hepatocyte duplicate. Re-administration of the AAV vector will prove in vain due to the activation of humoral immunity and hence the generation of neutralizing antibodies against the AAV vectors after the first administration (Calcedo and Wilson 2016) (Nathwani et al. 2007) (Wang et al. 2012). This is where genome editing comes in with a solution to permanently modify the hepatocytes for long-term expression (Barzel et al. 2015) Chen et al. 2019) (De Caneva et al. 2019) (De Giorgi et al. 2021) (Sharma et al. 2015) (Yang et al. 2016).

5.5 A gene targeting approach for Fabry disease

Genome editing is an alternative approach to permanently modify the genome to obtain a one-shot therapy while overcoming most of the concerns and limitations faced by AAV-based episomal gene therapy. Generally, two strategies can be used when correcting a monogenic genetic disorder, firstly a specific mutation causing the disease phenotype can be corrected by insertion or deletions, secondly, a therapeutic transgene can be integrated into a safe harbor locus in the genome. In both cases, the modified cells will transfer their corrected genome to the daughter cells.

Giulian Pavani and Mario Amendola in 2021, described the integration locus based on the functional characteristics. Transgenes can also be integrated into the coding sequence of endogenous genes to silence it to ameliorate the phenotype. Alternatively, the safe genomic harbors are regions that allow integration and robust expression of the transgene and their promoters without affecting the cell's physiology (Sadelain, Papapetrou, and Bushman 2012) like the AAVS1 locus used to treat Fanconi

anemia (Diez et al. 2017) and chronic granulomatous disease patients (De Ravin et al. 2016). CCR5 locus was used *ex vivo* to correct LSDs mouse models like MPS I (Gomez-Ospina et al. 2019) and Gaucher's disease (Scharenberg et al. 2020) and the Rosa26 locus was used to successfully target mouse liver to knock in human alpha-1-antitrypsin gene (Stephens et al. 2018) and the factor 9 gene (Stephens et al. 2019).

Gene targeting can also be exploited by integrating a promoterless functional transgene into a safe harbor and utilizing the endogenous gene promoter like in the case of X-SCID, where a functional copy of the gene IL2RG was integrated downstream its endogenous promoter *ex vivo* to restore expression (Genovese et al. 2014) (Schiroli et al. 2017). Due to the constraint of limited integration frequency high vector doses are needed to suffice the protein requirement to reach healthy thresholds. Therefore, endogenous genes with very strong promoters have also been used as safe genomic harbors for overexpression of the therapeutic transgenes. Rajiv Sharma *et. al.* first used the albumin locus as a safe genomic harbor due to its strong endogenous promoter by targeting the first intronic sequence of the albumin gene with a promoterless transgene bearing a splice acceptor. AAV vectors were coupled with ZFNs to achieve *in vivo* liver-directed targeting of human factor 8 and 9 and lysosomal enzymes α-Galactosidase A (Fabry disease), Acid β-Glucosidase (Gaucher disease), α-L-Iduronidase (Hurler syndrome) and Iduronate-2-sulfatase (Hunter syndrome) (Sharma et al. 2015). Although an elegant solution, this method observed a reduction the serum albumin levels. Barzel and his group applied a different strategy in hemophilia B mice by targeting the albumin locus downstream of its coding sequence without disrupting the open reading frame and achieved 5-20% Factor 9 levels with <1% integration events without the use of endonucleases (A Barzel et al. 2015). This strategy was applied to Haemophilia A mice using CRISPR/Cas9 system (Chen et al. 2019), to MPS II by ZFN-mediated genome targeting (Laoharawee et al. 2018), and a mouse model of Crigler-Najjar syndrome (Porro et al. 2017) (De Caneva, et al. 2019)

In this study, the approach was tested in Fabry KO mice with and without CRISPR/Cas9 system. Even with ~1% homologous recombination in hepatocytes, AAV-mediated donor vectors (3E+13 vg/kg) with albumin homology arms and human GLA transgene were able to reduce lyso-Gb3 accumulation in the blood plasma and tissues in juvenile mice (P30). However, this is an ideal strategy to exploit the advantage of a growing liver. Neonatal Fabry KO mice (P5) were treated in a dose-dependent manner with the same donor vector at 3E+13 vg/kg and 3E+14 vg/kg coupled with CRISPR/Cas9. As expected, the higher dose increased the percentage of homologous recombination of the donor vector into the albumin locus by a factor of 10x accompanied with 100% clearance of lyso-Gb3 accumulation in plasma. The biodistribution and uptake of the secreted GLA enzyme in tissues were also appreciable with a 90-100% reduction in animals treated with 3E+13vg/kg and a complete amelioration of the phenotype with the higher dose. The results obtained with the treatment in neonatal animals proved the efficacy of the promoterless approach when coupled with a nuclease with a stable GLA enzyme activity

and substrate reduction throughout the course of the treatment. Hence, proving that integrative vectors are a promising tool to overcome the challenge to treat the pediatric population with hepatocyte duplication and episomal vector loss.

5.6 Nuclease-free gene targeting in Fabry mice

Although CRISPR/Cas9 was used in the neonatal and juvenile Fabry KO animals and resulted in efficient disease phenotype amelioration, the drawbacks that come along with the use of nucleases like the potential off-target effect and the activation of oncogenes cannot be ignored. Alternatively, HR-enhancing drugs have been tested in cultured cells, but recent publications have studied the effect in somatic mammalian tissues. Fludarabine which is an FDA-approved drug known to increase HR was tested with an AAV donor vector containing hFIX transgene flanked by albumin homology arms targeting the liver and obtained a 2.7 to 4.6-fold higher human Factor 9 levels in the plasma of mice treated with fludarabine. When the AAV donor vector containing EGFP was coupled with Cas9 as well as fludarabine, the efficiency of the treatment increased from 1.8% to 5.7% with the drug (Tsuji et al. 2020).

In this study, 1-month-old Fabry KO animals were treated with an AAV8 donor vector with *hGLA* flanked by albumin homology arms coupled with a Fludarabine pre-treatment. There was no significant difference in the percentage of homologous recombination when measured with ddPCR however when the blood plasma was assessed, fludarabine treatment elevated enzyme activity by 1.4-5.5x accompanied by 1.3-2.2x higher substrate clearance, reducing it by ~80% when compared to only-donor vector treated samples. The effect of fludarabine treatment was also evident in the tissues. In the liver, the donor vector+ Drug was able to clear 95% of the substrate which is higher than when the animals are treated with the donor vector only (85-90% reduction). Similar effects were observed in the kidneys and heart where the lyso-Gb3 accumulation was reduced by 85-90% in Donor vector+ drug-treated animals which were always 10% more efficient than the animals treated with only the donor vector. Although, both the donor vectors hGLA_WT and hGLA_CO02 were used in this study, no significant differences in the results were found to conclude the supremacy of either one as in the case of episomal gene therapy or in the neonatal gene targeting where the hGLA_CO02 codon-optimized variant proved better than hGLA_WT.

Before testing the genome editing strategy with the drug in Fabry KO neonatal mice, a dose study was conducted with a donor vector containing EGFP transgene in C57BL/6 WT neonatal mice (P5) to determine a safe fludarabine concentration. By measuring the fused mRNA using primers in the EGFP region and the endogenous albumin outside the homology arm region, it was observed that when

animals were dosed with 190 mg/kg fludarabine twice per day for two consecutive days similar to the protocol used in the previous study (Tsuji et al. 2022), the expression increased by 75x compared to fused mRNA expression of only donor vector treated animals (baseline control). With the objective to optimize the treatment by reducing the dose of the drug or by reducing the number of booster doses, animals were treated with 95 mg/kg fludarabine twice per day for two consecutive days (reduced dose of the drug) or 190 mg/kg once a day for two consecutive days (reduced number of booster shots), the fused mRNA expression was 35x and 56x respectively. Since with the reduced dose or number of boosters the efficacy of the treatment is compromised, it was concluded that 190 mg/kg fludarabine given twice per day for two consecutive days will yield the best results. This treatment will be replicated in Fabry KO neonatal animals in the future.

5.7 Enzyme replacement therapy in Fabry KO mice: a comparative study

Enzyme replacement therapy is the only treatment available for patients suffering from Fabry disease. Replagal or Agalsidase alpha which is an Enzyme replacement therapy drug from Takeda pharmaceutical. It was granted European marketing authorization in 2001 and is being used in adults with Fabry disease across, the UK, Canada, Europe, and many more countries. Fabry patients are treated with the recommended dose of 0.2 mg/kg every other week (Keating 2012). According to a study published in 2011, a reduction in plasma lyso-Gb3 was observed in ERT-treated patients after 3 months of treatment which was stable for at least a year. ERT has proved to increase quality of life and reduce substrate however it was not able to completely clear the accumulation (van Breemen et al. 2011). When developing a new therapy, it is necessary to assess the efficiency with the available treatments. Therefore, many studies with Fabry disease have previously used these recombinant enzymes *in vivo* in mouse models to find new insights about the mechanism of ERT or to compare new therapies. In a study by Quinta *et. al.* in Fabry mice, a dose of 1.5 or 0.2 mg/kg was used in eight weekly administrations (Quinta et al. 2014), in another study focusing on the effect of ERT and Natural killer T cells, 1.5mg/kg Replagal was induced (Macedo et al. 2012). In an AAV gene therapy study by Jin-Ok Choi *et al.* using AAV2/8 in Fabry KO, the treatment was compared with ERT by treating animals at 1 mg/kg tail vein infusions once a week for six consecutive weeks (Choi et al. 2010). In order to study mRNA therapy and substrate therapy for Fabry disease, ERT at 1 mg/kg has been used as a comparative control (Marshall et al. 2010) (DeRosa et al. 2019). Following this optimized protocol, Replagal which was a kind gift from Dr Andrea Dardis was used as ERT control. In this study, 3 months old Fabry KO animals were treated with 1 mg/kg Replagal every week for two months. This treatment resulted in an increase in enzyme activity in plasma reaching GLA activity levels of untreated wild-

type animals. It was interesting to note the supraphysiological increase of GLA activity in the liver, kidneys, and heart. This elevation in activity led to 76% reduction in substrate accumulation in the liver, 67% in the kidneys, and 56% in the heart. Comparing these values with the substrate reduction obtained with episomal and integrative gene therapies is evidence of the efficacy of the gene-based therapies, since with one dose of AAV vector almost complete clearance of lyso-Gb3 can be achieved in all the tissues which sustained till 5 months of age. Long-term studied will allow a better evaluation of the effect of these liver-directed gene-based therapies. For now, it is safe to state that, comparing with available ERT this study is a more effective and cost-effective strategy.

5.8 Genome targeting approach for human albumin locus

The results obtained from the treatment with an AAV8 donor vector containing the transgene flanked by mouse albumin homology arms provided promising data. The next obvious step was to test the construct in human settings like human cell lines (HuH7).

Before proceeding with the construction and assembly of the human albumin homology arms, genetic polymorphism in the human albumin locus was taken into consideration. The importance of isogenic DNA in gene targeting has been previously demonstrated by H te Riele *et. al.* (te Riele, Maandag, and Berns 1992) With the help of the 1000 genome project, it was concluded that 95% of the 1000 genome samples belonged to two major groups of single nucleotide polymorphism or haplotypes at the region of interest in the ALB gene (http://www.1000genomes.org) (A. Barzel et al. 2015). Haplotype 1 (Hap1) and haplotype 2 (Hap2) constitute 50.14% and 44.69% of the human population respectively. The two donor vectors were assembled with eGFP transgene flanked by the albumin homology arms with SNPs corresponding to haplotype 1 or haplotype 2. This construct was packaged with the AAV LK03 serotype which transduces the human cells being species-specific (Lisowski et al. 2014). The importance of haplotype specificity was demonstrated by transducing HuH7 cells with AAV LK03_pAB_hALB_Hap1 or AAV LK03_pAB_hALB_Hap2 vectors. A noticeable 82% increase in target site integrated fusion mRNA expression was obtained with the Hap2 donor vector compared to the Hap1 donor vector. Upon genotyping the HuH7 for specific SNP, it was observed that the cells were haplotype 2 positive, which explains the observed effect of the variants during homologous recombination.

This experiment proved the efficacy of the constructs *in vitro*. However, in order to increase the HR rate, the constructs were coupled with either another AAV LK03 vector containing Cas9 and human albumin-specific guide RNA or Fludarabine while infecting HuH7 cells. Due to the haplotype specificity, the Hap2 donor vector was more efficient than the Hap1 donor vector. The Cas9 was able

to increase the efficiency of the treatment by 65% whereas the nuclease-free approach with fludarabine enhanced the therapy by 57% when compared to the effect of the vector alone.

Although the drug was not able to reach Cas9 levels, the nuclease-free approach significantly improved the efficacy of the treatment and can definitely be considered a safer alternative to CRISPR/Cas9 system.

Conclusion

In this study, we developed potential therapeutic treatments targeting late-onset and early-onset Fabry disease irrespective of the disease-causing mutation using AAV-based episomal gene therapy and integrative genome editing tools, respectively. In both approaches, we converted the liver into a GLA depot which abundantly expresses *hGLA* protein without the need for vector re-administration circumventing the existing cost of standard ERT or chaperone treatments for FD.

We provided a proof-of-concept and developed an efficient episomal liver-specific gene therapy AAV vector which when applied to juvenile Fabry KO mice was able to completely revert the diseased phenotype. This treatment has clinical potential for the treatment of late-onset FD and can be applied to juvenile/adult patients with different monogenic disorders.

To address early-onset FD, another platform using integrative genome editing was developed targeting the albumin locus in the liver using CRISPR/Cas9. This system was efficient in neonatal Fabry KO mice and has prospective applications in the treatment of neonatal/pediatric patients. A nuclease-free approach using fludarabine is being tested that can eventually be used in clinics as a safer genome editing treatment. The translational capabilities of the integrative strategy are being tested in human primary hepatocytes and humanized mice. Further studies are required to generate long-term pre-clinical data and fully assess the safety and implications of these strategies in the long period, in juvenile and neonatal FD mice.

References

Anderson, William. 1898. "A Case of 'Angeio-keratoma.'" *British Journal of Dermatology* 10(4):113–17.

Anzalone, Andrew V., Peyton B. Randolph, Jessie R. Davis, Alexander A. Sousa, Luke W. Koblan, Jonathan M. Levy, Peter J. Chen, Christopher Wilson, Gregory A. Newby, Aditya Raguram, and David R. Liu. 2019. "Search-and-Replace Genome Editing without Double-Strand Breaks or Donor DNA." *Nature* 576(7785):149–57.

Azparren-Angulo, Maria, Felix Royo, Esperanza Gonzalez, Marc Liebana, Bruno Brotons, Jesús Berganza, Felipe Goñi-de-Cerio, Nicoló Manicardi, Laia Abad-Jordà, Jordi Gracia-Sancho, and Juan M. Falcon-Perez. 2021. "Extracellular Vesicles in Hepatology: Physiological Role, Involvement in Pathogenesis, and Therapeutic Opportunities." *Pharmacology & Therapeutics* 218:107683.

Balakrishnan, Balaji and Giridhara R. Jayandharan. 2014. "Basic Biology of Adeno-Associated Virus (AAV) Vectors Used in Gene Therapy." *Current Gene Therapy* 14(2):86–100.

Bangari, Dinesh S., Karen M. Ashe, Robert J. Desnick, Colleen Maloney, John Lydon, Peter Piepenhagen, Eva Budman, John P. Leonard, Seng H. Cheng, John Marshall, and Beth L. Thurberg. 2015. "α-Galactosidase A Knockout Mice: Progressive Organ Pathology Resembles the Type 2 Later-Onset Phenotype of Fabry Disease." *The American Journal of Pathology* 185(3):651–65.

Barzel, A, N. K. Paulk, Y. Shi, Y. Huang, K. Chu, F. Zhang, P. N. Valdmanis, L. P. Spector, M. H. Porteus, K. M. Gaensler, and M. A. Kay. 2015. "Promoterless Gene Targeting without Nucleases Ameliorates Haemophilia B in Mice." *Nature* 517(7534):360–64.

Barzel, A., N. K. Paulk, Y. Shi, Y. Huang, K. Chu, F. Zhang, P. N. Valdmanis, L. P. Spector, M. H. Porteus, K. M. Gaensler, and M. A. Kay. 2015. "Promoterless Gene Targeting without Nucleases Ameliorates Haemophilia B in Mice." *Nature* 517(7534):360–64.

Bax, Bridget E. 2017. "Drug Development for Rare Diseases : Challenges and Regulatory Initiatives." *Archives of Science* 1(2):1000107.

Bertin, Berangere, Philippe Veron, Christian Leborgne, Jack-Yves Deschamps, Sophie Moullec, Yves Fromes, Fanny Collaud, Sylvie Boutin, Virginie Latournerie, Laetitia van Wittenberghe, Benoit Delache, Roger Le Grand, Nathalie Dereuddre-Bosquet, Olivier Benveniste, Philippe Moullier, Carole Masurier, Otto Merten, and Federico Mingozzi. 2020. "Capsid-Specific Removal of Circulating Antibodies to Adeno-Associated Virus Vectors." *Scientific Reports* 10(1):864.

Biferi, Maria Grazia, Mathilde Cohen-Tannoudji, Andrea García-Silva, Olga Souto-Rodríguez, Irene Viéitez-González, Beatriz San-Millán-Tejado, Andrea Fernández-Carrera, Tania Pérez-Márquez, Susana Teijeira-Bautista, Soraya Barrera, Vanesa Domínguez, Thibaut Marais, África González-Fernández, Martine Barkats, and Saida Ortolano. 2021. "Systemic Treatment of Fabry Disease Using a

Novel AAV9 Vector Expressing α-Galactosidase A." *Molecular Therapy - Methods & Clinical Development* 20:1–17.

Blair, Hannah A. 2022. "Valoctocogene Roxaparvovec: First Approval." *Drugs* 82(14):1505–10.

Boussettine, Rihabe, Najwa Hassou, Hlima Bessi, and Moulay Mustapha Ennaji. 2023. "Adenovirus Vectors for Vaccination and Cancer Gene Therapy." *Immunological Implications and Molecular Diagnostics of Genitourinary Cancer* 57.

Brady, Roscoe O., Andrew E. Gal, Roy M. Bradley, Erik Martensson, Andrew L. Warshaw, and Leonard Laster. 1967. "Enzymatic Defect in Fabry's Disease: Ceramidetrihexosidase Deficiency." *New England Journal of Medicine* 276(21):1163–67.

van Breemen, Mariëlle J., Saskia M. Rombach, Nick Dekker, Ben J. Poorthuis, Gabor E. Linthorst, Aeilko H. Zwinderman, Frank Breunig, Christoph Wanner, Johannes M. Aerts, and Carla E. Hollak. 2011. "Reduction of Elevated Plasma Globotriaosylsphingosine in Patients with Classic Fabry Disease Following Enzyme Replacement Therapy." *Biochimica et Biophysica Acta (BBA) - Molecular Basis of Disease* 1812(1):70–76.

De Caneva, Alessia, Fabiola Porro, Giulia Bortolussi, Riccardo Sola, Michela Lisjak, Adi Barzel, Mauro Giacca, Mark A. Kay, Kristian Vlahovicek, Lorena Zentilin, and Andrés F. Muro. 2019. "Coupling AAV-Mediated Promoterless Gene Targeting to SaCas9 Nuclease to Efficiently Correct Liver Metabolic Diseases." *JCI Insight* 4(15):1–15.

De Caneva, Alessia, Fabiola Porro, Giulia Bortolussi, Riccardo Sola, Michela Lisjak, Adi Barzel, Mauro Giacca, Mark A Kay, Kristian Vlahoviček, Lorena Zentilin, and Andrés F. Muro. 2019. "Coupling AAV-Mediated Promoterless Gene Targeting to SaCas9 Nuclease to Efficiently Correct Liver Metabolic Diseases." *JCI Insight* 5(15).

Chandler, Randy J., Leah E. Venturoni, Jing Liao, Brandon T. Hubbard, Jessica L. Schneller, Victoria Hoffmann, Susana Gordo, Shengwen Zang, Chih-Wei Ko, and Nelson Chau. 2021. "Promoterless, Nuclease-free Genome Editing Confers a Growth Advantage for Corrected Hepatocytes in Mice with Methylmalonic Acidemia." *Hepatology* 73(6):2223–37.

Chen, Hainan, Mi Shi, Avital Gilam, Qi Zheng, Yin Zhang, Ivka Afrikanova, Jinling Li, Zoya Gluzman, Ruhong Jiang, and Ling-Jie Kong. 2019. "Hemophilia A Ameliorated in Mice by CRISPR-Based in Vivo Genome Editing of Human Factor VIII." *Scientific Reports* 9(1):1–15.

Choi, Jin-Ok, Mi Hee Lee, Hae-Young Park, and Sung-Chul Jung. 2010. "Characterization of Fabry Mice Treated with Recombinant Adeno-Associated Virus 2/8-Mediated Gene Transfer." *Journal of Biomedical Science* 17(1):26.

Chu, Wing Sum and Joanne Ng. 2021. “Immunomodulation in Administration of RAAV: Preclinical and Clinical Adjuvant Pharmacotherapies.” *Frontiers in Immunology* 12:658038.

Collaud, Fanny, Giulia Bortolussi, Laurence Guianvarc’h, Sem J. Aronson, Thierry Bordet, Philippe Veron, Severine Charles, Patrice Vidal, Marcelo Simon Sola, Stephanie Rundwasser, Delphine G. Dufour, Florence Lacoste, Cyril Luc, Laetitia v. Wittenberghe, Samia Martin, Christine Le Bec, Piter J. Bosma, Andres F. Muro, Giuseppe Ronzitti, Matthias Hebben, and Federico Mingozzi. 2019. “Preclinical Development of an AAV8-HUGT1A1 Vector for the Treatment of Crigler-Najjar Syndrome.” *Molecular Therapy - Methods & Clinical Development* 12:157–74.

Cornel, Martina C., Rigter Tessel, Jansen Marleen E, and Henneman Lidewij. 2021. “Neonatal and Carrier Screening for Rare Diseases: How Innovation Challenges Screening Criteria Worldwide.” *Journal of Community Genetics (2021)* 12:257–65.

Coutinho, Maria F., Juliana I. Santos, and Sandra Alves. 2016. “Less Is More: Substrate Reduction Therapy for Lysosomal Storage Disorders.” *International Journal of Molecular Sciences* 17(7).

Cox, T. M., J. M. F. G. Aerts, N. Belmatoug, M. D. Cappellini, S. vom Dahl, J. Goldblatt, G. A. Grabowski, C. E. M. Hollak, P. Hwu, M. Maas, A. M. Martins, P. K. Mistry, G. M. Pastores, A. Tylki-Szymanska, J. Yee, and N. Weinreb. 2008. “Management of Non-Neuronopathic Gaucher Disease with Special Reference to Pregnancy, Splenectomy, Bisphosphonate Therapy, Use of Biomarkers and Bone Disease Monitoring.” *Journal of Inherited Metabolic Disease* 31(3):319–36.

Cunningham, S. C., C. Y. Kok, A. Spinoulas, K. H. Carpenter, and I. E. Alexander. 2013. “AAV-Encoded OTC Activity Persisting to Adulthood Following Delivery to Newborn Spfash Mice Is Insufficient to Prevent ShRNA-Induced Hyperammonaemia.” *Gene Therapy* 20(12):1184–87.

Cunningham, Sharon C., Allison P. Dane, Afroditi Spinoulas, Grant J. Logan, and Ian E. Alexander. 2008. “Gene Delivery to the Juvenile Mouse Liver Using AAV2/8 Vectors.” *Molecular Therapy : The Journal of the American Society of Gene Therapy* 16(6):1081–88.

DeRosa, Frank, Lianne Smith, Yinghua Shen, Yan Huang, Jing Pan, Hongsheng Xie, Barak Yahalom, and Michael W. Heartlein. 2019. “Improved Efficacy in a Fabry Disease Model Using a Systemic MRNA Liver Depot System as Compared to Enzyme Replacement Therapy.” *Molecular Therapy* 27(4):878–89.

Diez, Begoña, Pietro Genovese, Francisco J. Roman-Rodriguez, Lara Alvarez, Giulia Schiroli, Laura Ugalde, Sandra Rodriguez-Perales, Julian Sevilla, Cristina Diaz de Heredia, and Michael C. Holmes. 2017. “Therapeutic Gene Editing in CD 34+ Hematopoietic Progenitors from Fanconi Anemia Patients.” *EMBO Molecular Medicine* 9(11):1574–88.

Dirk, Grimm, Lee Joyce S., Wang Lora, Desai Tushar, Akache Bassel, Storm Theresa A., and Kay

Mark A. 2008. “In Vitro and In Vivo Gene Therapy Vector Evolution via Multispecies Interbreeding and Retargeting of Adeno-Associated Viruses .” *Journal of Virology* 82(12):5887–5911.

Domm, Jakob M., Sarah K. Wootton, Jeffrey A. Medin, and Michael L. West. 2021. “Gene Therapy for Fabry Disease: Progress, Challenges, and Outlooks on Gene-Editing.” *Molecular Genetics and Metabolism* 134(1–2):117–31.

Doudna, Jennifer A. 2020. “The Promise and Challenge of Therapeutic Genome Editing.” *Nature* 578(7794):229–36.

Dull, T., R. Zufferey, M. Kelly, R. J. Mandel, M. Nguyen, D. Trono, and L. Naldini. 1998. “A Third-Generation Lentivirus Vector with a Conditional Packaging System.” *Journal of Virology* 72(11):8463–71.

Duncan, Andrew W., Craig Dorrell, and Markus Grompe. 2009. “Stem Cells and Liver Regeneration.” *Gastroenterology* 137(2):466–81.

de Duve, Christian. 1963. “THE LYSOSOME.” *Scientific American* 208(5):64–73.

Earley, Joseph, Elena Piletska, Giuseppe Ronzitti, and Sergey Piletsky. 2023. “Evading and Overcoming AAV Neutralization in Gene Therapy.” *Trends in Biotechnology* 41(6):836–45.

Elmore, Zachary C., Daniel K. Oh, Katherine E. Simon, Marco M. Fanous, and Aravind Asokan. 2020. “Rescuing AAV Gene Transfer from Neutralizing Antibodies with an IgG-Degrading Enzyme.” *JCI Insight* 5(19).

Elsner, Carina and Jens Bohne. 2017. “The Retroviral Vector Family: Something for Everyone.” *Virus Genes* 53(5):714–22.

Favret, Jacob M., Nadav I. Weinstock, M. Laura Feltri, and Daesung Shin. 2020. “Pre-Clinical Mouse Models of Neurodegenerative Lysosomal Storage Diseases.” *Frontiers in Molecular Biosciences* 7:57.

Ganesh, Jaya, Patrick Deegan, Ozlem Goker-Alpan, Robert J. Hopkin, John Bernat, William Wilcox, Liching Cao, Michael Chen, Lisa Shiue, and Emma Bowden. n.d. “Preliminary Results of STAAR, a Phase I/2 Study of Isaralgagene Civaparvovec (ST-920) Gene Therapy in Adults with Fabry Disease and Long-Term Follow-Up.”

Gao, Guang-Ping, Mauricio R. Alvira, Lili Wang, Roberto Calcedo, Julie Johnston, and James M. Wilson. 2002. “Novel Adeno-Associated Viruses from Rhesus Monkeys as Vectors for Human Gene Therapy.” *Proceedings of the National Academy of Sciences* 99(18):11854–59.

Garman, Scott C. and David N. Garboczi. 2004. “The Molecular Defect Leading to Fabry Disease: Structure of Human α-Galactosidase.” *Journal of Molecular Biology* 337(2):319–35.

Genovese, Pietro, Giulia Schiroli, Giulia Escobar, Tiziano Di Tomaso, Claudia Firrito, Andrea Calabria, Davide Moi, Roberta Mazzieri, Chiara Bonini, and Michael C. Holmes. 2014. "Targeted Genome Editing in Human Repopulating Haematopoietic Stem Cells." *Nature* 510(7504):235–40.

Germain, Dominique P. 2010. "Fabry Disease." *Orphanet Journal of Rare Diseases* 5(1):30.

Germain, Dominique P., Derralynn A. Hughes, Kathleen Nicholls, Daniel G. Bichet, Roberto Giugliani, William R. Wilcox, Claudio Feliciani, Suma P. Shankar, Fatih Ezgu, Hernan Amartino, Drago Bratkovic, Ulla Feldt-Rasmussen, Khan Nedd, Usama Sharaf El Din, Charles M. Lourenco, Maryam Banikazemi, Joel Charrow, Majed Dasouki, David Finegold, Pilar Giraldo, Ozlem Goker-Alpan, Nicola Longo, C. Ronald Scott, Roser Torra, Ahmad Tuffaha, Ana Jovanovic, Stephen Waldek, Seymour Packman, Elizabeth Ludington, Christopher Viereck, John Kirk, Julie Yu, Elfrida R. Benjamin, Franklin Johnson, David J. Lockhart, Nina Skuban, Jeff Castelli, Jay Barth, Carrolee Barlow, and Raphael Schiffmann. 2016. "Treatment of Fabry's Disease with the Pharmacologic Chaperone Migalastat." *New England Journal of Medicine* 375(6):545–55.

Gilles, Anna F. and Michalis Averof. 2014. "Functional Genetics for All: Engineered Nucleases, CRISPR and the Gene Editing Revolution." *EvoDevo* 5(1):43.

Gillmore, Julian D., Ed Gane, Jorg Taubel, Justin Kao, Marianna Fontana, Michael L. Maitland, Jessica Seitzer, Daniel O'Connell, Kathryn R. Walsh, Kristy Wood, Jonathan Phillips, Yuanxin Xu, Adam Amaral, Adam P. Boyd, Jeffrey E. Cehelsky, Mark D. McKee, Andrew Schiermeier, Olivier Harari, Andrew Murphy, Christos A. Kyratsous, Brian Zambrowicz, Randy Soltys, David E. Gutstein, John Leonard, Laura Sepp-Lorenzino, and David Lebwohl. 2021. "CRISPR-Cas9 In Vivo Gene Editing for Transthyretin Amyloidosis." *New England Journal of Medicine* 385(6):493–502.

Gomez-Ospina, Natalia, Samantha G. Scharenberg, Nathalie Mostrel, Rasmus O. Bak, Sruthi Mantri, Rolen M. Quadros, Channabasavaiah B. Gurumurthy, Ciaran Lee, Gang Bao, and Carlos J. Suarez. 2019. "Human Genome-Edited Hematopoietic Stem Cells Phenotypically Correct Mucopolysaccharidosis Type I." *Nature Communications* 10(1):4045.

Gonçalves, Manuel A. F. V. 2005a. "Adeno-Associated Virus: From Defective Virus to Effective Vector." *Virology Journal* 2(1):43.

Gonçalves, Manuel A. F. V. 2005b. "Adeno-Associated Virus: From Defective Virus to Effective Vector." *Virology Journal* 2(1):43.

Guérard, Nicolas, Daniel Oder, Peter Nordbeck, Christian Zwingelstein, Olivier Morand, Richard W. D. Welford, Jasper Dingemanse, and Christoph Wanner. 2018. "Lucerastat, an Iminosugar for Substrate Reduction Therapy: Tolerability, Pharmacodynamics, and Pharmacokinetics in Patients With Fabry Disease on Enzyme Replacement." *Clinical Pharmacology & Therapeutics* 103(4):703–11.

Van Haele, Matthias, Janne Snoeck, and Tania Roskams. 2019. "Human Liver Regeneration: An Etiology Dependent Process." *International Journal of Molecular Sciences* 20(9):2332.

Hiroyuki, Nakai, Yant Stephen R., Storm Theresa A., Fuess Sally, Meuse Leonard, and Kay Mark A. 2001. "Extrachromosomal Recombinant Adeno-Associated Virus Vector Genomes Are Primarily Responsible for Stable Liver Transduction In Vivo." *Journal of Virology* 75(15):6969–76.

Hughes, Derralynn A. 2008. "Early Therapeutic Intervention in Females with Fabry Disease?" *Acta Paediatrica* 97(s457):41–47.

Jayathilaka, Krishanthi, Sean D. Sheridan, Tyler D. Bold, Katarzyna Bochenska, Hillary L. Logan, Ralph R. Weichselbaum, Douglas K. Bishop, and Philip P. Connell. 2008. "A Chemical Compound That Stimulates the Human Homologous Recombination Protein RAD51." *Proceedings of the National Academy of Sciences* 105(41):15848–53.

Jeyakumar, Jey M., Azadeh Kia, Lawrence C. S. Tam, Jenny McIntosh, Justyna Spiewak, Kevin Mills, Wendy Heywood, Elisa Chisari, Noemi Castaldo, Daniël Verhoef, Paniz Hosseini, Petya Kalcheva, Clement Cocita, Carlos J. Miranda, Miriam Canavese, Jaminder Khinder, Cecilia Rosales, Derralynn Hughes, Rose Sheridan, Romuald Corbau, and Amit Nathwani. 2023. "Preclinical Evaluation of FLT190, a Liver-Directed AAV Gene Therapy for Fabry Disease." *Gene Therapy*.

Katsigianni, Eleni Ioanna and Panagiotis Petrou. 2022. "A Systematic Review of the Economic Evaluations of Enzyme Replacement Therapy in Lysosomal Storage Diseases." *Cost Effectiveness and Resource Allocation* 20(1):51.

Kattenhorn, Lisa M., Christopher H. Tipper, Lorelei Stoica, Deborah S. Geraghty, Teresa L. Wright, K. Reed Clark, and Samuel C. Wadsworth. 2016. "Adeno-Associated Virus Gene Therapy for Liver Disease." *Human Gene Therapy* 27(12):947–61.

Keating, Gillian M. 2012. "Agalsidase Alfa." *BioDrugs* 26(5):335–54.

Kellner, Max J., Jeremy G. Koob, Jonathan S. Gootenberg, Omar O. Abudayyeh, and Feng Zhang. 2019. "SHERLOCK: Nucleic Acid Detection with CRISPR Nucleases." *Nature Protocols* 14(10):2986–3012.

Khirallah, Jennifer, Maximilan Eimbinder, Yamin Li, and Qiaobing Xu. 2023. "Clinical Progress in Genome-Editing Technology and in Vivo Delivery Techniques." *Trends in Genetics* 39(3):208–16.

Khosla, Neil and Rodolfo Valdez. 2018. "A Compilation of National Plans, Policies and Government Actions for Rare Diseases in 23 Countries." *Intractable and Rare Diseases Research* 7(4):213–22.

Kido, Jun, Keishin Sugawara, and Kimitoshi Nakamura. 2023. "Gene Therapy for Lysosomal Storage Diseases: Current Clinical Trial Prospects." *Frontiers in Genetics* 14(January):1–16.

Klamroth, Robert, Gregory Hayes, Tatiana Andreeva, Keith Gregg, Takashi Suzuki, Ismail Haroon Mitha, Brandon Hardesty, Midori Shima, Toni Pollock, Patricia Slev, Johannes Oldenburg, Margareth C. Ozelo, Natalie Stieltjes, Sabine-Marie Castet, Johnny Mahlangu, Flora Peyvandi, Rashid Kazmi, Jean-François Schved, Andrew D. Leavitt, Michael Callaghan, Brigitte Pan-Petesch, Doris V Quon, Jayson Andrews, Alex Trinh, Mingjin Li, and Wing Yen Wong. 2022. "Global Seroprevalence of Pre-Existing Immunity Against AAV5 and Other AAV Serotypes in People with Hemophilia A." *Human Gene Therapy* 33(7–8):432–41.

Klingelhöfer, Doris, Markus Braun, Rebekka K. Seeger-Zybok, David Quarcoo, Dörthe Brüggmann, and David A. Groneberg. 2020. "Global Research on Fabry's Disease: Demands for a Rare Disease." *Molecular Genetics & Genomic Medicine* 8(9):e1163.

von Knebel Doeberitz, Magnus and Nicolas Wentzensen. 2008. "CHAPTER 1 - The Cell: Basic Structure and Function." Pp. 3–22 in, edited by M. Bibbo and D. B. T.-C. C. (Third E. Wilbur. Edinburgh: W.B. Saunders.

Laoharawee, Kanut, Russell C. DeKelver, Kelly M. Podetz-Pedersen, Michelle Rohde, Scott Sproul, Hoang-Oanh Nguyen, Tam Nguyen, Susan J. St Martin, Li Ou, and Susan Tom. 2018. "Dose-Dependent Prevention of Metabolic and Neurologic Disease in Murine MPS II by ZFN-Mediated in Vivo Genome Editing." *Molecular Therapy* 26(4):1127–36.

Lin, Hsiang-Yu, Kah-Wai Chong, Ju-Hui Hsu, Hsiao-Chi Yu, Chun-Che Shih, Cheng-Hung Huang, Shing-Jong Lin, Chen-Huan Chen, Chuan-Chi Chiang, Huey-Jane Ho, Pi-Chang Lee, Chuan-Hong Kao, Kang-Hsiang Cheng, Chuen Hsueh, and Dau-Ming Niu. 2009. "High Incidence of the Cardiac Variant of Fabry Disease Revealed by Newborn Screening in the Taiwan Chinese Population." *Circulation: Cardiovascular Genetics* 2(5):450–56.

Lisowski, Leszek, Allison P. Dane, Kirk Chu, Yue Zhang, Sharon C. Cunningham, Elizabeth M. Wilson, Sean Nygaard, Markus Grompe, Ian E. Alexander, and Mark A. Kay. 2014. "Selection and Evaluation of Clinically Relevant AAV Variants in a Xenograft Liver Model." *Nature* 506(7488):382–86.

Lu, Yaoyao, Cedric Happi Mbakam, Bo Song, Eli Bendavid, and Jacques-P. Tremblay. 2022. "Improvements of Nuclease and Nickase Gene Modification Techniques for the Treatment of Genetic Diseases." *Frontiers in Genome Editing* 4.

Luzio, J. P., B. A. Rous, N. A. Bright, P. R. Pryor, B. M. Mullock, and R. C. Piper. 2000. "Lysosome-Endosome Fusion and Lysosome Biogenesis." *Journal of Cell Science* 113(9):1515–24.

Macedo, Maria Fatima, Rui Quinta, Catia Sofia Pereira, and Maria Clara Sa Miranda. 2012. "Enzyme Replacement Therapy Partially Prevents Invariant Natural Killer T Cell Deficiency in the Fabry Disease

Mouse Model." *Molecular Genetics and Metabolism* 106(1):83–91.

Makarova, Kira S., Daniel H. Haft, Rodolphe Barrangou, Stan J. J. Brouns, Emmanuelle Charpentier, Philippe Horvath, Sylvain Moineau, Francisco J. M. Mojica, Yuri I. Wolf, Alexander F. Yakunin, John van der Oost, and Eugene V Koonin. 2011. "Evolution and Classification of the CRISPR–Cas Systems." *Nature Reviews Microbiology* 9(6):467–77.

Marshall, John, Karen M. Ashe, Dinesh Bangari, KerryAnne McEachern, Wei-Lien Chuang, Joshua Pacheco, Diane P. Copeland, Robert J. Desnick, James A. Shayman, Ronald K. Scheule, and Seng H. Cheng. 2010. "Substrate Reduction Augments the Efficacy of Enzyme Therapy in a Mouse Model of Fabry Disease." *PloS One* 5(11):e15033.

McCafferty, Emma H. and Lesley J. Scott. 2019. "Migalastat: A Review in Fabry Disease." *Drugs* 79(5):543–54.

Meliani, Amine, Florence Boisgerault, Romain Hardet, Solenne Marmier, Fanny Collaud, Giuseppe Ronzitti, Christian Leborgne, Helena Costa Verdera, Marcelo Simon Sola, Severine Charles, Alban Vignaud, Laetitia van Wittenberghe, Giorgia Manni, Olivier Christophe, Francesca Fallarino, Christopher Roy, Alicia Michaud, Petr Ilyinskii, Takashi Kei Kishimoto, and Federico Mingozzi. 2018. "Antigen-Selective Modulation of AAV Immunogenicity with Tolerogenic Rapamycin Nanoparticles Enables Successful Vector Re-Administration." *Nature Communications* 9(1).

Michaud, Martin, Wladimir Mauhin, Nadia Belmatoug, Roselyne Garnotel, Naiya Bedreddine, Florian Catros, Sophie Ancellin, Olivier Lidove, and Francis Gaches. 2020. "When and How to Diagnose Fabry Disease in Clinical Pratice." *The American Journal of the Medical Sciences* 360(6):641–49.

Mindy, Li. 2018. "Enzyme Replacement Therapy: A Review and Its Role in Treating Lysosomal Storage Diseases." *Pediatric Annals* 47(5):e191–97.

Miyoshi, H., U. Blömer, M. Takahashi, F. H. Gage, and I. M. Verma. 1998. "Development of a Self-Inactivating Lentivirus Vector." *Journal of Virology* 72(10):8150–57.

Motabar, Omid, Ellen Sidransky, Ehud Goldin, and Wei Zheng. 2010. "Fabry Disease - Current Treatment and New Drug Development." *Current Chemical Genomics* 4:50–56.

Naso, Michael F., Brian Tomkowicz, William L. Perry, and William R. Strohl. 2017. "Adeno-Associated Virus (AAV) as a Vector for Gene Therapy." *BioDrugs* 31(4):317–34.

Nguengang Wakap, Stéphanie, Deborah M. Lambert, Annie Olry, Charlotte Rodwell, Charlotte Gueydan, Valérie Lanneau, Daniel Murphy, Yann Le Cam, and Ana Rath. 2020. "Estimating Cumulative Point Prevalence of Rare Diseases: Analysis of the Orphanet Database." *European Journal of Human Genetics* 28(2):165–73.

Nguyen, M. T. and K. Charlebois. 2015. “The Clinical Utility of Whole-Exome Sequencing in the Context of Rare Diseases-the Changing Tides of Medical Practice.” *Clinical Genetics* 88(4):313–19.

Ohshima, Toshio, Gary J Murray, William D. Swaim, Glenn Longenecker, Jane M. Quirk, Carol O. Cardarelli, Yoshikazu Sugimoto, Ira Pastan, Michael M. Gottesman, and Roscoe O. Brady. 1997. “α-Galactosidase A Deficient Mice: A Model of Fabry Disease.” *Proceedings of the National Academy of Sciences* 94(6):2540–44.

Ohshima, Toshio, Gary J. Murray, William D. Swaim, Glenn Longenecker, Jane M. Quirk, Carol O. Cardarelli, Yoshikazu Sugimoto, Ira Pastan, Michael M. Gottesman, Roscoe O. Brady, and Ashok B. Kulkarni. 1997. “α-Galactosidase A Deficient Mice: A Model of Fabry Disease.” *Proceedings of the National Academy of Sciences of the United States of America* 94(6):2540–44.

Parenti, Giancarlo, Generoso Andria, and Kenneth J. Valenzano. 2015. “Pharmacological Chaperone Therapy: Preclinical Development, Clinical Translation, and Prospects for the Treatment of Lysosomal Storage Disorders.” *Molecular Therapy* 23(7):1138–48.

Parkinson-Lawrence, Emma J., Tetyana Shandala, Mark Prodoehl, Revecca Plew, Glenn N. Borlace, and Doug A. Brooks. 2010. “Lysosomal Storage Disease: Revealing Lysosomal Function and Physiology.” *Physiology* 25(2):102–15.

Pavan, Sonia, Kathrin Rommel, María Elena Mateo Marquina, Sophie Höhn, Valérie Lanneau, and Ana Rath. 2017. “Clinical Practice Guidelines for Rare Diseases: The Orphanet Database.” *PLoS ONE* 12(1):1–14.

Petri, Karl and Vikram Pattanayak. 2018. “SHERLOCK and DETECTR Open a New Frontier in Molecular Diagnostics.” *The CRISPR Journal* 1(3):209–11.

Pisani, Antonio, Bianca Visciano, Graciana Diez Roux, Massimo Sabbatini, Caterina Porto, Giancarlo Parenti, and Massimo Imbriaco. 2012. “Enzyme Replacement Therapy in Patients with Fabry Disease: State of the Art and Review of the Literature.” *Molecular Genetics and Metabolism* 107(3):267–75.

Pompen, A. W. M., M. Ruiter, and H. J. G. Wyers. 1947. “Angiokeratoma Corporis Diffusum (Universale) Fabry, as a Sign of an Unknown Internal Disease; Two Autopsy Reports.” *Acta Medica Scandinavica* 128(3):234–55.

Porro, Fabiola, Giulia Bortolussi, Adi Barzel, Alessia De Caneva, Alessandra Iaconcig, Simone Vodret, Lorena Zentilin, Mark A. Kay, and Andrés F. Muro. 2017. “Promoterless Gene Targeting without Nucleases Rescues Lethality of a Crigler-Najjar Syndrome Mouse Model.” *EMBO Molecular Medicine* 9(10):1346–55.

Powell, Sara Kathleen, Ricardo Rivera-Soto, and Steven James Gray. 2015. “Viral Expression Cassette

Elements to Enhance Transgene Target Specificity and Expression in Gene Therapy." *Discovery Medicine* 19(102):49–57.

Quinta, Rui, Daniel Rodrigues, Marisa Assunção, Maria Fatima Macedo, Olga Azevedo, Damião Cunha, Pedro Oliveira, and Maria Clara Sá Miranda. 2014. "Reduced Glucosylceramide in the Mouse Model of Fabry Disease: Correction by Successful Enzyme Replacement Therapy." *Gene* 536(1):97–104.

Ran, F. Ann, Le Cong, Winston X. Yan, David A. Scott, Jonathan S. Gootenberg, Andrea J. Kriz, Bernd Zetsche, Ophir Shalem, Xuebing Wu, Kira S. Makarova, Eugene V Koonin, Phillip A. Sharp, and Feng Zhang. 2015. "In Vivo Genome Editing Using Staphylococcus Aureus Cas9." *Nature* 520(7546):186–91.

De Ravin, Suk See, Andreas Reik, Pei-Qi Liu, Linhong Li, Xiaolin Wu, Ling Su, Castle Raley, Narda Theobald, Uimook Choi, and Alexander H. Song. 2016. "Targeted Gene Addition in Human CD34+ Hematopoietic Cells for Correction of X-Linked Chronic Granulomatous Disease." *Nature Biotechnology* 34(4):424–29.

te Riele, H., E. R. Maandag, and A. Berns. 1992. "Highly Efficient Gene Targeting in Embryonic Stem Cells through Homologous Recombination with Isogenic DNA Constructs." *Proceedings of the National Academy of Sciences of the United States of America* 89(11):5128–32.

Rombach, Saskia M., Bouwien E. Smid, Machtelt G. Bouwman, Gabor E. Linthorst, Marcel G. W. Dijkgraaf, and Carla E. M. Hollak. 2013. "Long Term Enzyme Replacement Therapy for Fabry Disease: Effectiveness on Kidney, Heart and Brain." *Orphanet Journal of Rare Diseases* 8(1):47.

De Sabbata, Giulia, Florence Boisgerault, Corrado Guarnaccia, Alessandra Iaconcig, Giulia Bortolussi, Fanny Collaud, Giuseppe Ronzitti, Marcelo Simon Sola, Patrice Vidal, and Jeremy Rouillon. 2021. "Long-Term Correction of Ornithine Transcarbamylase Deficiency in Spf-Ash Mice with a Translationally Optimized AAV Vector." *Molecular Therapy-Methods & Clinical Development* 20:169–80.

Sachin Navale, Kaveri Bhosale, Mahesh Mohite, and Swapnali Navale. 2022. "Hemgenix as First Gene Therapy for Treatment of Haemophilia B." *International Journal of Advanced Research in Science, Communication and Technology* 2(1):89–94.

Sadelain, Michel, Eirini P. Papapetrou, and Frederic D. Bushman. 2012. "Safe Harbours for the Integration of New DNA in the Human Genome." *Nature Reviews Cancer* 12(1):51–58.

Sarvari, Raana, Mohammad Nouri, Samira Agbolaghi, Laila Roshangar, Amirhouman Sadrhaghighi, Alexander M. Seifalian, and Peyman Keyhanvar. 2022. "A Summary on Non-Viral Systems for Gene Delivery Based on Natural and Synthetic Polymers." *International Journal of Polymeric Materials and*

Polymeric Biomaterials 71(4):246–65.

Scharenberg, Samantha G., Edina Poletto, Katherine L. Lucot, Pasqualina Colella, Adam Sheikali, Thomas J. Montine, Matthew H. Porteus, and Natalia Gomez-Ospina. 2020. "Engineering Monocyte/Macrophage− Specific Glucocerebrosidase Expression in Human Hematopoietic Stem Cells Using Genome Editing." *Nature Communications* 11(1):3327.

Schiroli, Giulia, Samuele Ferrari, Anthony Conway, Aurelien Jacob, Valentina Capo, Luisa Albano, Tiziana Plati, Maria C. Castiello, Francesca Sanvito, and Andrew R. Gennery. 2017. "Preclinical Modeling Highlights the Therapeutic Potential of Hematopoietic Stem Cell Gene Editing for Correction of SCID-X1." *Science Translational Medicine* 9(411):eaan0820.

Sharma, Rajiv, Xavier M. Anguela, Yannick Doyon, Thomas Wechsler, Russell C. DeKelver, Scott Sproul, David E. Paschon, Jeffrey C. Miller, Robert J. Davidson, David Shivak, Shangzhen Zhou, Julianne Rieders, Philip D. Gregory, Michael C. Holmes, Edward J. Rebar, and Katherine A. High. 2015. "In Vivo Genome Editing of the Albumin Locus as a Platform for Protein Replacement Therapy." *Blood* 126(15):1777–84.

Silva, Amanda K. A., Corinne Sagné, Florence Gazeau, and Ibane Abasolo. 2022. "Enzyme Replacement Therapy: Current Challenges and Drug Delivery Prospects via Extracellular Vesicles." *Rare Disease and Orphan Drugs Journal* 1(3):13.

Spada, Marco, Severo Pagliardini, Makiko Yasuda, Turgut Tukel, Geetha Thiagarajan, Hitoshi Sakuraba, Alberto Ponzone, and Robert J. Desnick. 2006. "High Incidence of Later-Onset Fabry Disease Revealed by Newborn Screening*." *The American Journal of Human Genetics* 79(1):31–40.

Stephens, Calvin J., Elena Kashentseva, William Everett, Lyudmila Kaliberova, and David T. Curiel. 2018. "Targeted in Vivo Knock-in of Human Alpha-1-Antitrypsin CDNA Using Adenoviral Delivery of CRISPR/Cas9." *Gene Therapy* 25(2):139–56.

Stephens, Calvin J., Elvin J. Lauron, Elena Kashentseva, Zhi Hong Lu, Wayne M. Yokoyama, and David T. Curiel. 2019. "Long-Term Correction of Hemophilia B Using Adenoviral Delivery of CRISPR/Cas9." *Journal of Controlled Release* 298:128–41.

Taguchi, Atsumi, Hiroki Maruyama, Masaaki Nameta, Tadashi Yamamoto, Junichiro Matsuda, Ashok B. Kulkarni, Hidekatsu Yoshioka, and Satoshi Ishii. 2013. "A Symptomatic Fabry Disease Mouse Model Generated by Inducing Globotriaosylceramide Synthesis." *Biochemical Journal* 456(3):373–83.

Tambuyzer, Erik. 2010. "Rare Diseases, Orphan Drugs and Their Regulation: Questions and Misconceptions." *Nature Reviews Drug Discovery* 9(12):921–29.

Taub, Rebecca. 2004. "Liver Regeneration: From Myth to Mechanism." *Nature Reviews Molecular*

Cell Biology 5(10):836–47.

Thomas, Clare E., Theresa A. Storm, Zan Huang, and Mark A. Kay. 2004. “Rapid Uncoating of Vector Genomes Is the Key Toefficient Liver Transduction with Pseudotyped Adeno-Associated Virusvectors.” *Journal of Virology* 78(6):3110–22.

Tsuji, Shinnosuke, Calvin J. Stephens, Giulia Bortolussi, Feijie Zhang, Gabriele Baj, Hagoon Jang, Gustavo de Alencastro, Andrés F. Muro, Katja Pekrun, and Mark A. Kay. 2022. “Fludarabine Increases Nuclease-Free AAV- and CRISPR/Cas9-Mediated Homologous Recombination in Mice.” *Nature Biotechnology* 40(8):1285–94.

Tsuji, Shinnosuke, Calvin Stevens, Giulia Bortolussi, Feijie Zhang, Katja Pekrun, Gabriele Baj, Gustavo de Alencastro, Andres Muro, and Mark Kay. 2020. “Improving the Efficiency of Liver Targeting RAAV-Mediated Homologous Recombination Using Ribonucleotide Reductase Inhibitors.” *ResearchSquare* 1–28.

Verma, Sumit, Stella N. Nwosu, Raj Razdan, Saila R. Upadhyayula, Han C. Phan, Abubakarr A. Koroma, Isai Leguizamo, Natalie S. Correa, Michael Kuipa, David Lee, Thomas H. Vanderford, and Matthew R. Gardner. 2022. “Seroprevalence of Adeno-Associated Virus Neutralizing Antibodies in Males with Duchenne Muscular Dystrophy.” *Human Gene Therapy*.

Wang, Joy Y. and Jennifer A. Doudna. 2023. “CRISPR Technology: A Decade of Genome Editing Is Only the Beginning.” *Science* 379(6629):eadd8643.

Wang, Lili, Peter Bell, Suryanarayan Somanathan, Qiang Wang, Zhenning He, Hongwei Yu, Deirdre McMenamin, Tamara Goode, Roberto Calcedo, and James M. Wilson. 2015. “Comparative Study of Liver Gene Transfer With AAV Vectors Based on Natural and Engineered AAV Capsids.” *Molecular Therapy* 23(12):1877–87.

Wang, Lili, Hiroki Morizono, Jianping Lin, Peter Bell, David Jones, Deirdre McMenamin, Hongwei Yu, Mark L. Batshaw, and James M. Wilson. 2012. “Preclinical Evaluation of a Clinical Candidate AAV8 Vector for Ornithine Transcarbamylase (OTC) Deficiency Reveals Functional Enzyme from Each Persisting Vector Genome.” *Molecular Genetics and Metabolism* 105(2):203–11.

Weterings, Eric and David J. Chen. 2008. “The Endless Tale of Non-Homologous End-Joining.” *Cell Research* 18(1):114–24.

Whittington, Ruth and Karen L. Goa. 1995. “Alglucerase.” *PharmacoEconomics* 7(1):63–90.

Xu, Yuanyuan and Zhanjun Li. 2020. “CRISPR-Cas Systems: Overview, Innovations and Applications in Human Disease Research and Gene Therapy.” *Computational and Structural Biotechnology Journal* 18:2401–15.

Yan, Zhonghai, Hao Yan, and Hailong Ou. 2012. “Human Thyroxine Binding Globulin (TBG) Promoter Directs Efficient and Sustaining Transgene Expression in Liver-Specific Pattern.” *Gene* 506(2):289–94.

Yasuda, Makiko, Marshall W. Huston, Silvere Pagant, Lin Gan, Susan St. Martin, Scott Sproul, Daniel Richards, Stephen Ballaron, Khaled Hettini, Annemarie Ledeboer, Lillian Falese, Liching Cao, Yanmei Lu, Michael C. Holmes, Kathleen Meyer, Robert J. Desnick, and Thomas Wechsler. 2020. “AAV2/6 Gene Therapy in a Murine Model of Fabry Disease Results in Supraphysiological Enzyme Activity and Effective Substrate Reduction.” *Molecular Therapy - Methods and Clinical Development* 18:607–19.

Zabaleta, Nerea, Carmen Unzu, Nicholas D. Weber, and Gloria Gonzalez-Aseguinolaza. 2023. “Gene Therapy for Liver Diseases — Progress and Challenges.” *Nature Reviews Gastroenterology & Hepatology* 20(5):288–305.

Zhao, Liyuan, Zixuan Yang, Minhui Zheng, Lei Shi, Mengyun Gu, Gang Liu, Feng Miao, Yan Chang, Fanghua Huang, and Naping Tang. 2023. “Recombinant Adeno-Associated Virus 8 Vector in Gene Therapy: Opportunities and Challenges.” *Genes & Diseases*.

Zhu, Xuling, Ling Yin, Matt Theisen, Jenny Zhuo, Summar Siddiqui, Becca Levy, Vladimir Presnyak, Andrea Frassetto, Jaclyn Milton, Timothy Salerno, Kerry E. Benenato, Joe Milano, Andy Lynn, Staci Sabnis, Kristine Burke, Gilles Besin, Christine M. Lukacs, Lin T. Guey, Patrick F. Finn, and Paolo G. V. Martini. 2019. “Systemic MRNA Therapy for the Treatment of Fabry Disease: Preclinical Studies in Wild-Type Mice, Fabry Mouse Model, and Wild-Type Non-Human Primates.” *American Journal of Human Genetics* 104(4):625–37.

Zimran, Ari, Gheona Altarescu, and Deborah Elstein. 2013. “Pilot Study Using Ambroxol as a Pharmacological Chaperone in Type 1 Gaucher Disease.” *Blood Cells, Molecules, and Diseases* 50(2):134–37.

Zimran, Ari, Deborah Elstein, Ephrat Levy-Lahad, Shoshana Zevin, I. Hadas-Halpern, Y. Bar-Ziv, J. Foldes, A. J. Schwartz, and A. Abrahamov. 1995. “Replacement Therapy with Imiglucerase for Type 1 Gaucher’s Disease.” *Lancet (London, England)* 345(8963):1479–80.